EXAMINING NANOPARTICLE CHARACTERISTICS AND REMOVAL THROUGH DIRECT FILTRATION TREATMENT

By

Elsadig Abdallah

Submitted in partial fulfilment of the requirements
for the degree of Doctor of Philosophy

at

Dalhousie University
Halifax, Nova Scotia
August 2012

DALHOUSIE UNIVERSITY

DEPARTMENT OF CIVIL AND RESOURCE ENGINEERING

The undersigned hereby certify that they have read and recommend to the Faculty of Graduate Studies for acceptance a thesis entitled "**Examining Nanoparticle Characteristics and Removal Through Direct Filtration Treatment**" by Elsadig Ahmed Mohamed Abdallah in partial fulfilment of the requirements for the degree of Doctor of Philosophy.

Dated: August 30, 2012

External Examiner: _____

Research Supervisor: _____

Examining Committee: _____

_____

Departmental Representative: _____

DALHOUSIE UNIVERSITY

DATE: August 30, 2012

AUTHOR: Elsadig Abdallah

TITLE: **Examining Nanoparticle Characteristics and Removal Through Direct Filtration Treatment**

DEPARTMENT OR SCHOOL: Department of Civil and Resource Engineering

DEGREE: PhD CONVOCATION: May YEAR: 2013

_____

Signature of Author

DEDICATION

I dedicate this dissertation to the spirit of my parents
who are peacefully lying in their eternity.

I would also like to dedicate this dissertation to my brother Salah Ahmed
who introduced me to the wonders of science at a very early age and encouraged me to obtain this Ph.D. degree.

TABLE OF CONTENTS

LIST OF TABLES

LIST OF FIGURES

ABSTRACT

Water utilities in Nova Scotia face numerous challenges treating low turbidity water and complying with stringent guidelines and treatment standards. Problems associated with the treatment of low-turbidity water are not confined to Nova Scotia; several other provinces, British Columbia, Manitoba and Ontario share similar water characteristics of drinking water sources. The treatment of low turbidity water is a challenge for these utilities as it requires maintaining the appropriate coagulant dosage that will ensure adequate particle and natural organic matter removal, while at the same time not enhancing the formation of disinfection by-products. Another concern associated with the treatment of such water is that when the particle content of the water is very low, charge neutralization will not be effective due to the weak contact between destabilized particles. Currently, nanoparticles are not regulated as water contaminants, and thus it is unclear whether the existing filtration treatment practices are capable of removing them from drinking water. Obtaining in-depth information on nanoparticle characteristics in drinking water sources will provide a valuable resource that can assist in the development of future treatment strategies.

In this research, characteristics of four synthetic nanoparticles cerium dioxide (CeO_2), ferric oxide (Fe_2O_3), silicon dioxide (SiO_2) and titanium dioxide (TiO_2) were investigated in Milli-Q water for particle size, surface area, and surface potential using different characterization techniques. Water samples from Pockwock Lake were also characterized for naturally occurring nanoparticles. After initial testing, titanium dioxide (TiO_2) nanoparticles were selected to examine particle removal at bench-scale filtration experiments, under operating conditions similar to those practiced at the J.D. Kline Water Supply Plant, Halifax, NS, Canada. Filter performance for the deposition of TiO_2 nanoparticles was evaluated through the calculation of its attachment efficiency and coefficient under various water chemistry conditions. The calculated filter efficiency was then applied to simulate natural nanoparticles removal from water.

The results of the research indicate that the investigated nanoparticles behaved similar to natural particles and formed aggregates with larger particle sizes in Milli-Q water. Among the tested nanoparticles, only titanium dioxide could be coagulated with alum, as its negative surface charge and zero point of charge were closer to that of alum. Filtration experiments revealed that TiO_2 nanoparticles, when present in water, could successfully be removed by an alum dose of 8 mg/L. Indeed, removal in excess of 99.5% was achieved under the study conditions. Under the investigated water chemistry conditions, very low attachment efficiencies (α) of 0.001, 0.002 and 0.01, and filter coefficients (λ) of -0.003, -0.001 and -0.02 were determined for the filters. Based on the calculated attachment efficiencies, and under the studied conditions, natural nanoparticles remain dispersed in the water and would not likely to be removed by direct filtration. The overall research findings represent a major step forward in nanoparticle removal by direct filtration.

LIST OF ABBREVIATIONS AND SYMBOLS USED

AFM	Atomic Force Microscopy
Ar	Argon Gas
A_s	Porosity function, Dimensionless
BET	Burnauer Emmet and Teller
C	Effluent Particle Concentration
$Ca(NO_3)_2$	Calcium Nitrate
CeO_2	Cerium Dioxide
cm	centimeter
C_o	Influent Particle Concentration
D	Particle Diffusion Coefficient,
d_c	Collector Diameter
DEL	Doppler Electrophoretic Light scattering
DLS	Dynamic Light Scattering
DLVO	Derjagiun Landau Verwey Overbeek
d_p	Particle Diameter
f	Particle Friction Coefficient
Fe_2O_3	Ferric Dioxide
g	Acceleration of Gravity
Ha	Hamaker Constant
HCl	Hydrochloric Acid
ICP-MS	Inductively Coupled Plasma Mass Spectrometry
kB	Boltzmann Constant (1.381 × 10 -23 J/K)

L	Media Bed depth
MFI	Micro Flow Imaging
mg/L	milligram per liter
mmol/L	millimole per litre
mS/cm	microsiemens per centimeter
mV	millivolt
NaCl	Sodium Chloride
$NaNO_3$	Sodium Nitrate
NaOH	Sodium Hydroxide
N_G	Dimensionless Gravitational Force Number
N_{LO}	London Group Dimensionless Number or Van Der Waals Number
nm	nanometer
N_R	Relative-size Group Dimensionless
NTU	Nephliometric Turbidity Unit
ºC	Degrees Celsius
Pe	Peclet Number Dimensionless
PSD	Particle Size Distribution
QA/QC	Quality Assurance/Quality Control
R	Ratio of Particle to Collector size = d_p/d_c,
R_H	Particle Hydrodynamic Diameter
SEM	Scanning Electron Microscopy
SiO_2	Silicon Dioxide
std	Standard Deviation

T	Absolute Temperature K (273+ °C),
TEM	Transmission Electron Microscopy
TiO_2	Titanium Dioxide
U/AAS	Ultrasonic/Acoustic Attenuation Spectroscopy
V_F	Superficial Velocity above the Media Bed
V_s	Stokes Settling Velocity,
α	Empirical Collision Attachment Efficiency
γ	Porosity Function Dimensionless
$\mathcal{E}$	Porosity
η	Water Viscosity
λ	Filter Coefficient
μ	Absolute Viscosity of Fluid
μm	Micrometer
η_D	Single Contact Efficiency by Diffusion
η_G	Single Contact Efficiency by Gravity
η_I	Single Contact Efficiency by Interception
η_o	The Overall Single Collector Efficiency
ρ	Mass Density of Fluid
ρ_s	Density of particle

ACKNOWLEDGEMENT

I would like to thank my supervisor, Dr. Graham Gagnon, for his guidance as well as his technical and financial support throughout my graduate studies. I would also like to thank him for his constructive criticism, which has been invaluable for the development of this research.

In addition, I would like to thank my supervisory committee members, Dr. Craig Lake and Dr. Su-Ling Brooks. Their technical advice and contributions to this manuscript have been highly appreciated.

I would also like to thank Dr. Manfred H. Jericho from the Department of Physics at Dalhousie University for his magnanimity and generosity, not only for providing access to his laboratory, but also for showing me how doing the AFM analysis and answering all of my questions.

My thanks are likewise extended to Eliman Camara, for assisting me in conducting the filtration experiments, to John Bergese, Jessica MacKay, Matt Follett and Sara Payne, for providing me with water samples throughout this research.

As well, my sincere thanks go to Yamun Vadasarukkai and Sadra Monfared, whose leniency makes the office a joyous place for discussions and frolic.

Finally, my thanks go to everyone who contributed to the successful completion of this research.

CHAPTER 1: INTRODUCTION

Most surface waters in Nova Scotia are characterized by low pH (5.5-6.5), low turbidity (less than 2 NTU), low alkalinity (less than 5 mg/L as $CaCO_3$), and moderate to high color and dissolved natural organic matter (O'Leary et al., 2003). The treatment of such water poses several challenges, as it requires a trade-off between natural organic matter removal that would meet disinfection by-product goals, and filtration treatment that would ensure adequate particle removal. This can be achieved through proper adjustment of chemical additions during the coagulation process, which reduces the natural organic matter and prevents disinfection by-product formation.

Previous studies have shown that coagulation of water with low particle content is associated with ineffective charge neutralization due to the weak contact between destabilized particles (Petrusevski, 1999). It is also established that increasing coagulant dosages to remove natural organic matter would lead to the excessive floc formation, fast filter clogging, fast head loss development, and short filter run time. Therefore, in order to achieve effective filtration treatment, proper coagulation and flocculation processes need to be maintained (Cleasby & Logsdon, 1999).

Water from Pockwock Lake in Nova Scotia is treated at the J.D. Kline Water Supply Plant, which is equipped with a direct filtration facility. The water is treated through coagulation with an 8 mg/L alum dose, flocculation with hydraulic mixing, followed by direct filtration and disinfection with free chlorine. The filters at the plant operate for approximately 60 hours before being backwashed (O'Leary et al., 2003). Eisnor et al. (2001) assessed particle removal at JD Kline Water Supply Plant based on particle counts

and found that the filters degraded from a greater than 2-log removal to around a 1-log removal over the course of the filter run for particles greater than 2 μm. Moreover, a recent study by Vadasarukkai et al., (2011) indicated that a computational fluid dynamics modeling of flocculation tanks at the plant identified several stagnant regions where little to no mixing had occurred, which can affect filtration performance. Vadasarukkai et al. (2011) also elaborated that inadequate mixing has several negative consequences on overall particle removal efficiency; these include poor floc formation, reliance on additional flocculant aids, and increased filters load. Therefore, proper mixing is required for effective binding and pinpoint floc formation.

Although *Giardia* and *Cryptosporidium* have not been detected in the plant's source water (Pockwock Lake), Canadian drinking water quality guidelines require that a 3-log reduction for these protozoa should be achieved in treated water (Health Canada Guidelines, 2004). Therefore, there is a need for more effective evidence of particle removal that could be used to improve filtration treatment for the removal of particles with size smaller than 2 μm. It is believed that improving particle removal will also reduce natural organic matter and the formation of disinfection by-products.

Various particles have been used as particle sources in filtration studies to evaluate filter performance (e.g., Styrene Beads, inactivated *Giardia* and *Cryptosporidium parvum*). However, these particles are too large (e.g. 3 – 8 μm) for many of the naturally occurring nanoparticles in Pockwock Lake water. Therefore, particles with size smaller than 2 μm are required to be used to investigate the ability of direct filtration for efficient particle

and pathogen removal. This research utilizes nanoparticles as a source particle for removal during filtration. It focuses on assessing filter performance using nanoparticles as surrogates for particle removal in a water source characterized by low pH, turbidity and alkalinity. Problems associated with the treatment of low-turbidity water are not confined to Nova Scotia, several other provinces; British Columbia, Manitoba and Ontario (Braul et al., 2001) share similar water characteristics of drinking water sources.

Currently, nanoparticles are not regulated as water contaminants, and thus it is unclear whether the existing filtration treatment practices are capable of removing them from drinking water. Obtaining in-depth information on nanoparticle characteristics in drinking water sources will provide a valuable resource that can assist in the development of future treatment strategies. Therefore, examining surface water in Nova Scotia for particle removal at bench-scale filtration studies using nanoparticles, and under operating conditions similar to those practiced at JD Kline Water Supply Plant, will help tailor appropriate treatment options in the plant and assist other regions with similar water characteristics to optimize their treatment processes.

1.1. Research Hypothesis and Objective

The fundamental hypothesis of this dissertation was that synthetic nanoparticles can aggregate in a similar manner to natural particles and therefore can be removed by direct filtration from surface water characterized by low levels of pH, turbidity and alkalinity.

The main objective of the dissertation was to examine direct filtration treatment for the removal of synthetic nanoparticles as a surrogate for natural particles in low turbidity

water, and under operating conditions similar to those practiced at the JD Kline Water Supply Plant. To test this hypothesis, the main objective was further broken down into several sub-objectives:

Objective 1. To characterize and select appropriate synthetic nanoparticles that can further be used as surrogate for evaluating particle removal in low turbidity water.

Objective 2. To characterize water samples from Pockwock Lake for naturally occurring nanoparticles.

Objective 3. To evaluate filter performance for the deposition of TiO_2 nanoparticles under various water chemistry and simulated conditions.

Objective 4. To examine direct filtration for the removal of TiO_2 nanoparticles at a bench scale level and under operating conditions similar to those practiced at the J.D. Kline Water Supply Plant in Halifax, Nova Scotia Canada.

1.2. Organization of the Dissertation

The chapters of this dissertation are organized as manuscripts, with the intention for them to be submitted to refereed journals for publication. Hence, each of these chapters consists of an abstract, introduction, material and method, results and discussion, and a conclusion section.

Chapter 1 provides a general introduction of the dissertation rationale and the challenges faced when treating low turbidity water by direct filtration. It also outlines the dissertation hypothesis and its main objective.

Chapter 2 presents general background information on particles in water, fundamental theories that govern particle interaction and stability in water, filtration mechanisms, direct filtration, and particle characterization techniques.

Chapter 3 describes water sample sources, chemicals, experimental conditions, and analytical techniques used in **Chapters 4, 5, 6, and 7**; any material and method that are chapter-specific are described within that chapter.

Chapter 4 presents the results and findings from nanoparticle characterization and selection in Milli-Q water using various analytical techniques.

Chapter 5 presents a procedure and findings for the characterization of water samples from Pockwock Lake for naturally occurring nanoparticles.

Chapter 6 presents findings from filtration experiments for the deposition of TiO_2 nanoparticles onto porous media under various water chemistry and simulated conditions.

Chapter 7 presents findings from bench-scale filter experiments for the removal of TiO_2 nanoparticles under operating conditions similar to those practiced at JD Kline Water Supply Plant.

Chapter 8 provides the overall summary of Chapters 1 through 7 presented in this dissertation.

Chapter 9 provides the overall dissertation conclusions and recommended future work beyond the scope of this dissertation that needs to be studied or investigated further.

CHAPTER 2: BACKGROUND

2.1. Particles in Water

Particles in water are a complex mixture of physical, chemical and biological nature, with sizes ranging from 0.001 to 1 μm (Lead and Muirhead 2005). In terms of composition, particles can be silt, clay or natural organic matter, and can have globular, fibrous or irregular shapes (Gregory 2005; Crittenden et al., 2005; Santschi et al., 1998). Particles in water possess unique properties (e.g., large surface area and small size) that enable them to play a profound role in determining the fate and behavior of an entire aquatic system, including particle transport, deposition, and toxicity (Lead and Muirhead 2005).

A substantial number of these particles fall under the category of nanoparticles (i.e. 1-100 nm). Currently there is no uniform internationally recognized definition of nanoparticles, which is something that would be required for regulatory purposes at the international level. The ASTM E2456-06 defines nanoparticles as "a sub-classification of ultrafine particle with lengths in two or three dimensions greater than 0.001 micrometer (1 nanometer) and smaller than about 0.1 micrometer (100 nanometers) and which may or may not exhibit a size-related intensive property". Although uniformity in terminology exists, the ASTM definition is somewhat controversial due to its size range and size-related aspects; the definition emphasizes length rather than size, and the length scale could be a hydrodynamic diameter or a geometric length relevant to the intended use of nanoparticles. Moreover, this definition includes nanoparticles as well as materials that are not quite nanoparticles but have nano-sized features (e.g., DNA) such as surfaces,

topography or structure. Therefore, the 100 nanometer upper cut-off limit for nanoparticles does not seem to be directly linked to the physical phenomenon length.

However, the presence of particles in water is generally not desired, for a number of reasons. Muirhead and Lead (2003) indicated that particles in water can inhibit metal bioavailability due to chemical kinetic and mass transport constraints, and can also affect transport in water due to their propensity to remain unstable under the influence of diffusion and convection processes. As well, they can increase water turbidity and reduce the amount of light passing through the water body. Additionally, Guo and Ma (2006) found that particles can absorb humic acids and trace metals in water due to their high surface area, and can therefore extend their transport. Another problem associated with the particle presence in water is that they can seriously impair the disinfection process by shielding pathogens and preventing the inactivation process (Korich et al., 1990).

Particle interaction is affected by their surface charge and by the chemical functional group attached to them. This interaction is essential because it involves two types of particles in water: hydrophobic and hydrophilic. Hydrophobic particles are less attracted to water, are thermodynamically unstable, and tend to form aggregates over time, whereas hydrophilic particles are water-attracted and can easily bind to their polar ionized surface functional groups. Hydrophilic particulates in water may be metal oxides, proteins, humic or fulvic acids, or biological formations (Crittenden et al., 2005). Another complexity associated with particles is that it is difficult to determine their exact role in water, as they can be polydisperse, polyelectrolytic or polyfunctional. Moreover, it is also

not easy to determine their exact structure, as they are pH and ionic strength-dependent (Santschi et al., 1998).

While surface waters share similar characteristics, significant variations in the quality of water can be found in different sources. Hence, the characterization of each water source for naturally occurring nanoparticles will provide information on their properties and related removal mechanisms. Some studies have been conducted in Europe to investigate the properties of submicron particles in fresh and groundwater sources, using a number of advanced analytical techniques such as atomic force microscopy (AFM), and transmission electron microscopy (TEM) (Lead and Muirhead 2005; Kaegi et al., 2008; Hassellov and Kaegi 2009; Perret et al., 1994; Plaschke et al., 2002). These studies found that three populations of submicron particles with different shapes and morphologies were detected in the studied natural waters. Nevertheless, comparative studies in other regions are required to analyze the properties of these particles elsewhere.

Although submicron particles (< 0.45 μm) are presently not regulated as water contaminants, obtaining information on their occurrence and characteristics in drinking water sources will assist in developing future treatment solutions. Furthermore, identifying natural nanoparticles in drinking water sources will provide valuable information that will assist in developing removal mechanisms, as it is unclear whether the water treatment practices currently available are capable of removing nanoparticles from water (Hahn & O'Melia, 2004; Tufenkji & Elimelech, 2004). It is believed that, due to the complexity of particles in natural water sources and the limitations of analytical

techniques, nanoparticle characteristics need to be investigated. In addition, the identification of nano-scale particles in natural water sources will further our understanding of their behavior and fate during the treatment process.

2.2. The DLVO (Derjaguin-Landau-Verwey-Overbeek) Theory and Particle Stability in Water

The DLVO theory suggests that particle stability in a suspension is a function of the total potential energy, which is the sum of potential energy due to a solvent, attractive forces and repulsive forces (Yiacoumi and Letterman, 2011). The potential energy of a solvent is usually neglected, as it has a very minor effect at separation distances in the nanometer range. Thus, attractive and repulsive forces are the major contributors to total potential energy, as they can act at much larger distances. Therefore, according to the DLVO theory, the stability of a colloidal system is determined by the sum of the attractive (Van der Waals) forces and the electric double layer repulsive forces that exist between particles when they approach each other, as per Brownian motion (Hahn & O'Melia, 2004). The DLVO theory also shows that an energy barrier due to repulsive forces impedes particles from reaching each other and adhering together.

When conditions allow particles to reach each other and collide with sufficient energy, they can easily overcome this barrier, as attraction forces pull them to adhere together. If the repulsion forces between particles are sufficiently strong, the colloidal system is considered to be stable. However, if the repulsion forces are weak or are reduced to a minimum for some reason, then the attractive forces come into play and permit particles

to adhere together. In such a case, the colloidal system eventually becomes destabilized, creating a better environment for flocculation.

Hahn and O'Melia (2004) explained that when two charged surfaces are brought close to each other in a suspension, the attraction between surfaces at small separating distances results in a minimum energy barrier. Moreover, as the attraction between the surfaces continues, a maximum energy barrier at large separating distances is created. However, between the minimum and maximum energy barriers, a secondary minimum is observed. The secondary minimum was attributed to coulombic electrostatic repulsion forces, which decay exponentially with separating distances, whereas Van Der Waals attractive forces decay more slowly and with increased separation distances. In order to achieve a successful deposition of particles onto a porous media surface, the repulsive energy barriers should be overcome to allow for successful transport and subsequent attachment.

During water filtration, both particles and filter media usually possess surface charges; if the charges are opposite, filtration conditions are considered favorable. This is because attractive interactions are expected between particles and media grains. Otherwise, when charges are similar, filtration conditions are regarded as unfavorable due to the expected repulsive interaction with media grains, as similar charges repel each other (Jegatheesan & Vigneswaran, 2005). Nonetheless, filtration usually occurs under unfavorable conditions because filter media such as sand, glass beads and particulates in water are known to have negative surface charges (Crittenden et al., 2005). Often, during filtration, chemicals are added to alter water chemistry and create favorable filtration conditions.

The rate of particle deposition on a collector surface with regards to its rate of collision with that collector surface is regarded as the collision attachment efficiency, α. The attachment efficiency is found to be a function of the attractive Van Der Waals forces, electrical double layer interaction, steric interactions, and particle hydrophobicity (Lecoanet et al., 2004). The collision attachment efficiency has a value of unity when there are favorable conditions and a zero when there are unfavorable conditions (Crittenden et al., 2005). Particle transport and attachment are expressed as attachment efficiency (η_r) and collector efficiency (η_o). According to Cleasby and Logsdon (1999), if the particles are not adequately destabilized, the removal efficiency of the collector will be less than η_o. Therefore, the attachment efficiency can be used to evaluate filter performance, as the value of unity of α would indicate that repulsive forces are eliminated and favorable conditions have been created during the filtration process.

Researchers suggest that the DLVO theory comes up short in explaining particle interactions and colloid formation in dilute dispersion systems under low ionic strengths and particle attachment under unfavorable conditions, as the theory considers particle attachment to be a function of particle size and ionic strength in a suspension, which is not supported by experimental results (Lecoanet et al., 2004; Hahn & O'Melia, 2004). In addition, Lecoanet and co-workers argued that models describing attachment efficiency based on the balance between electrostatic and Van der Waals forces looked at changes over separation distances of many nanometers.

To overcome the shortcomings of the DLVO theory, Lecoanet et al. (2004) examined the attachment efficiency as an empirical parameter that captures all particle aspects related to deposition, a perspective that has not yet been described by the most extensively validated particle transport models. Based on Yao et al. (1971), the collision attachment efficiency, α, can be calculated using experimental data collected from filtration experiments.

2.3. Filtration Treatment

Filtration is an essential process in most water treatment plants with the final goal to remove particles and to protect public health from pathogens. Since the early 1960s, filtration has been extensively studied and a considerable body of knowledge has been developed around the mechanisms of particle removal within a filter (Amirtharajah, 1988; O'Melia & Stumm, 1967; Rajagopalan & Tien, 1976; Kawamura, 1975; Tien & Payatake, 1979; Tobiason & O'Melia 1988; Mahmood et al., 2000; Kim & Tobiason, 2004; Yao et al., 1971). At their core, filtration mechanisms involve particle destabilization, transport, attachment and detachment processes, and can be explained by two distinctive models: phenomenological (macroscopic) and fundamental (microscopic). While both models attempt to predict particle removal within a filter, only the fundamental models consider the mechanism of particle transport and attachment (Cleasby & Logsdon, 1999).

The removal of particles within a filter involves at least two separate steps. Suspended particles are transported and brought into close contact with the filter media, after which they attach to the media surface (Yao et al., 1971). Filtration transport models for water

treatment were derived from models developed for air filtration (Yao et al., 1971). The attachment mechanism may involve either electrostatic interactions, such as the Van Der Waals forces, or surface chemical interactions. Design and operation of an effective filtration process requires a thorough understanding of the physical and chemical characteristics of both the media and the water source (Crittenden et al., 2005; O'Melia & Stumm, 1967). Media characteristics include grain size, shape, density and bed depth. Granular media, such as sand, anthracite and granular-activated carbon, are used as particle removal media. Water source characteristics include turbidity, particulate matter concentration, pH, temperature, and natural organic matter characteristics. Operation conditions that can significantly affect filter performance are filtration rate, filter run time, and backwashing sequence.

Transport mechanisms are also described as diffusion, sedimentation, interception, and inertia. It is generally accepted that under the conditions of water filtration, the dominant mechanisms are diffusion and sedimentation (Amirtharajah, 1988). Diffusion is the transport resulting from random Brownian motion or random collision of particles by molecules of water. These models predict that suspended particles larger than 1μm in size are transported to the filter media by sedimentation and interception. Smaller particles are again effectively transported by Brownian diffusion (Yao et al., 1971). The mechanism of sedimentation is due to the force of gravity and the associated settling velocity of the particles, which causes them to cross streamlines and reach the collector (medium grain). For this mechanism, temperature and particle density play important roles (Amirtharajah, 1988).

Interception occurs when particle motion along a streamline is close enough to the collector for attachment to occur. In earlier studies of filtration, interception was considered a distinctive transport mechanism, but in more recent research it has been incorporated as a boundary condition for attachment resulting from diffusion and sedimentation (Amirtharajah, 1988). Each transport mechanism is expressed in terms of theoretical single collector efficiency, η, which is the ratio of the number of successful collisions to the total number of potential collisions in the projected cross-sectional area of the collector and it is dimenssionless. The overall collector efficiency is the sum of the three individual collector efficiencies due to interception, inertia, and diffusion ($\eta_o = \eta_D + \eta_I + \eta_G$).

If the particles are not adequately destabilized, the removal efficiency of the collector will be less than η_o. It is found that to improve filtrate quality, a value of collision efficiency, α should be equal to 1, which eliminates repulsive forces. Empirical collision attachment efficiency, α, is applied to account for this, so that the actual single removal efficiency is calculated as:

$$\eta = \alpha\eta_o \qquad (2.1)$$

The trajectory analysis has been developed for the analysis of particles not significantly affected by Brownian motion. The rigorous use of trajectory analysis to predict particle capturing requires correction for hydrodynamic interaction as the particles approach a grain surface (Cleasby & Logsdon, 1999). These interactions significantly slow the rate of deposition of particles. Based on the results of trajectory analysis, an approximation for η_o is given by Equation (2.2), as follows (Crittenden et al., 2005):

$$\eta_o = \ 4.0{A_s}^{1/3}\left(\frac{D_\infty}{V d_c}\right) + A_s {N_{LO}}^{1/8} R^{15/8} + (3.38 \times 10E-3) A_s {N_G}^{1.2} R^{-0.4} \quad (2.2)$$

where A_s is a dimensionless porosity function to account for the effect of neighboring collectors in the flow field around a single collector, D_∞ is the bulk particle diffusion coefficient, N_{LO} is the dimensionless Van Der Waals number or London group number, R is a dimensionless ratio of particle to collector size = d_p/d_c or the relative-size group number, N_G is a dimensionless gravitational force number, d_c is collector diameter in mm, d_p is particle diameter in mm, and V is velocity in m/s. The single collector efficiency can then be related to the removal efficiency of a clean bed of uniform spheres with the following equation by Yao et al. (1971):

$$ln\left(\frac{C}{C_o}\right) = -\frac{3}{2}\frac{(1-\mathcal{E})\alpha\eta_o L}{d_c} \quad (2.3)$$

Where C is the effluent particle concentration in mg/L, C_o is the influent particle concentration in mg/L, α is the empirical collision attachment efficiency dimensionless, L is the filter bed depth in m, η_o is the overall collector efficiency dimensionless, ε is the porosity in %, and d_c is the collector diameter in mm. Crittenden et al. (2005) suggested the following equations for calculating the removal efficiency of the filter:

$$\eta_\circ = 4{A_s}^{1/3} Pe^{-2/3} + A_s {N_{LO}}^{1/8} {N_R}^{15/8} + 3.88 \times 10^{-3} A_s {N_G}^{1.2} {N_R}^{-0.4} \quad (2.4)$$

$$A_s = \frac{2(1-\gamma^5)}{2-3\gamma+3\gamma^5-2\gamma^6} \quad (2.5)$$

$$N_{LO} = \frac{4Ha}{9\pi\mu {d_p}^2 \nu} \quad (2.6)$$

$$N_R = \frac{d_p}{d_c} \quad (2.7)$$

$$N_G = \frac{V_s}{V_F} = \frac{(\rho_s-\rho_w) g {d_p}^2}{18\mu V_F} \quad (2.8)$$

$$Pe = \frac{3\pi\mu d_p d_c \nu}{k_B T} \quad (2.9)$$

$$\lambda = \frac{-3(1-\varepsilon)\alpha\eta}{2d_c} \quad (2.10)$$

Where A_s is the porosity function dimensionless, N_{LO} is as described earlier, N_R is as described earlier, γ is the porosity function dimensionless, *Ha* is the Hamaker constant J, V_s is the Stokes settling velocity (m/s), V_F is the superficial velocity above the bed (m/s), *Pe* is the Peclet number (dimensionless), *kB* is the Boltzmann constant which equals to 1.381E -23 J/K, *T* is the absolute temperature in Kelvin, μ is the water viscosity in kg/m.s, and λ is the filter coefficient in m^{-1}.

2.4. Direct Filtration

Direct filtration is a surface water treatment process that includes coagulation through rapid mixing, and flocculation followed by filtration (Cleasby & Logsdon, 1999). Direct filtration is suitable for the treatment of source waters characterized by low turbidity of less than 10 NTU, such as river and reservoir waters. After being coagulated, the water undergoes flocculation by means of slow mixing and then passes through media filters to remove pinpoint flocs formed during the flocculation process. In terms of media, direct filtration can be achieved using mono, dual, or tri-media. In practice, dual-media filters are more common and are traditionally designed as 0.45 – 0.6 m of anthracite over 0.23 – 0.3 m of sand. The combination of granular activated carbon and sand is also commonly encountered in practice. Dual media are found to be more robust than monomedia filters (Crittenden et al., 2005).

The first direct filtration plant was built in the United States in 1884, but the rapid clogging of the filters limited its feasibility (Petrusevski, 1996). Nearly a century later,

the first Canadian direct filtration plant was built in Toronto, Ontario, in 1964, followed by additional facilities in that province; including the F.J. Horgan water treatment plant. Thirteen years later, in 1977, the J.D. Kline Water Supply Plant was built in Halifax, Nova Scotia. Today, direct filtration is practiced worldwide, and is particularly popular in the United States.

The use of direct filtration is favored because it has several advantages over conventional filtration treatment, including lower capital costs due to low sludge production and the omission of a sedimentation facility. Moreover, as it requires lower coagulation dosages to generate a filterable pinpoint floc, it has lower operation and maintenance costs (Cleasby & Logsdon, 1999). However, direct filtration has some drawbacks in that it is limited to the treatment of source waters of low turbidity only (< 10 NTU). It is challenging to maintain an effective filtration treatment, especially when the concentration of dissolved natural organic matter is high in the source water, as it requires high coagulant dosages. Excessive coagulant dosages increase floc formation, overload the filter, and hasten its clogging, leading to swift head loss development, which consequently shortens the filter run time. Additionally, when particle content in the water is very low, charge neutralization is ineffective due to the lack of contact opportunities between destabilized particles.

2.5. Characterization Techniques

Nanoparticle characterization is achieved through a number of techniques drawn primarily from materials science. Some of the techniques used in this research include scanning electron microscopy (SEM), transmission electron microscopy (TEM),

ultrasonic/acoustic attenuation spectroscopy (U/AAS), Brunauer Emmett Teller (BET) surface area, dynamic light scattering (DLS), zeta potential, atomic force microscopy (AFM), micro flow imaging (MFI), and inductively coupled plasma mass spectrometry (ICP-MS).

SEM is a characterization technique that uses an electron beam in a vacuum to generate an image of the specimen and provide information about its surface properties. SEM creates various high-resolution images by focusing a high-energy beam of electrons onto a sample surface. SEM images are useful for understanding the morphology, shape, surface structure and elemental composition of a sample (Zhang et al., 2009).

TEM is a microscopy technique where a beam of electrons is transmitted through a specimen and passes through a series of lenses (Sellers, 2009). It determines the image resolution and obtains a magnified image using an image processing system such as a computer or a camera (Zhang et al., 2009). A typical TEM system is comprised of an electron source, a high voltage generator, a sample chamber, a series of electromagnetic lenses, and a data acquisition and analysis system (Jing et al., 2005). Rose et al. (2007) indicated that the potential drawback of SEM and TEM is that, in some cases, particle shape induces indirect modification of the spectroscopic signal, which then becomes a source of error in the measurement.

U/AAS is a method for fluid and dispersed particles characterization. U/AAS measures acoustic attenuation versus frequency of sound of colloidal dispersions and is mainly applied to determine the zeta potential of particles and particle size distribution (PSD).

The zeta potential and PSD of nanoparticles were measured using Zeta-APS, which uses an electroacoustic technique called electrokinetic sonic amplitude (ESA) to measure the zeta potential of a suspension. A zeta sensor applies short high-frequency pulses to a sample located within the electrode region of the zeta sensor. These pulses last about 30 micro-seconds at a frequency range of 0.5 – 3.5 MHz and with amplitudes of 100 – 600 volts. Sample particles move back and forth due to their surface electric charge, which produces an output sound wave of the same frequency as the applied sound wave, provided that there is a particle/solvent density difference of at least 2% (Zeta-APS Operation Manual, 2004).

BET measures the specific surface area through the physical adsorption of nitrogen gas molecules on a sample surface under specific measurement conditions. The sample is prepared through heating, degasification with nitrogen gas, and exposure to a mixture of nitrogen-helium gas. The BET surface area is calculated from the amount of nitrogen gas adsorbed by the sample (Zhang et al., 2009).

DLS, also known as correlation spectroscopy or quasi-elastic light, is a technique for particle size analysis. DLS measures fluctuations in light-scattering intensity induced by particles in the sample at short time intervals, and uses special software to process the data in an autocorrelation function. The autocorrelation function encompasses all information related to the particle diffusion coefficient (D). A correlation exists between the particle diffusion coefficient and the decay time of the autocorrelation function, from which the hydrodynamic diameter of the particle is calculated using Stoke's Einstein

relationship for diffusion – Zetasizer Nano Series User Manual (Instruments 2007), which is:

$$D = \frac{\mathrm{kBT}}{f} = \frac{\mathrm{kBT}}{6\pi\eta \mathrm{R_H}} \quad (2.1)$$

$$f = 6\pi\eta \mathrm{R_H} \quad (2.2)$$

Where kB, T, f, η, and R_H are the Boltzmann constant, absolute temperature, particle friction coefficient, water viscosity, and particle hydrodynamic diameter, respectively. The hydrodynamic diameter of a particle is actually the diameter of a hypothetical sphere that has the same diffusivity as the particle being measured. The analytical applications of DLS for particle size measurements have been comprehensively discussed by Filella et al. (1997).

The average particle size produced by DLS could be presented as an intensity, volume, or number distribution. However, the reported average particle size is always an intensity mean size (also called a cumulant mean). The size distribution describes the frequency of encountering a certain particle size within the analyzed sample volume. Thus, number distribution shows the number of particles in the sample, volume distribution shows particle volume, and intensity distribution shows the magnitude of the light scattered by particles in the sample. In other words, intensity distribution puts more emphasis on the presence of large particles, while number distribution emphasizes the presence of smaller particles. However, both number and intensity distributions describe the same particle aspect, though in different ways.

AFM is a microscopic technique that gives a 3D image of a sample. In AFM, a small cantilever (usually 200 μm long and made of silicon or silicon nitride) with a sharp tip or probe is scanned over a sample surface (Zhang et al., 2009). To map the topography of a surface, the tip is brought into gentle contact with the sample surface (this is called contact mode imaging) and is then scanned in a raster fashion over the surface. Topographic features cause cantilever deflections, which are recorded by measuring the deflection of a laser beam focused on the end of the cantilever. The deflected laser beam falls on a split photo detector and the voltage difference from the two photo detectors is a measure of the size of the cantilever deflection and hence the size of the imaged object. Tip position and cantilever deflections are recorded by a computer that processes the data into an image of the sample topography. The entire sample surface is scanned, and its topography can be viewed with sub-nanometer precision.

MFI is described by Sharma et al. (2010) as a flow microscopy technology, where bright field images are captured in successive frames as a continuous sample stream passes through a flow cell centered in the field-of-view of a custom magnification system having a well characterized and extended depth-of-field. The extended depth-of-field is defined as the distance over which an object remains in focus for a given magnification or lens setting. The MFI uses two flow cell depths of 100 and 400 μm, with magnifications of 13.86x and 4.88x, respectively (MFI^{TM} threshold, sensitivity and depth-of-field overview - www.brightwelltech.com). The MFI system consists of five components: a light source, a sample cell or detection zone, an optical system with digital camera, a peristaltic pump, and a computer system equipped with special software for data processing and analysis.

MFI uses digital imaging of a flowing sample stream to measure the size, shape and concentration of the flowing particles in the sample.

ICP-MS is a mass spectrometry technique for the measurement of trace metal and non-metal element concentrations. It consists of several integrated components, such as a sample injection system, inductively coupled plasma, plasma sampling interface, mass analyzer, detector and computer. ICP-MS combines a high temperature ICP source with MS, which means that the ICP converts all of the element's atoms to ions. These ions are then detected by the MS as a mass concentration of the given element. ICP-MS has the following advantages: high detection limits for most of the elements; the ability to handle both simple and complex matrices with less interference due to the high temperature of the ICP; the ability to detect numerous elements in one sample at the same time; and the ability to provide isotopic information of elements (Wolf, 2005).

Therefore, it is believed that examining nanoparticle characteristics using the above mentioned techniques will assist understanding their properties in water and provide invaluable information that can help developing appropriate future treatment solutions.

CHAPTER 3: MATERIALS AND METHODS

This chapter describes the water samples that were used and the experimental conditions that were common for most of the experiments in this dissertation. Material and method that are chapter-specific will be described within the respective chapters.

3.1. Water Samples

3.1.1. Pockwock Lake

Water samples used to conduct some of the experiments were collected from Pockwock Lake and from the pumping station at the J.D. Kline Water Supply Plant. Pockwock Lake is a protected watershed located in Hants County, Nova Scotia, Canada. The lake occupies an area of approximately 5660 hectares and is the main drinking water source for the city of Halifax and the surrounding counties. Pockwock water is known for its low water quality parameters: a pH of around 5.5, an alkalinity of less than 5 mg/L as $CaCO_3$, and a turbidity of less than 0.5 NTU. Pockwock water also has moderate to higher color and natural organic matter content. The microbiological growth in the lake is extremely low and *Cryptosporidium* or *Giardia* have never been detected there (O'Leary et al., 2003).

Table 3.1 presents the measured water quality parameters of Pockwock Lake water in this research. It is seen from this table that Pockwock water has low turbidity (0.4 NTU), low pH (5.4), and moderate organic matter content (expressed as TOC and DOC; 2.6 and 2.4 mg/L, respectively). The treatment of this type of water is challenging, as it requires maintaining an optimal chemical dosage (e.g., coagulants, disinfectants) in such a way

that it does not enhance the disinfection by-product formation or compromise the removal of natural organic matter. Similar water quality parameters are encountered in many regions in Atlantic Canada.

Table 3.1: The Measured Water Quality Parameters of Pockwock Lake Water in This Research.

Parameter	pH	Turbidity	Alkalinity	TOC	DOC	Fe	Mg
Measured value	5.4	0.4 NTU	4 mg/L	2.6 mg/L	2.4 mg/L	< MDL*	0.51 mg/L

*Method Detection Limit.

3.1.2. JD Kline Water Supply Plant

Water from Pockwock Lake is treated at the J.D. Kline Water Supply Plant, a direct filtration facility built in 1977 with a design capacity of 220,000 m^3/d and currently operates at 90,000 m^3/d (Halifax Regional Municipality website – accessed on February 13, 2012). Figure 3.1 describes the plant process flow diagram. The water is treated at the plant through coagulation with 8 mg/L dose of alum and hydraulic flocculation, followed by direct filtration and chlorine disinfection.

The plant treatment process description is as follows. The raw water is pre-screened to remove large impurities and then pumped through six vertical turbine pumps to the treatment facility, where chemicals are added for: iron and manganese oxidation, pH adjustment, and optimum coagulation condition. During the cold weather months (November to June), a cationic polymer is added to strengthen floc formation. Chlorine is also added to control any biological activity that might occur in the filters and for disinfection throughout the distribution system. Finally polyphosphate is dosed for

corrosion inhibition, and fluoride is added for dental care. The finished water then flows by gravity into the distribution system to satisfy the needs of Halifax residents. Oxidized water from the plant was used to perform the jar testing and filtration experiments in this research.

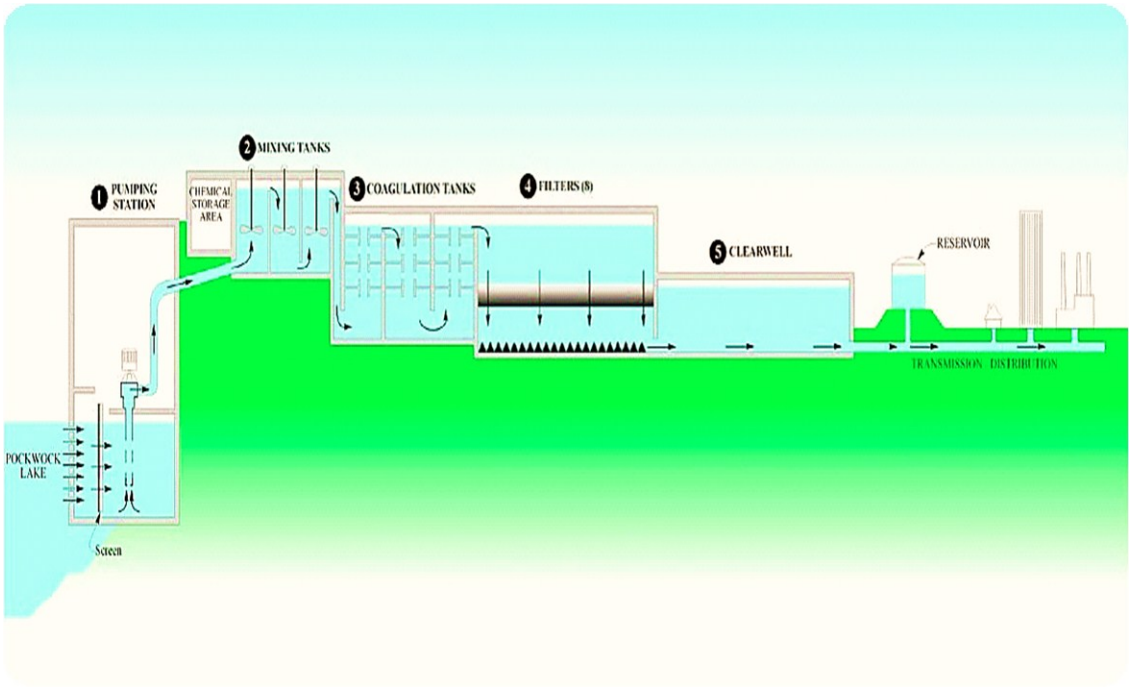

Figure 3.1: Process Flow Diagram of the J.D. Kline Water Supply Plant, Halifax, Nova Scotia, Canada (taken from - www.halifax.ca/hrwc/documents/WaterReport200506.pdf).

3.2. Experimental Conditions

3.2.1. Nanoparticles Preparation

Four types of commercially available synthetic nanoparticles were selected to conduct the characterization experiments in this research: cerium dioxide oxide (CeO_2), with a particle size of < 20 nm and a refractive index of 2; ferric oxide (Fe_2O_3), with a particle size of between 20 and 25 nm and a refractive index of 2.9; silicon dioxide (SiO_2), with a particle size of 5 to 10 nm and a refractive index of 1.5; and titanium dioxide (TiO_2), with

a particle size of 5 to 10 nm and a refractive index of 2.5. These nanoparticles were purchased from Sigma Aldrich and received in their powder forms (with the exception of cerium oxide, which was received as 5 wt% stock solution). The selection of these nanoparticles was based on their extensive applications in many consumer based products (Sellers et al., 2009). Solutions of 10 mg/L and 5 mg/L were prepared from the powders and the cerium stock solution, respectively, and used for nanoparticle characterization.

3.2.2. Glassware

All laboratory experiments were treated according to the procedure described in the Standard Methods for the Examination of Water and Wastewater (Franson 1995). To avoid contamination, glassware used for sample collection and preservation was detergent dish-washed, soaked in a 10% nitric acid (HNO_3) solution for 24 hours, rinsed several times in Milli-Q water, dried, covered with parafilm plastic (Pechiney Plastic Packing, Chicago, IL), and stored in a dry and dust-free place prior to use.

3.2.3. Chemicals and Milli-Q Water

All chemicals and reagents used to conduct the experiments were of a high analytical grade and were prepared according to procedures described in the Standard Methods for the Examination of Water and Wastewater (Franson 1995). High quality Milli-Q water produced by Millipore SAS 67120, Molsheim, France, was used for all experimental purposes, such as dilution, solution preparation, etc.

3.2.4. Statistical Analysis

Quality control/assurance (QC/QA) practices have been incorporated into all stages of this research, including experiment planning, data analyzing, and results interpretation. All experiments were conducted in duplicate or triplicate, to allow for reproducibility and verification of the results. QC/QA practices were considered in all laboratory analyses; method blanks were analyzed to ensure the cleanliness of the equipment and of the Milli-Q water, and to ensure that there were no particle background concentrations that might skew the results during the analysis and characterization. A brief description of the analytical techniques common to all experiments is given below. However, each chapter will include a section to discuss relevant technique, where appropriate.

3.3. Analytical Techniques

Several analytical techniques were used during the course of this research to characterize nanoparticles in water and to explore the properties that determine their behavior and fate in water. Analytical techniques include scanning electron microscopy (SEM), transmission electron microscopy (TEM), Brunauer Emmett Teller surface area (BET), zeta potential, dynamic and doppler electrophoretic light scattering (DLS & DEL), micro flow imaging (MFI), atomic force microscopy (AFM), and ultrasonic acoustic attenuation spectroscopy (U/AAS). A brief description of how these techniques were utilized is given below.

3.3.1. SEM

To obtain SEM images, a small amount of each type of the nanoparticle powder was mixed with acetone / Milli-Q water, and a flat circular 1-inch aluminum stub was

polished and heated at 50 ºC for about a minute. While the stub was still hot, a droplet of the acetone-mixed nanoparticles was placed and spread on its surface, where the acetone evaporated and the nanoparticles were firmly pasted into the stub. The stub was then mounted on the multiport sample holder at a suitable height (an exception was made for cerium oxide, as a drop of it was air dried on the stub and then imaged in the same way as the other nanoparticles). Finally, the samples were inserted in the sample chamber and the images were captured using the HITACH S-4700 at the Minerals Engineering Centre, Dalhousie University.

3.3.2. TEM

Sample preparation for TEM imaging is crucial, as the quality of the image is governed not only by the acceleration voltage of electrons but also by the sample nature and structure. The TEM images of the four nanoparticles were generated using the FEI Tecnai-12, Japan, with a MegaView II camera and AnalySIS software (Scientific Imaging Suite, the Life Science Building at Dalhousie University). A 10 mg/L solution of TiO_2, SiO_2, Fe_2O_3, and a 5 w% solution of CeO_2 was prepared and sonicated for about a minute before a droplet of it was placed on a 200-mesh gold grid of carbon film (Electron Microscopy Sciences, Hatfield, PA, USA). The 200-mesh grid was set on tissue paper and allowed to dry before being placed in a special holder and loaded under a vacuum in the FEI Tecnai-12 for image capturing.

3.3.3. BET Surface Area

The nanoparticle surface areas were determined using a FlowSorb II2300 nitrogen gas adsorption surface area analysis (Micromeritics, the Material Engineering Lab at

Dalhousie University). In this research, the BET surface area was measured by placing 2 to 3 grams of their powers into sample bottles and heating them at 150 °C for 2 hours to remove any gases that might be absorbed by the sample. The cerium surface area was not measured but taken directly from the literature (Limbach et al., 2008.) After the degasification process, the sample bottles were immersed in a liquid nitrogen bath, after which the bottles were exposed to a mixture of nitrogen-helium gas under ambient pressure. As the sample surfaces absorbed a certain amount of nitrogen gas, the surface area of the sample was determined by recording the nitrogen content in the sample bottles before and after absorption.

3.3.4. Zeta Potential

The electric surface potential of nanoparticles was measured using a Zeta-Meter System 4.0 (GENEQinc., Montreal, Canada), following the procedure described by Zhang et al. (2008). The ionic strength of the samples was altered by the addition of 0.1M $NaNO_3$, and the pH was adjusted either by 0.1N HCl or 0.2N NaOH. The nanoparticles' zero point of charge (pH_{zpc}) was determined through the titration technique by varying the pH of the water sample.

3.3.5. DLS & DEL

The average particle size and size distribution of nanoparticles were determined through DLS, using a Zetasizer Nano Series from Malvern Instruments Ltd., UK. The Zetasizer is equipped with a 633 nm wavelength of green laser and was operated at a non-invasive back scattering angle of 173°. Water was used as a dispersion medium, with a refractive index of 1.33 and a viscosity of 0.8872 cP at 25°C. The average particle size of the

nanoparticles was measured while 5µg/L was being added to 50 mL of the Mill-Q water. A 1.3 mL portion of this sample was filled in a cuvette, which was then capped, cleaned from the outside, and loaded in the Zetasizer cell for the size measurement.

The zeta potential of nanoparticles is obtained through the measurement of their electrophoretic mobility by using doppler electrophoretic light scattering (DEL) and then applying Henry's equation to calculate the zeta potential via electrophoretic mobility. Electrophoretic mobility is determined by conducting an electrophoresis experiment on the sample and measuring the velocity of the particles using laser doppler velocimetry. Approximately 0.75 mL of the sample is filled in a folded capillary cell using a syringe, after which the cell is checked for air bubbles and then loaded into the Zetasizer for a zeta potential measurement (the detailed procedure for sample preparation and measurement for both particle size and zeta potential are described in the Zetasizer User Manual).

3.3.6. MFI

The number concentration, size, and shape of nanoparticles were determined through MFI – Model DP A4100 from BrightWell Technologies Inc., Montreal, Canada. As a sample is drawn through the flow cell using a peristaltic pump, and as the sample passes through the flow cell, particles are imaged in a real time. The displayed images give visual feedback on the nature of the particles in terms of morphological characteristics. Particle characteristics can be displayed as intensity, equivalent circular diameter, ferret's diameter, area, perimeter and circularity. It takes 5 minutes for the MFI to process a sample and provide size and shape statistics on hundreds of thousands of particles in an actual sample volume of less than 0.75 mL.

3.3.7. ICP-MS

ICP-MS works as a stream Ar gas, liquid or solid samples are introduced from sample injection systems into hot plasma, which serves as an efficient source of positively charged analyte ions. The Ar plasma is generated and maintained at the end of the glass torch located inside the loops of a water-cooled copper load coil. A radio frequency (RF) potential applied to the coil produces an electromagnetic field in the part of the torch located within its loops. A short electrical discharge from a wire inside the torch provides the electrons to ignite the plasma. In the electromagnetic field of the load coil, these electrons are accelerated and collide with Ar atoms in the Ar gas flowing through the torch, producing Ar^+ ions and free electrons. Further collisions cause an increasing number of Ar atoms to be ionized and result in the formation of plasma. The plasma-forming process rapidly becomes self-sustaining and may be maintained as long as Ar gas continues to flow through the torch (www.gso.uri.edu/icpms/how_does.htm, accessed in February 2012).

3.4. Jar Test and Filtration Experiments

Oxidized water from the JD Kline Water Supply Plant was used to conduct the jar test and filtration experiments. Prior to its use and in order to create ideal coagulation conditions, the pH of the oxidized water was adjusted to 5.5 using 0.1 N HCl. TiO_2 nanoparticles were added at a concentration of 5µg/L (turbidity of 4.2 NTU) in the oxidized water. The water was then jar-tested following the same sequence practiced at the JD Kline Water Supply Plant. Rapid mixing for a minute at 142 rpm (i.e. velocity gradient or G = 100 s^{-1}) was followed by 3 rounds of slow mixing for 12.5 min each, at 37rpm (i.e. velocity gradient or G = 30s^{-1}), 26 rpm (i.e. velocity gradient or G = 20s^{-1}),

and 17rpm (i.e. $G = 10s^{-1}$), respectively. Next, the coagulated/flocculated water was run through the laboratory filter columns to mimic direct filtration treatment. Filtration experiments were carried out using Plexiglas columns with an inside diameter of 25 mm and a length of 220 mm. The Plexiglas columns were filled with a 100 mm bed of anthracite (effective size or d_{10} 0.8 mm and a uniformity coefficient of 1.76), over a 50 mm bed of Ottawa sand (effective size or d_{10} of 0.5 mm and a uniformity coefficient of 1.53). The columns were run at a filtration rate of 0.167 cm/s. Samples were collected and analyzed for turbidity (using the HACH 2100 spectrophotometer) and for TiO_2 concentration in the finished water using the ICP-MS.

CHAPTER 4: CHARACTERIZATION OF NANOPARTICLES IN MILLI-Q WATER

4.1. Abstract

The objective of this study was to characterize and select appropriate synthetic nanoparticles that can further be used as surrogate for evaluating particle removal in low turbidity water. Characteristics of four synthetic nanoparticles cerium dioxide (CeO_2), ferric oxide (Fe_2O_3), silicon dioxide (SiO_2) and titanium dioxide (TiO_2) were investigated in Milli-Q water for particle size, surface area, and surface potential using different characterization techniques. The effect of ionic strength and pH on these nanoparticles at 10 and 20 mmol sodium chloride and pH of 4 and 10 were also investigated. The analytical techniques used in this investigation were scanning electron microscopy (SEM), transmission electron microscopy (TEM), dynamic light scattering (DLS), Brunauer-Emmet-Teller (BET) surface area, and zeta potential. SEM images showed that synthetic nanoparticles possessed different shapes and morphological structures, such as irregular, spherical, cotton-like, and elliptical shapes for CeO_2, Fe_2O_3, SiO_2, and TiO_2, respectively. TEM images, however, showed that all these nanoparticles form aggregates in water with particle sizes far larger than the initial size reported to them by the vendors. The average particle sizes measured for these nanoparticles by dynamic light scattering (DLS) were 163, 370, 1554, and 2169 nm for CeO_2, Fe_2O_3, SiO_2, and TiO_2 respectively, with particle sizes measured by the three techniques correlating well with each other. Brunauer-Emmet-Teller (BET) surface areas of 445.9 m^2/g, 120.1 m^2/g, and 35.7 m^2/g were measured for SiO_2, Fe_2O_3, and TiO_2 respectively, whereas the BET surface area of CeO_2 was taken from literature. Zeta potential of 22.5, 16, -20.8, and -23.8 mV and zero point of charge of 8.2, 7.5, 1.8 and 5.4 were measured for CeO_2, Fe_2O_3, SiO_2, and TiO_2, respectively. It was found that increasing solution ionic strength at a pH of 4 decreased the zeta potential for TiO_2 and Fe_2O_3 and increased it for CeO_2, whereas the zeta potential of SiO_2 changed slightly. Increasing the ionic strength from 10 to 20 mmol NaCl increased the zeta potential of the four investigated nanoparticles. The average particle size of the studied nanoparticles appeared to be pH and ionic strength dependent. The obtained characteristics of nanoparticles in this study correlate well with those reported for similar nanoparticles in the pertinent literature. Based on the characterization results, TiO_2 nanoparticles were selected to perform all filtration experiments throughout the remainder of the research.

4.2. Introduction

Today, nanoparticles are found in many applications of modern human life; food industry, cosmetics, medicine, pharmaceuticals, electronics, and environmental remediation (Abdallah & Gagnon, 2009; French et al., 2009; Hassellov et al., 2008; Nowack & Bucheli, 2007). Currently, nanoparticles are not regulated as water contaminants, and thus it is unclear whether the existing treatment practices are capable of removing them from drinking water. However, obtaining in-depth information on their characteristics in drinking water sources will provide a valuable resource that can assist in creating alternative treatment solutions.

Nanoparticle characterization in terms of physicochemical properties that dictate their behavior and fate during water treatment is somewhat lacking in the literature, especially for low turbidity waters such as those in Nova Scotia. Due to their small size and large surface area, nanoparticles in water are expected to exhibit a high reactivity. Some research related to nanoparticle characterization in water has already been done (Zhang et al., 2008; Hassellov et al., 2008; Kaegi et al., 2008; Domingos et al. 2009; Lead et al., 1997; Nurmi et al., 2005; and Limbach et al., 2008). But most of this research focused on characterization at high concentrations, and no research has tested the removal of nanoparticles in low turbidity water, which makes this study unique. For example, Zhang et al. (2008) studied the stability of commercial metal oxide nanoparticles in water, finding that the fate of the studied nanoparticles depended on their surface charge, size, and interaction with other substances present in the water. Additionally, Wigginton et al. (2007) reported that when seawater was mixed with river water, inorganic nanoparticles

were removed from the sample due to salt-induced aggregation; thus, changing ionic strength can drastically alter nanoparticles stability in water.

It is believed that a thorough characterization of nanoparticles in water will lead to a better understanding of their characteristics and enhance the development of future treatment strategies. The objective of this study was to characterize and select the appropriate type of synthetic nanoparticle that can be further used as surrogate for particle removal in low turbidity water. Thus, characterizing these nanoparticles in water and to investigating the effect of pH and solution ionic strength on them, will assist determining which one among them can be used as the potential surrogate for particle removal from low turbidity water going forward in this research.

4.3. Materials and Methods

4.3.1. Nanoparticles

Cerium dioxide (CeO_2), ferric oxide (Fe_2O_3), silicon dioxide (SiO_2), and titanium dioxide (TiO_2), nanoparticles were purchased from Sigma Aldrich and received in powder forms (with the exception of cerium oxide, which was received as 5 wt% stock solution). Solutions of 10 mg/L and 5 mg/L were prepared from the powders and the cerium stock solution, respectively, and used for characterization purposes. For pH and ionic strength investigations, water samples spiked with nanoparticles were prepared in 10 and 20 mmol NaCl ionic strength solutions and with pH values of 4 and 10 to ensure that zeta potential measurements were performed under constant conductivity for each pH.

4.3.2. Water Source

The water used in the characterization experiments was Milli-Q water produced by Millipore SAS 67120, Molsheim, France. All chemicals and reagents used were of a high analytical grade and were prepared according to the procedures described in the Standard Methods for the Examination of Water and Wastewater (Franson 1995). All glassware used for sample collection and preservation was detergent dish-washed, soaked in a 10% nitric acid (HNO_3) solution for 24 hours, rinsed several times with Milli-Q water, dried, covered with parafilm plastic (Pechiney Plastic Packing, Chicago, IL), and stored in a dry and dust-free place prior to use. All experiments were performed in laboratories at Dalhousie University.

4.3.3. Characterization Techniques

Several characterization techniques were used during the course of this study to characterize nanoparticles and to explore the properties that determine their behavior and fate in water. Those techniques include scanning electron microscopy (SEM), transmission electron microscopy (TEM), Brunauer Emmett Teller surface area (BET), zeta potential, dynamic light scattering (DLS). Additional details about these techniques can be found in Zhang et al. (2009).

The sample preparation for SEM consisted of mixing a small amount of each nanoparticle powder in acetone. Next, a flat circular 1-inch aluminum stub was polished and heated at 50 ºC for approximately one minute. While it was still hot, a droplet of the acetone-mixed nanoparticle was placed and spread on the stub surface. The acetone evaporated and the nanoparticles were firmly fixed onto the stub surface. The aluminum

stub was then mounted on a multiport sample holder at a suitable height (except for cerium oxide, as a drop of it was air-dried on the stub and then imaged in the same way as the other nanoparticles). Finally, the samples were inserted into the sample chamber, where nanoparticles images were generated using the HITACH S-4700 (Japan) at the Mineral Engineering Lab, Dalhousie University.

The TEM images were obtained using the FEI Tecnai-12 with a MegaView II camera and AnalySIS software (Japan) at the Life Sciences Lab, Dalhousie University. A 10 mg/L solution of TiO_2, SiO_2, Fe_2O_3 and a 5 w% solution of CeO_2 was prepared and sonicated for one minute before a droplet of each was placed on a 200-mesh gold grid of holy carbon film (Electron Microscopy Sciences, Hatfield, PA, USA). The 200-mesh grid was set on tissue paper and allowed to dry before being placed in a special holder and loaded under a vacuum in the FEI Tecnai-12 for image capturing.

The nanoparticle surface area was measured using N_2- absorption methods (Micromeritics FlowSorb II2300, Physics Department, Dalhousie University). The cerium dioxide surface area was not measured but taken from literature (Limbach et al., 2008). Two to three grams of the nanoparticle powders were placed into sample bottles and heated at 150 °C for two hours to remove any gases that might be absorbed by the sample. Following the degasification process, sample bottles were immersed in a liquid nitrogen bath, after which the bottles were exposed to a mixture of nitrogen-helium gas under ambient pressure. The sample surfaces absorbed a certain amount of nitrogen gas,

and by recording nitrogen content in the sample bottles before and after absorption, the surface area of the sample was determined from the amount of nitrogen absorbed.

The average particle size of nanoparticles was determined by applying the DLS technique and using the Zetasizer Nano Series (Malvern Instruments Ltd, Mississauga, Ontario, Canada). The Zetasizer is equipped with 633 nm wavelengths of green laser and is operated at a non-invasive back scattering angle of 173°. Here, water was used as a dispersion medium, with a refractive index of 1.33 and a viscosity of 0.8872 cP at 25°C (Zetasizer Nano Series User Manual 2008). The average particle size was measured as 5µg/L of nanoparticles were added to 50 mL of the twice-filtered (0.45 µm, membrane filter). Afterwards, analyses were performed according to the instructions stated in the Zetasizer Nano User Manual (Instruments 2007).

The zeta potentials and the zero point of charge of nanoparticles were measured using Zeta-Meter System 4.0, following a procedure described by Zhang et al. (2008). The ionic strength of the samples was made up by the addition of 0.1M $NaNO_3$, and the pH was adjusted either by 0.1N HCl or 0.2N NaOH.

4.4. Results and Discussion

4.4.1. Characterization Experiments

Table 4.1 summarizes the physicochemical characteristics of nanoparticles measured in Milli-Q water, along with some comparative values reported by others. The average sizes measured for nanoparticles by DLS were 163, 370, 1554, and 2169 nm for cerium

dioxide, ferric oxide, silicon dioxide, and titanium dioxide, respectively (Table 4.1). It is evident that all these nanoparticles in the Milli-Q water had an average particle size greater than their initial size reported by the vendors.

Table 4.1 also presents the nanoparticle BET surface areas measured in this study, along with their standard deviations. The measurements reported by others are also presented (with the exception of the cerium dioxide BET surface area, which was taken from Limbach et al. 2008). It is seen that silicon dioxide had the largest surface area (445.9 m^2/g), followed by titanium dioxide (120.1 m^2/g) and ferric oxide (35.7 m^2/g). As noted in Table 4.1, cerium dioxide had the smallest surface area 32 m^2/g, based on results reported in the literature. Surface areas of SiO_2 between 4 and 1200 m^2/g were reported for tabular SiO_2 nanoparticles in synthesized form in the literature.

Table 4.1: Summary of the Measured Physicochemical Characteristics of Nanoparticles in Milli-Q Water

Nanoparticles type	CeO_2	Fe_2O_3	SiO_2	TiO_2	Reference
Particle size, nm	< 20	20 – 25	<10	5 – 10	Sigma Aldrich (product specification material)
Initial Nanoparticle's form	5 wt%	Powder	Powder	Powder	Sigma Aldrich (product specification material)
Refractive index	2	2.9	1.5	2.5	Sigma Aldrich (product specification material)
Average particle size by DLS in [nm]	163	370	1554	2169	This study
Zeta potential (std) in [mV] at pH 6	22.5 (0.4)	16.0 (0.3)	-20.8 (1.9)	-23.8 (2.1)	This study
Zeta potential in [mV] by others at pH 6	24	16	-20	-25	Zhang et al., 2008; Limbach et al., 2008
$pH_{zpc}^{\dagger}$	8.2	7.5	1.8	5.4	This study
$pH_{zpc}^{\dagger}$ by others	8.1	6.5	1.8	5.2	Zhang et al., 2008; Limbach et al., 2008
BET surface area (std) in [m^2/g]	N/M*	35.7 (0.2)	455.9 (0.9)	120.11 (0.3)	This study
BET surface area in [m^2/g] by others	32	33.5 – 50	135 – 236	219 ±3	Nurmi et al., 2005; Pettibone et al., 2008; Wang & Zhang 1997, Lien and Zhang 2001

*Not Measured, $pH_{zpc}^{\dagger}$ – zero point of charge; std – standard deviation.

A surface area of 219 ± 3 m^2/g was reported for TiO_2 by Pettibone et al. (2008), who investigated the effects of pH, size, and aggregation of nanoparticles on the adsorption of organic acids on TiO_2 nanoparticles. Surface areas of 25 – 33 m^2/g were reported for Fe_2O_3 (particle size range 38 – 45 nm) by Nurmi et al. (2005), who studied the electrochemistry kinetics of metallic iron nanoparticles. Surface areas of 33.5 and 35 m^2/g for Fe_2O_3 (particle size 1 -100 mm) were reported by Lien and Zhang (2001) and Wang and Zhang (1997), who investigated iron nanoparticles for complete dechlorination of halogenated compounds and chlorinated ethenes. Regardless of the differences under which experimental conditions were performed, surface areas obtained for nanoparticles in this study were consistent and within the range of those reported by other researchers.

Table 4.1 also shows the measured zeta potentials for nanoparticles in this study and those reported by Zhang et al. (2008) and Limbach et al. (2008). Zeta potential values of 22.5, 16.0, - 20.8, and - 23.8 mV were measured for CeO_2, Fe_2O_3, SiO_2, and TiO_2, respectively, following the protocol developed by Lien and Zhang (2001). The measured zeta potentials of nanoparticles agreed with those reported by Zhan et al. (2008) and Limbach et al. (2008), and that the observed deviations in the results could be due to differences in the conditions under which the experiments were conducted. Deviated results could also be attributed to the fact that Zhang et al. (2008) used KNO_3 for ionic strength as opposed to $NaNO_3$ used in the present study, and Limbach et al. (2008) used a 1 wt% stock solution of cerium dioxide as opposed to the 5 wt% solution used in this study.

SEM images of nanoparticles prepared in Milli-Q water are presented in Figures 4.1, 4.2, 4.3 and 4.4. The images show the different shapes and morphologies of the nanoparticles. For instance, cerium dioxide (Fig. 4.1) had an irregular shape, ferric oxide (Fig. 4.2) had a spherical shape, silicon dioxide (Fig. 4.3) showed a cotton-like shape and titanium dioxide (Fig. 4.4) had an elliptical shape. With the exception of cerium dioxide, all of these nanoparticles seemed to form aggregates with a larger particle size in water compared to their initial sizes reported by the vendors. This result is in line with other researchers' findings (Zhang et al., 2008; Wiesner & Bottero, 2007).

TEM images of CeO_2, Fe_2O_3, SiO_2, and TiO_2 nanoparticles are shown in Figures 4.5 through 4.8. Here again, it is apparent that cerium dioxide nanoparticles (Fig. 4.5) remained loosely aggregated in the suspension, with a particle size almost identical to the one reported by the vendor (less than 20 mm), whereas ferric oxide (Fig. 4.6), silicon dioxide (Fig. 4.7), and titanium dioxide nanoparticles (Fig. 4.8) all formed aggregates with sizes greater than 160 mm. Of this group, titanium dioxide had the largest aggregate formation (greater than 2150 mm, as measured by the DLS and confirmed by the TEM image).

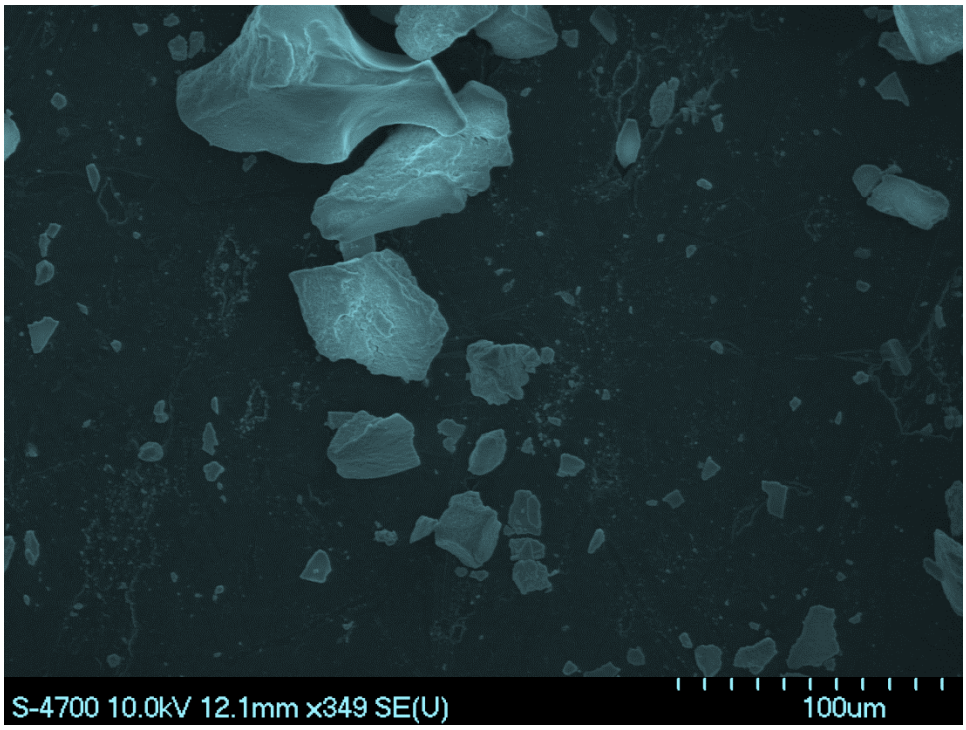

Figure 4.1: SEM Images of Cerium Dioxide Nanoparticles.

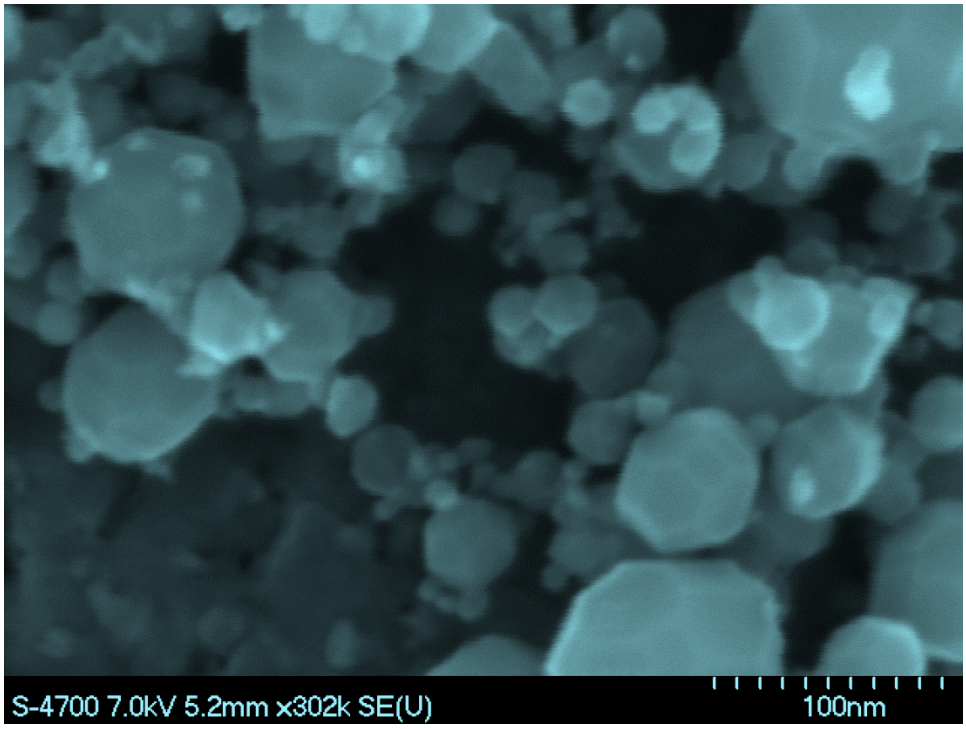

Figure 4.2: SEM Images of Ferric Oxide Nanoparticles.

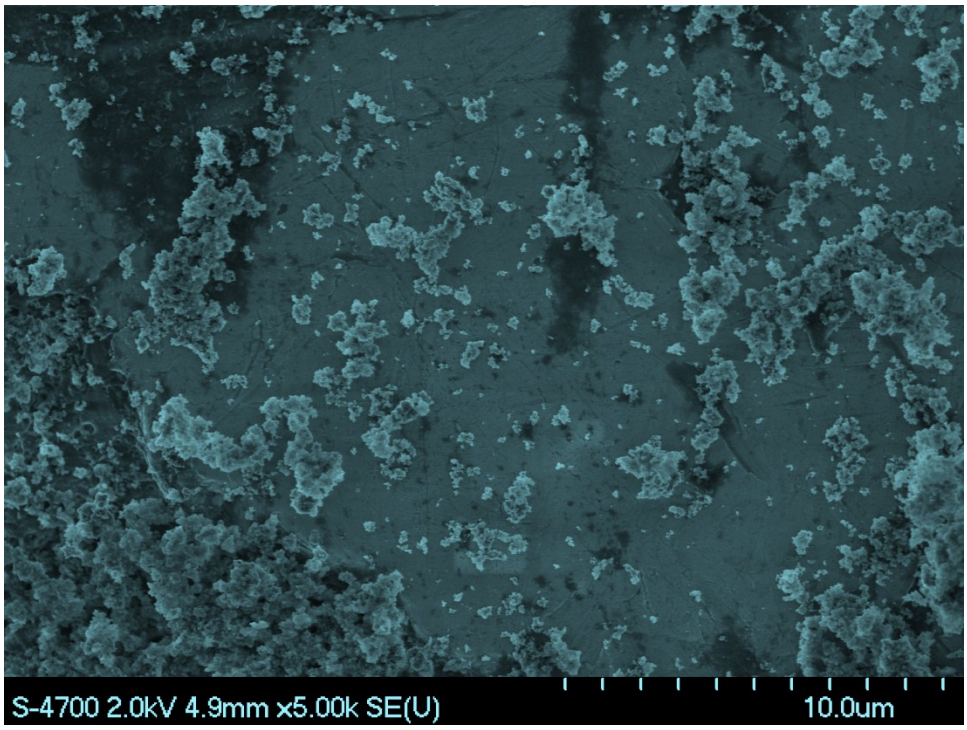

Figure 4.3: SEM Images of Silicon Dioxide Nanoparticles.

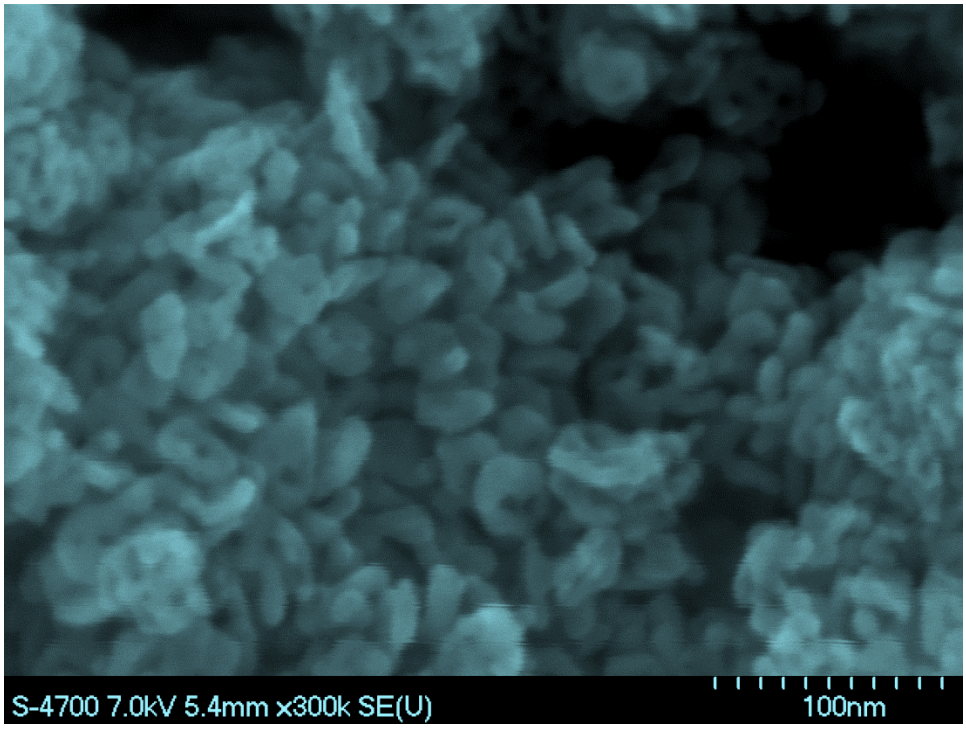

Figure 4.4: SEM Images of Titanium Dioxide Nanoparticles.

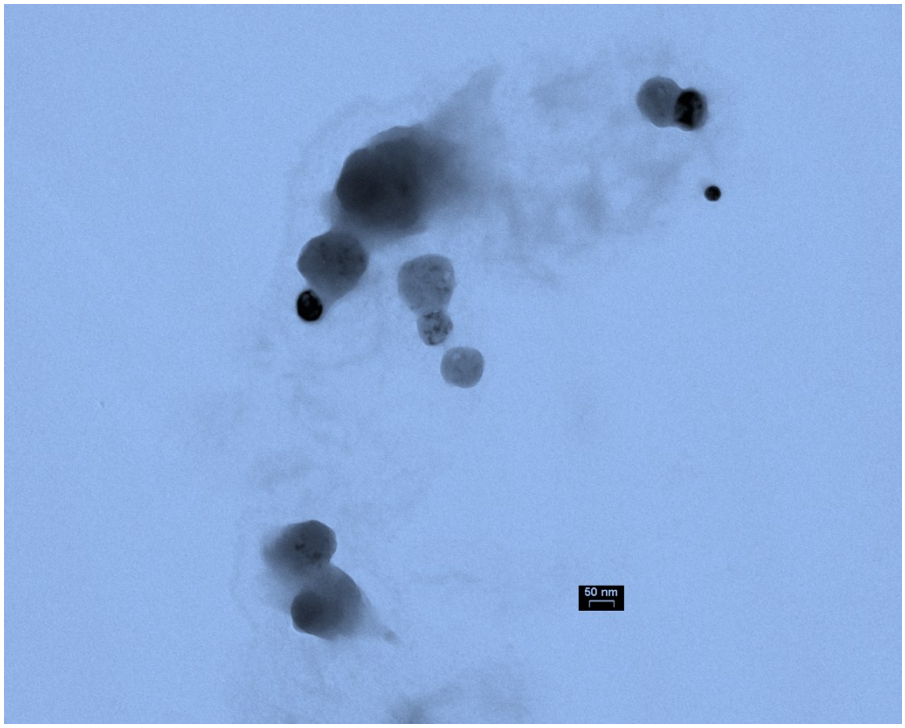

Figure 4.5: TEM Images of Cerium Dioxide Nanoparticles.

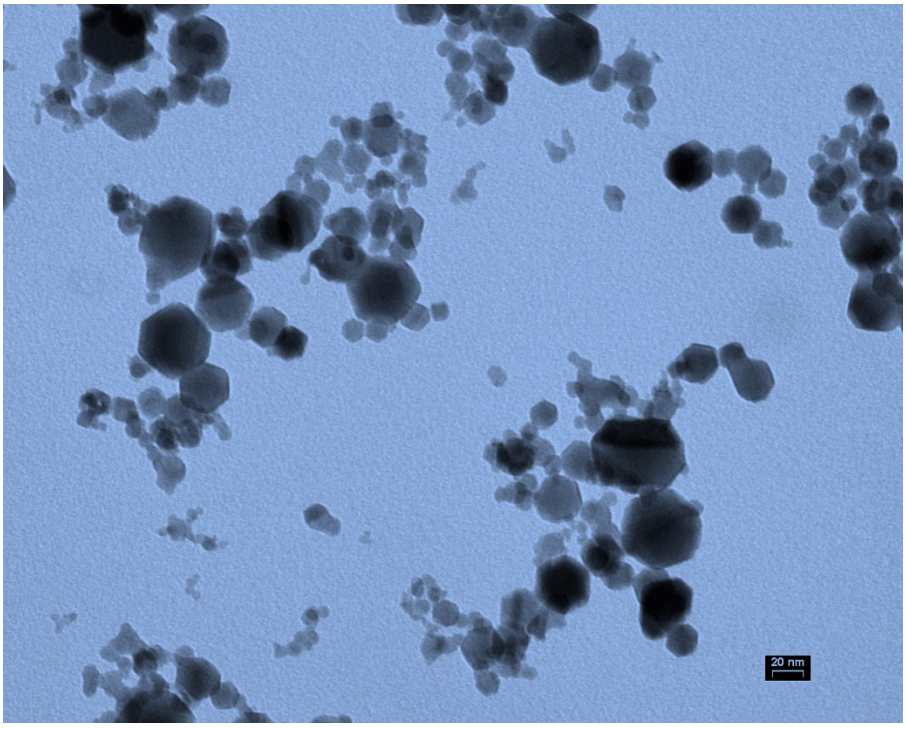

Figure 4.6: TEM Images of Ferric Oxide Nanoparticles in Milli-Q Water.

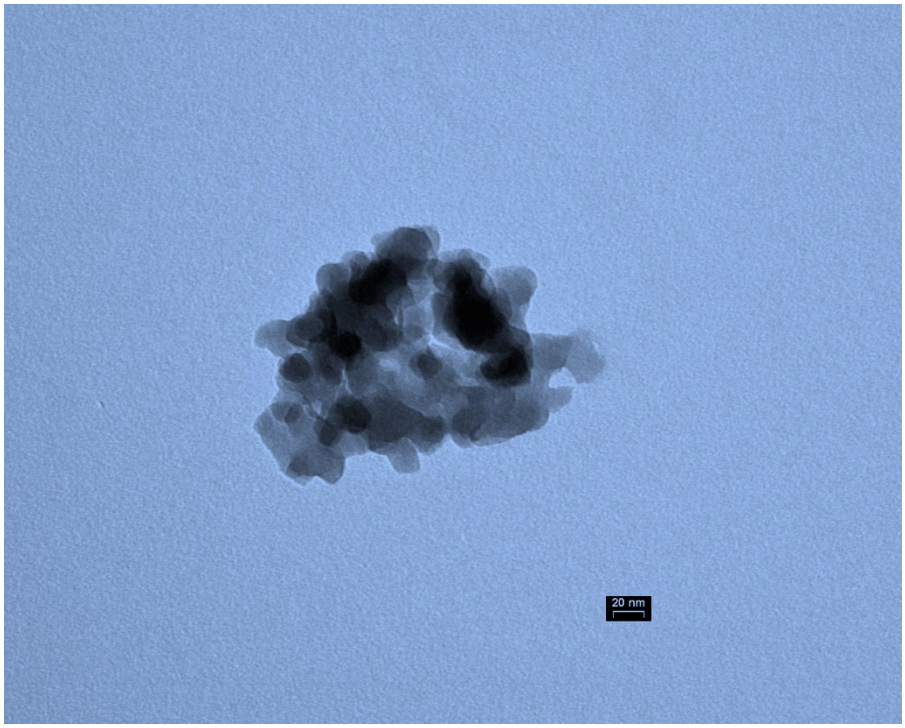

Figure 4.7: TEM Images of Silicon Dioxide Nanoparticles.

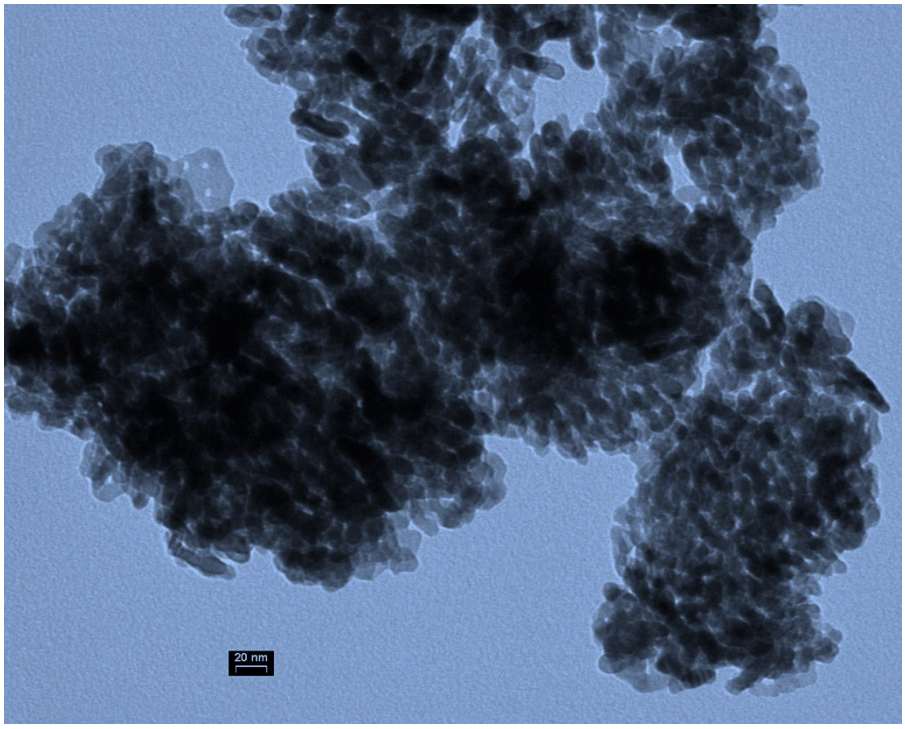

Figure 4.8: TEM Images of Titanium Dioxide Nanoparticles.

4.4.2. Zeta Potential of Nanoparticles

Generally speaking, most nanoparticles in water carry an electrical surface charge, with the origin of the charge depending on the nature of nanoparticles and their characteristics in the water. Additionally, it is known that ionization or dissociation of acidic groups on the surface of nanoparticles can increase their negative charge, while basic groups can increase their positive charge (Bratby, 2006). Nevertheless, the magnitude of the surface charge can be decreased to zero by pH reduction (in cases of negatively-charged nanoparticles) or by a pH increase (in cases of positively-charged nanoparticles). Thus, the magnitude of the zeta potential dictates the stability of nanoparticles in water, such that nanoparticles with a large negative or positive charge will repel each other and remain dispersed.

Nonetheless, when the zeta potential is low or close to zero, the likelihood that nanoparticles will come together and form an aggregate is increased. It is generally accepted that particles with a zeta potential beyond ± 30 mV are considered to be dispersed in water (i.e., stable). Acidity and alkalinity can change the zeta potential of nanoparticles, which is why a zeta-potential-versus-pH plot is positive at low pH values and negative at high pH values. Moreover, the point where the plot crosses zero is called the zero point of charge (zpc). The zpc is important with regards to water treatment, as it indicates destabilization of colloidal particles and promotes their subsequent removal by means of filtration treatment.

A plot of zeta potential versus pH measured for nanoparticles is shown in Figure 4.9. The dotted line in Figure 4.9 represents the optimum alum dose for these nanoparticles. On

the right side of the dotted line (at higher pH values), the nanoparticles appear to have a positive surface potential, as Fe_2O_3 and CeO_2 both showed a pH_{zpc} greater than 7 and positive zeta potentials. From coagulation chemistry, however, it is known that alum is positively charged and is mainly added to destabilize the negative charge that suspended particles have while in water (Crittenden et al., 2005; Bratby, 2006). Therefore, alum is not expected to be a suitable coagulant for Fe_2O_3 and CeO_2 nanoparticles because they have positive surface potential (similar charges repel each other and a more stable system would be created). Based on this interpretation of the results, ferric and cerium oxide nanoparticles were excluded as a potential surrogate for jar and filtration testing. In the case of TiO_2 and SiO_2, both had negative surface potentials (- 20.78 and - 23.76 mV at pH 6).

Figure 4.9 also shows that titanium and silicon dioxide fall on the left-hand side of the dotted line (at acidic pH values), which means that they were negatively charged at lower pH values and thus can be readily destabilized by alum. However, Figure 4.9 also shows that TiO_2 was unstable and tended to form aggregates in the pH range of 3.8 to 7. In the case of silicon dioxide, however, Hunter (1981) indicated that its surface potential reaches asymptotically an isoelectric point close to pH_{zpc} of 2; therefore, silicon dioxide nanoparticles are anticipated to remain stable at pH above 7, which is the case in the current experiment. In other words, the silicon dioxide nanoparticles' region of stability starts at a zeta potential less than - 20 mV. This result means that it is hard to treat silicon dioxide nanoparticles by coagulation at such low pH. Water treatment practices, however,

prove that silica dioxide, if it becomes an issue in water, can be treated by means of lime softening or precipitated along with magnesium and iron.

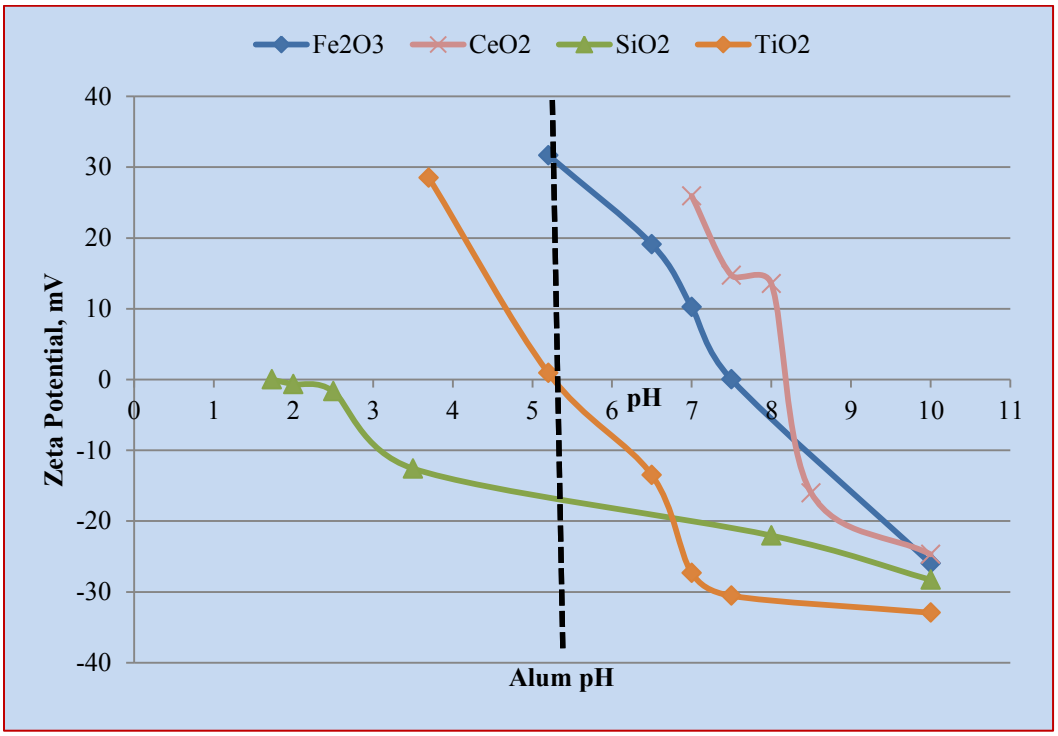

Figure 4.9: Plot of Nanoparticles Zeta Potential versus pH in Milli-Q Water.

The message that can be taken from Figure 4.9 is that TiO_2 nanoparticles have a pHzpc very close to that of alum, and this closeness of pHzpc values would make TiO_2 nanoparticles easily aggregate and destabilize by alum addition during water treatment. Based on the results of the study above, bench-scale filtration experiments in this study were performed with TiO_2 nanoparticles only.

The measured zeta potentials for titanium dioxide (- 23.8 mV), silicon dioxide (- 20.8 mV) and ferric oxide nanoparticles (16.0 mV) in this study were in agreement with those reported by Zhang et al. (2008), who reported zeta potentials of - 25, 20, and 16 mV with

pH_{zpc} of 5.2, 1.8, and 7.5, respectively, for those nanoparticles. However, the measured pHzpc for ferric oxide nanoparticles of 7.5 deviated from Zhang et al.'s (2008) findings. This deviation could be due to the difference in experimental conditions, temperature and zeta meter, or the $NaNO_3$ used in the current study for the solution ionic strength make-up as opposed to the KNO_3 used by them. For cerium dioxide, a surface potential of 22.5 mV and pH_{zpc} of 8.2 were measured. These results agree with Limbach et al. (2008), who measured 24 mV and pH_{zpc} of 8.1. Here, the deviation in zeta values could also be due to differences in the conditions under which the two experiments were performed.

Additionally, the observed deviation between measurements in this study and the reported zero point of charge and zeta potential could be due to the fact that the zpc of metal oxide nanoparticles is sensitive to impurities that contaminate them during their production (U.S. EPA 2010). Nanoparticle structure (i.e., amorphous versus crystalline) can also play a role in the zero point of charge and zeta potential values. For instance, anatase crystal and the rutile structure of titanium dioxide nanoparticles were found to have different zero points of charge (4 and 7, respectively) and most commercially available titanium dioxide would be a mixture of these two forms (U.S. EPA 2010). This also applies to many other metal oxide nanoparticles.

4.4.3. Effect of pH and Ionic Strength on Nanoparticles in Mill-Q Water

Table 4.2 summarizes the values of the zeta potential and the standard deviation obtained for the four synthetic nanoparticles prepared in 10 and 20 mmol NaCl solutions at pH 4 and pH 10. These results illustrate the conductivity values at which zeta potentials were measured and also shows that, during zeta potential measurements, conductivity

remained constant for the given pH and ionic strength, indicating the quality of the measuring procedure. Specifically, conductivity remained constant at pH 4 and pH 10 for the 10 mmol NaCl; however, for the 20 mmol NaCl, the conductivity at pH 10 was almost twice that at pH 4 (e.g., 4.66 mS/cm vs 2.56 mS/cm for the four studied metal oxide nanoparticles). The differences in the nanoparticles' zeta potentials reported in Table 4.2 were a result of changes in the ionic strength when the pH is fixed at 4 or 10.

Table 4.2. Nanoparticle Zeta Potential Measurements

0.01% w/v nanoparticles in 10 mmol NaCl at pH 4			
Nanoparticles	Zeta Potential, mV	Conductivity, mS/cm	Std, mV
CeO_2	-5.08	1.35	3.60
SiO_2	-6.57	1.34	3.39
TiO_2	11.50	1.36	4.22
Fe_2O_3	9.36	1.37	3.34
0.01 % w/v nanoparticles in 20 mmol NaCl at pH 4			
Nanoparticles	Zeta Potential, mV	Conductivity, mS/cm	Std, mV
CeO_2	-8.58	2.56	5.11
SiO_2	-6.03	2.59	3.55
TiO_2	5.63	2.57	6.26
Fe_2O_3	4.21	2.62	5.34
0.01 % w/v nanoparticles in 10 mmol NaCl at pH 10			
Nanoparticles	Zeta Potential, mV	Conductivity, mS/cm	Std, mV
CeO_2	-41.30	1.32	5.40
SiO_2	-35.10	1.34	6.18
TiO_2	-41.30	1.32	5.56
Fe_2O_3	-35.30	1.32	4.59
0.01 % w/v nanoparticles in 20 mmol NaCl at pH 10			
Nanoparticles	Zeta Potential, mV	Conductivity, mS/cm	Std, mV
CeO_2	-31.40	4.72	5.60
SiO_2	-33.60	4.66	7.47
TiO_2	-39.30	4.66	5.52
Fe_2O_3	-33.50	4.62	5.04

0Figure 4.10 shows the zeta potential of each of the four synthetic nanoparticles at two different ionic strengths and pH values in the Milli-Q water. At pH 4 and 10 mmol NaCl, CeO_2, and SiO_2 had negative zeta potentials, whereas TiO_2 and Fe_2O_3 had positive zeta potentials. When the ionic strength was increased to 20 mmol NaCl and the pH remained at 4, a decrease or increase in the CeO_2 and SiO_2 zeta potential values was observed (from -5.1 to -8.6 mV and from -6.6 to -6 mV, respectively). For TiO_2 and Fe_2O_3, however, decreases in zeta potential values were noticed (from 11.5 to 5.6 mV, and 9.4 to 4.2 mV, respectively). At the higher pH value of 10 and at 10 mmol NaCl ionic strength, all nanoparticles showed negative zeta potential values of less than -30 mV, which means that at this pH and ionic strength, these nanoparticles remain stable in the water. However, at fixed pH, the increase of ionic strength (i.e., the increased concentration of an indifferent electrolyte, such as NaCl) should lead to a nanoparticle zeta potential reduction due to double layer shrinkage. This result shows that increasing ionic strength decreases zeta potential at low pH and increases it at higher pH values.

It is worth mentioning that the used values of pH (4 and 10) and the ionic strength of (10 and 20 mmol) in this study (see Figure 4.9 and Table 4.2), represent typical ranges encountered in natural waters. And as the focus here is placed on TiO_2 nanoparticles, it is clear that at these pH and zeta potential ranges, TiO_2 nanoparticles can be destabilized and coagulated by alum during the treatment process; usually lime is added in the treatment (as the case of JD. Kline Water Supply Plant), which raises the pH of the water to over 10 and had to be adjusted to 5-6 to create the optimal coagulation condition.

Therefore, TiO_2 nanoparticles can easily be treated under these pH and ionic strength ranges.

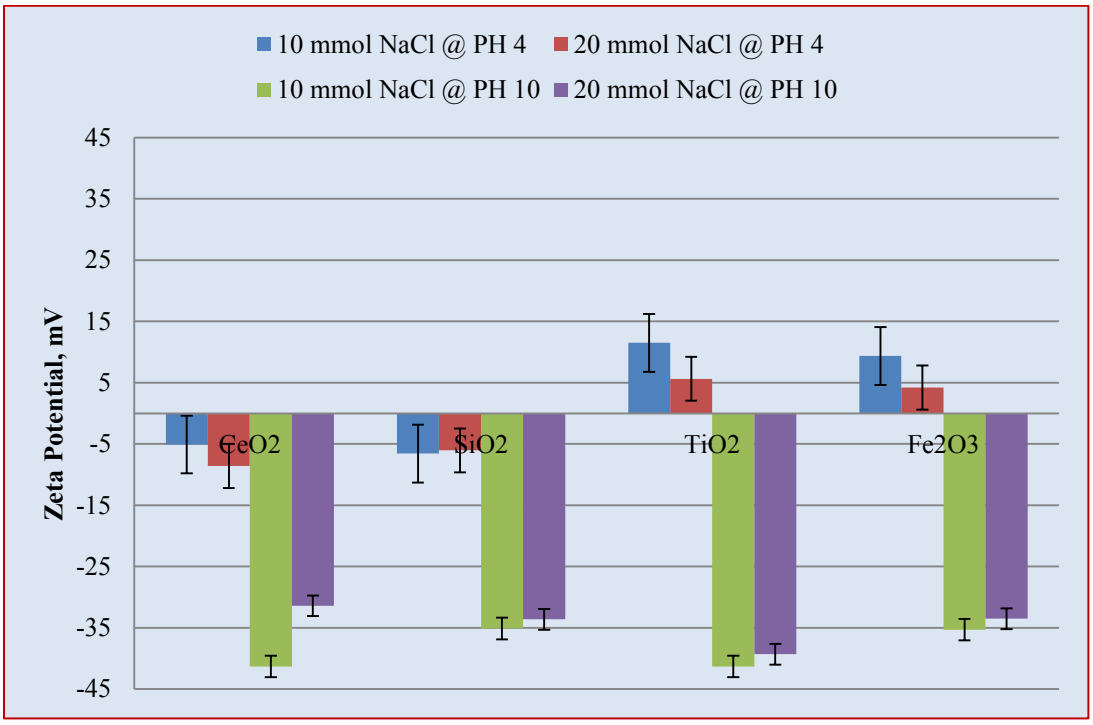

Figure 4.10: Effect of pH and Ionic Strength on Nanoparticles Zeta Potential in Milli-Q Water.

Figure 4.11 shows the effect of pH and ionic strength on nanoparticles' average particle size. Average nanoparticle size seems to decrease under acidic conditions (i.e., pH of 4) and a high ionic strength (i.e., 20 mmol NaCl). Specifically, the particle size decreased from 709 to 608 nm, 2040 to 2027 nm, 1481 to 1466 nm, and 2011 to 1934 for CeO_2, SiO_2, TiO_2, and Fe_2O_3 respectively. Moreover, under basic conditions (i.e., pH of 10) and low ionic strength (i.e., 10 mmol NaCl), the average particle size is lower for all of the studied nanoparticles. However, at higher pH (10) and increased ionic strength (20 mmol NaCl), the average particle size increased for all nanoparticles, from 272 to 500

nm, 903 to 1383 nm, 730 to 1484 nm, and 1936 to 2132 nm for CeO_2, SiO_2, TiO_2, and Fe_2O_3, respectively. These results show that the particle size distribution of synthetic nanoparticles in water is pH- and ionic strength-dependent, as increasing ionic strength at low pH leads to an average particle size decrease, while increasing ionic strength at high pH leads to an average particle size increase. These results are consistent with finding from Wigginton et al. (2007), who attributed the increase of particle size to the salt-induced aggregation effect.

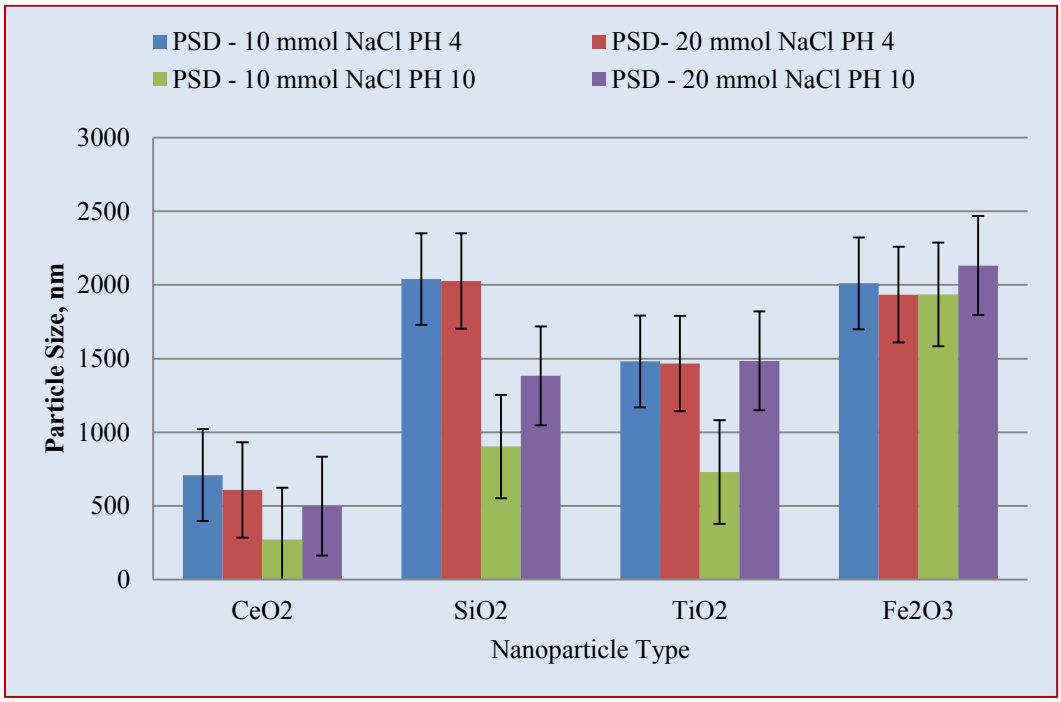

Figure 4.11: Effect of pH and Ionic Strength on Nanoparticles Average Size in Milli-Q Water.

4.5. Conclusions

The objective of this study was to characterize and select an appropriate synthetic nanoparticle that could be utilized as a surrogate for examining bench scale nanoparticle removal in low turbidity water using typical treatment approaches (i.e. coagulation and/or

filtration). Four synthetic nanoparticles (CeO_2, Fe_2O_3, SiO_2, and TiO_2) were initially examined for particle size, shape, aggregation and zeta potential characterization. Nanoparticle zeta potential measurements were performed under different pH and ionic strength conditions to examine their potential for removal under anticipated coagulation conditions for water treatment.

SEM images showed that the studied nanoparticles had different shapes and morphologies roughly analogous to spherical, irregular, ellipsoidal and cotton-like shapes. TEM images and DLS revealed that the nanoparticles in water formed aggregates with particle sizes far greater than the sizes declared by suppliers. The average particle size of the synthetic nanoparticles in water appeared to be pH and ionic strength-dependent. Increasing ionic strength at low pH generally led to a particle size decrease, whereas increasing ionic strength at high pH generally led to an average particle size increase. The zeta potential was found to be an effective tool to predict nanoparticle destabilization in water. Based on the characterization results, TiO_2 nanoparticles were selected to perform all filtration experiments throughout the following chapters of the research.

CHAPTER 5: PROCEDURE FOR CHARACTERIZATION OF NATURALLY OCCURRING NANOPARTICLES IN POCKWOCK LAKE WATER

5.1. Abstract

The objective of this chapter was to develop a procedure for the characterization of low turbidity water for naturally occurring nanoparticles. Water samples from Pockwock Lake were characterized for natural nanoparticles applying a stepwise filtration procedure using 0.45, 0.1, and 0.05 μm membrane filters. Afterwards, three analytical techniques – dynamic light scattering (DLS), transmission electron microscopy (TEM), and atomic force microscopy (AFM) were used to generate particle size measurements. The results obtained through these techniques correlate well with each other with regards to particle size and shape. Three distinctive populations of natural nanoparticles were identified in Pockwock Lake water through DLS. The first population had an average particle size of 2.3 nm, the second population had an average particle size of 15.7 nm, and the third population had an average particle size of 58.8 nm. TEM images of the raw water samples showed nanoparticles of spherical, elongated, and irregular shapes, with diameters ranging from 1 to 200 nm. AFM images of the raw water sample revealed that the same shapes imaged by TEM had spherical and irregular shapes. The three dimensional (3D) AFM plot showed that the structure of those nanoparticles appeared to have hill-like structures with a sharp apex, a diameter of 0.5 to 40 nm, and a height of 0.5 to 33 nm. Similar structures (spherical, fibrous, and irregular) have been reported for clay and humic acid nanoparticles in the ground and fresh water. However, the height histograms of the filtered through 0.45, 0.1, and 0.05 μm water samples, showed nanoparticles with diameter and height of 44 and 20 nm, 33 and 4nm, and 15.5 and 1.4 nm for the three populations, respectively. These dimensions also agree with those reported in the literature for humic acids in water. This study found that natural nanoparticles in Lake Pockwock water could be characterized as a complex mixture of humic acids, clay, and other inorganic nanoparticles. The study results represent a key step in characterizing low turbidity water for natural nanoparticles, and it is anticipated that its findings would assist in the optimization of filtration treatment for the removal of these kinds of particles.

5.2. Introduction

Particles in water are considered to be a complex mixture of different physical, chemical, and biological nature with sizes ranging between 0.001 and 1 μm (Lead and Muirhead 2005). A substantial number of these particles fall under the category of nanoparticles (i.e. < 100 nm). In nature, particles can be silt, clay, and natural organic matter, and are generally defined as globular, fibrous, or irregular in shape (Gregory 2005; Crittenden et al., 2005; Santschi et al., 1998). Their unique properties (i.e., large surface area and small size) enable them to play a profound role in determining the fate and behavior of an entire aquatic system, including particle transport, deposition, and toxicity (Lead and Muirhead 2005).

The presence of particles in water is not desired for a number of reasons. Muirhead and Lead (2003) indicated that particles in water can inhibit metal bioavailability due to chemical kinetic and mass transport constraints, and can affect colloidal transport in water due to their propensity to remain unstable under the influence of diffusion and convection processes. Particles can also increase water turbidity and reduce the amount of light passing through the water body. Additionally, Guo and Ma (2006) found that particles can absorb humic acids and trace metals in water due to their high surface area, and therefore can extend their transport. Another problem associated with particles in water is that they can negatively impact disinfection treatment, as they may shield pathogens and impair the pathogen inactivation process (Korich et al., 1990).

Particle interaction with water is affected by their surface charge as well as the chemical functional group attached to them. This interaction is essential because it involves two

types of particles in water: hydrophobic and hydrophilic. Hydrophobic particles are generally less attracted to water, are thermodynamically unstable, and tend to form aggregates over time, while hydrophilic particles are water-attracted and can easily bind to their polar ionized surface functional groups. Hydrophilic particulates in water can be metal oxides, proteins, humic or fulvic acids, and biological formations (Crittenden et al., 2005). Another complexity associated with particles is that it is difficult to determine their exact role in the water, as they can be polydisperse, polyelectrolytic, or polyfunctional. It is also not easy to determine their exact structure, due to it being pH- and ionic strength-dependent (Santschi et al., 1998).

While surface waters have similar characteristics, significant variations in the quality of water can be found in different sources. Hence, the characterization of each water source for naturally occurring nanoparticles will provide information on their properties and related removal mechanisms. Some studies have been conducted in Europe to investigate the properties of submicron particles in fresh and groundwater sources, using a number of advanced analytical techniques such as atomic force microscopy (AFM), and transmission electron microscopy (TEM) (Lead et al., 1997, 2003, 2005, and De Momi and Lead 2008; Kaegi et al., 2008; Hassellov and Kaegi 2009; Perret et al., 1994; Plaschke et al., 2002). These studies found that three populations of submicron particles with different shapes and morphologies were detected in the studied natural waters. To compare those submicron nanoparticles, comparative studies are required to be conducted in other drinking water sources elsewhere (e.g. Atlantic Canada).

Although nano-scale particulates are presently not regulated as water contaminants, acquiring in-depth information on their occurrence and characteristics in drinking water sources will assist in developing future treatment solutions. Furthermore, identifying nanoparticles in drinking water sources will assist in the development of removal mechanisms. Currently, it is unclear whether the available water treatment practices are capable of removing nanoparticles from water (Hahn & O'Melia, 2004; Tufenkji & Elimelech, 2004). Nevertheless, it is believed that, due to the complexity of particles in natural water sources and the limitations of analytical techniques, particle characterization in drinking water sources needs to be investigated to further our understanding of their behavior and fate during the treatment process. The objective of this study was to develop a procedure for the characterization of water samples from Pockwock Lake for naturally occurring nanoparticles using various analytical techniques. It is anticipated that such characterization will help evaluate the removability of nanoparticles during water treatment.

5.3. Materials and Methods

5.3.1. Water and Sample Preparation

Water samples used to conduct the experiments were collected from Pockwock Lake and from the pumping station at the J.D. Kline Water Supply Plant. Pockwock Lake is a protected watershed located in Hants County, Nova Scotia, Canada. The lake occupies an area of around 5660 hectares and is the main drinking water source for the city of Halifax and the surrounding counties. Pockwock water is known for its low water quality parameters: a pH of around 5.5, an alkalinity of less than 5 mg/L as $CaCO_3$, and a

turbidity of less than 0.5 NTU; it also has moderate to higher color and natural organic matter. The microbiological growth in the lake is extremely low and *Cryptosporidium* or *Giardia* have never been detected (O'Leary et al., 2003).

A stepwise filtration procedure for sample fractionation was developed to characterize Pockwock Lake water for natural nanoparticles. Through this procedure all particles with size greater than 0.45 μm were removed from the sample via membrane filtration. The water sample was left un-agitated for 24 hours, at room temperature (20 ºC), to allow large particles to settle, and then the samples were stepwise filtered through different pore-size membrane filters, (i.e., 0.45, 0.1, and 0.05 μm filters from Nuclepore Etched Membranes Filters from Whatman, USA). To avoid sample contamination, all glassware employed to collect samples were soaked in a 10 % nitric acid (HNO_3) solution, rinsed with twice-filtered Milli-Q water, dried, covered with parafilm plastic (Pechiney Plastic, Chicago, USA), and stored in a clean drawer prior to use. Milli-Q water produced by Millipore SAS67120, Molsheim, France was used to conduct all other work related to sample preparation and experimental performance.

5.3.2. Analytical Methods

Three analytical techniques – dynamic light scattering (DLS), transmission electron microscopy (TEM), and atomic force microscopy (AFM) – were used to characterize Pockwock water for natural nanoparticles. These techniques have been proven to be capable of generating adequate and accurate particle size measurements, provided that artifacts associated with sample preparation and measuring are reduced to a minimum (Zhang and Kumar 2009). Among these techniques, AFM is considered to be a powerful

analytical technique for determining nanoparticle characteristics, but it would be most beneficial when used in conjunction with other techniques to allow for result comparison. Altogether, these techniques provide invaluable information on quantifying the nanoparticle size in water samples.

5.3.2.1. Dynamic light scattering (DLS)

In dynamic light scattering (DLS), the sample is illuminated with a laser beam, and the fluctuation in the intensity of the scattered light is detected (measured) and converted into a particle hydrodynamic diameter using Stokes Einstein equation (Wiesner and Bottero, 2007). The hydrodynamic diameter of a particle is actually the diameter of a hypothetical sphere that has the same diffusivity as the particle being measured (Wiener and Bottero 2007). Here, it is worth mentioning that DLS applies only to particles undergoing Brownian motion that remain fully suspended in water. Brownian motion is the random movement of particles due to collisions between liquid molecules and particles that occupy the liquid. The drawback of the DLS is that it cannot measure the size of a discrete particle but instead measures the average particle size. The analytical applications of DLS for particle size measurements of natural particles have been discussed in detail by Filella et al. (1997).

The DLS equipment used in this study was the Zetasizer Nano Series (Malvern Instruments Ltd. Mississauga, Ontario, Canada), equipped with a 633 nm green laser wavelength and operated at a non-invasive back scattering angle of 173°. Water was used as a dispersion medium, with a refractive index of 1.33 and a viscosity of 0.8872 cP at 25°C. The volume of the sample was 1.3 mL loaded in special cuvettes provided for this

purpose. The sample was treated strictly according to the instructions described in the user manual of the Zetasizer Nano Series from Malvern Instruments Ltd.

5.3.2.2. Transmission Electron Microscopy (TEM)

In transmission electron microscopy (TEM), a beam of electrons is transmitted through a sample and allowed to pass through a series of lenses (Zhang and Kumar 2009). It determines the image resolution and obtains the magnified image with the help of a computer processor and a special camera attached to the system. Sample preparation for TEM imaging is crucial, as the quality of images is governed not only by the acceleration voltage of electrons but also by the sample nature and structure. The TEM images of a raw water sample were generated using an FEI Tecnai-12 Microscope at 80 kV power and with a Gatan 832 camera. A droplet of the sample was placed on a 200-mesh gold grid of a holy carbon film (Electron Microscopy Sciences, Hatfield, PA, USA). The 200-mesh grid was placed on a piece of tissue paper in a covered Petri dish and allowed to dry for 24 hours before being placed in a special holder and loaded into the FEI Tecnai-12 for image capturing.

5.3.2.3. Atomic Force Microscopy (AFM)

During AFM imaging, a small cantilever (usually 200 um long and made of silicon or silicon nitride) with a sharp tip or probe is scanned over a sample surface (Zhang and Kumar 2009). To map the topography of a surface, the tip is brought into gentle contact with the sample surface (this is called contact mode imaging) and is then scanned in a raster fashion over the surface. Topographic features cause cantilever deflections, which are recorded by measuring the deflection of a laser beam that is focused on the end of the

cantilever. The deflected laser beam falls on a split photo detector and the voltage difference from the two photo detectors is a measure of the size of the cantilever deflection and hence the size of the imaged object. Tip position and cantilever deflections are recorded by a computer that processes the data into an image of the sample topography. Thus, the entire sample surface was scanned and its topography viewed with sub-nanometer precision.

Before the sample was analyzed, a sheet of mica was adhered to it using ordinary sticky tape, after which 40 μL of the sample was poured on the mica and left to dry in an incubator (133000 Boekel Scientific, Life Science Laboratory, Dalhousie University) at 37° C for a half an hour. The water evaporated, leaving only nanoscale materials on the mica surface. The mica and its content were then cooled to room temperature (20°C) before being analyzed by the AFM instrument. AFM images were captured using a Molecular Imaging AFM instrument in contact mode. The cantilevers had spring constants of 0.03 N/m. The height and width of the nanoparticles were obtained from cross-sections taken on height images of the sample surface. Nanotech software WSxM 5.0 was used to analyze the AFM images (Horcas et al., 2007).

5.3.3.4. AFM Artifacts

AFM is a tool that can be used to investigate the nanoparticle structure in an aqueous environment with a great precision. However, as with all other analytical methods, the veracity of AFM images is affected by artifacts that can significantly distort the generated image and consequently lead to an inadequate interpretation of the results. AFM lateral dimensions often overestimate the size of nanoparticles because the radius of curvature of

the AFM tip is usually in the size range of these nanoparticles (Lead and Muirhead 2005). Thus, AFM heights were found to be more accurate to estimate nanoparticle diameter rather than the size.

Therefore, the aggregate formation seen in some of the AFM images is attributed to the fact that, when the sample was placed on the mica surface and left to dry, the water had a bow or half-circle shape. While drying, the sample gradually shrunk and most of its particles accumulated at the circle circumference, creating the aggregate formation seen in the images. Another possible artifact is associated with the force exerted by the tip on the sample surface. When AFM operates in contact mode, the applied force is extremely high; thus, particles that are not firmly adhered to the surface can drift due to the tip movement. Fortunately, this artifact was not expected to have happened during the imaging process, as the force used was only 0.03 N/m and no drifting, tilting, streaking, or bowing can be seen in any of the images.

5.4. Results and Discussion

Figure 5.1 shows particle size distributions obtained by DLS according to the number of nanoparticles detected in 0.45 μm of the twice-filtered Pockwock water. Particle size distribution describes how frequently a certain size of particle within the analyzed sample is encountered. Particle sizes obtained by DLS are always the mean or average size, which is a major drawback of the DLS technique, as it cannot measure the size of a discrete particle.

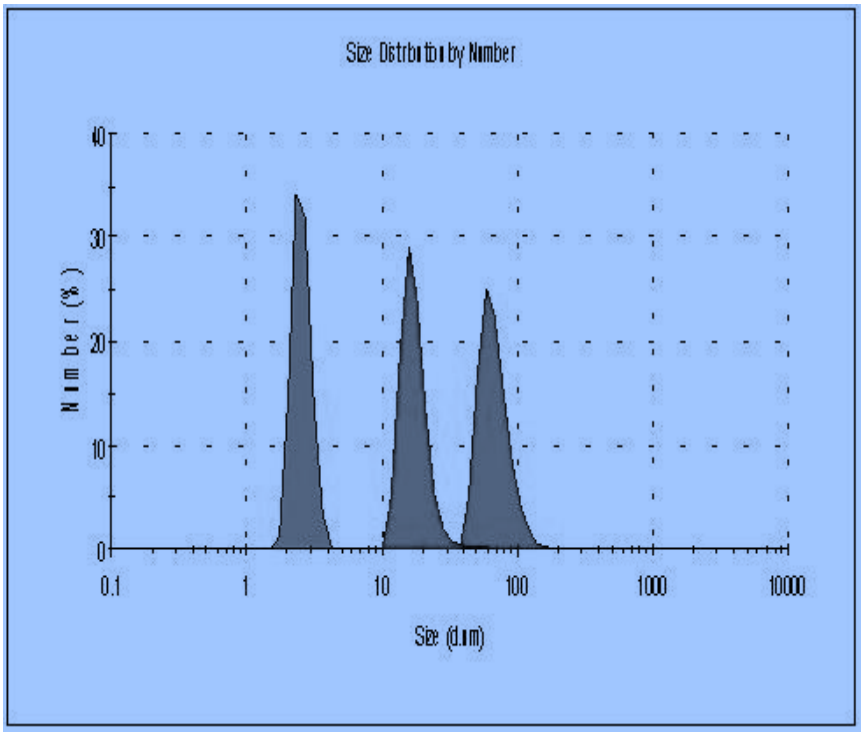

Figure 5.1: Particle Size Distribution by Number of the 0.45 μm Twice-Filtered Pockwock Water Obtained by DLS.

From Figure 5.1, it can clearly be seen that there are three distinctive populations of naturally occurring nanoparticles identified in Pockwock water. The first population represented 34.2% of the total particle number in the sample and had an average size of 2.33 nm, the second population represented 29.1% of the total particle number in the sample and had an average size of 15.7 nm, and the third population occupied 25.1% of the total sample particle number and had an average size of 58.8 nm. These particle size ranges are consistent with those obtained by Hassellov and Kaegi (2009), who studied nanoparticles in water from Lengg Lake in Zurich, Switzerland, and by Lead and Muirhead (2005), who characterized freshwater for natural aquatic colloids using atomic force microscopy. As will be discussed later in the AFM section, and based on Lead and Muirhead's findings, it is assumed that these populations belong to organic nanoparticles

(e.g., humic acids) or inorganic nano-structures such as metallic nanoparticles. However, they could also belong to other nano-formations in the water.

Figure 5.2 provides a TEM micrograph of various nanoparticles with different size, shape, structure and morphology detected in the raw Pockwock water sample. Three distinctive shapes that were observed in Figure 5.2 are spherical, elliptical or elongated, and irregular (see the circled areas in Figure 5.2). These three nanoparticle structures have diameters ranging from 1 – 80 nm. However, most of the spherical particles had a diameter between 1 – 20 nm, which is consistent with the sizes measured by DLS. Particle size distribution of nanoparticles in Pockwock water obtained by DLS in this research indicated that the dominant nanoparticle species had a diameter of 2.3 nm (34.2 %). The same sizes of nanoparticle were visible in the AFM images; they will be discussed later in the AFM section. Hassellov and Kaegi (2009) suggested that the spherical aggregates are probably humic acid aggregates, with a diameter up to 60 nm, and the elongated or fibrous particles are likely to be polysaccharides, with a diameter up to several hundred nanometers. Santschi et al. (1998) drew similar conclusions when studying fibrillar polysaccharides in macromolecular organic matters in different waters; they compared colloidal distribution using AFM and TEM techniques and determined the nature of colloidal fractions based on their microscopic structure. They were able to contrast surface water colloidal structure with those in deep and marine waters.

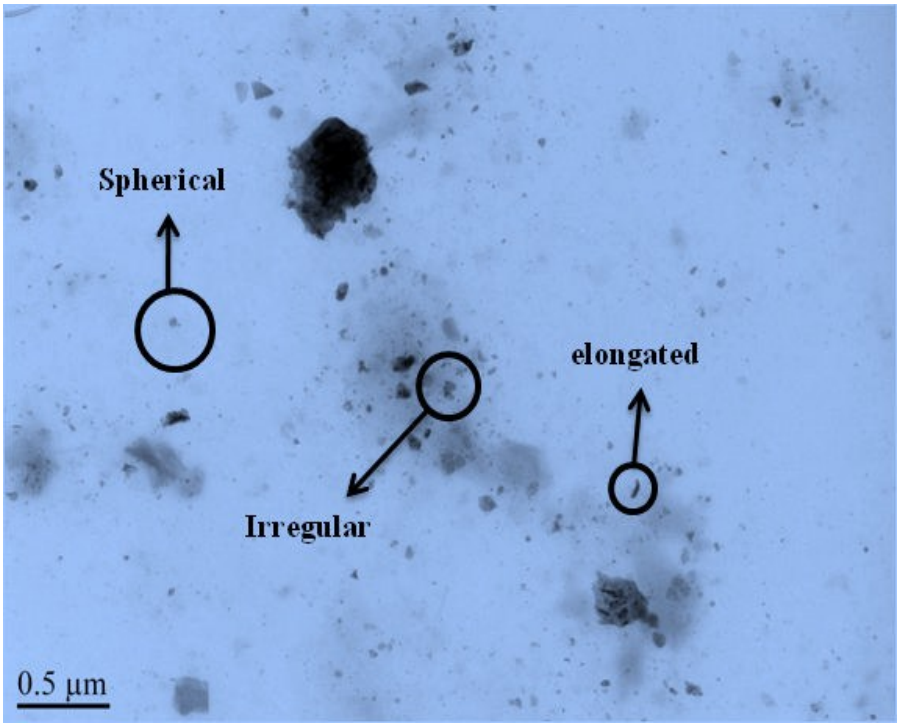

Figure 5.2: TEM Image of Raw Water from Pockwock Lake.

Figure 5.3A shows nanoparticle and nanoparticle aggregates along with their particle size distribution in raw Pockwock Lake water obtained through the AFM. Mostly spherical and irregular shapes are seen, with sizes between 10 nm to several hundred nm, and most are aggregates. Similar shapes have been reported by others (Lead and Muirhead 2005; Guo & Ma, 2006; Domingos et al., 2009; Plaschke et al., 2002). For example, Lead and Muirhead (2005) measured the size and structure of natural aquatic colloids in Suwannee River water using atomic force microscopy, reporting 2 – 3 nm nanoparticles, globular in shape (they regarded them as humic acid). They also observed natural aquatic colloids with fibrous and irregular shapes and structures. Specifically, they identified irregular nano-structure with sizes between 1 – 70 nm, mostly made of oxide and organic origin, and fibrous nano-colloids with diameters of 1 – 10 nm, mostly of microbiological origin (polysaccharides).

Plaschke et al., (2002) reported spherical and elongated structures for nano-scale colloids in Gorleben groundwater. The spherical structure they observed had a diameter and height in the range of 100 to 60 nm, and the elongated species had a diameter and height ranging from 280 to 80 nm, respectively. Plaschke et al., (2002) also observed a third irregularly-shaped structure, with diameter and height between 600 and 23 nm, respectively, and assumed it to be a lignite particle. From the AFM image artifacts, it was anticipated that the measured particle sizes on the surface often look larger than expected; however, when the particle height is measured by a line profile, the correct size is given. Therefore, based on the AFM artifacts (www.cma.fcen.uba.ar/files/Guide_AFM.pdf, accessed in February 2012), it is considered that nanoparticle height would be a more precise way of reporting particle diameter rather than the size measured at the surface plane.

Based on findings from others (e.g., Plaschke et al., 2002; De Momi & Lead, 2008; Domingos et al., 2009), it is presumed that the dominant species could be regarded as humic acid formations, which would be normal for Pockwock Lake, based on its low turbidity (< 0.5 NTU), low pH (<5.5) and moderate concentration of total organic carbon (2.6 mg/L). The 15.9 nm (29.1 %) spherical nanoparticles detected in Pockwock water, according to the literature cited earlier could be considered metal oxide and organic materials. Finally, the 58.8 nm (25.1 %) nanoparticles could be of organic or other nano-formation origin. The particle size ranges obtained in this work using the three analytical techniques are consistent with those obtained by other researchers in different natural water sources.

Figure 5.3B shows a histogram of particle size distribution derived from a roughness analysis by AFM. The histogram shows that natural nanoparticles in Pockwock water have heights between 0.5 to 28.5 nm and a mean particle diameter of 15 nm. This result agrees with those reported by Muirhead and Lead (2003) and Plaschke et al. (2002), who presumed the irregular nano-colloid aggregates to be inorganic colloids coated with organic matter. It is believed that this is the case with the irregularly-structured nanoparticles observed in Pockwock water. In addition, the interaction between water molecules and hydrophobic substances might contribute to the formation of the observed nanoparticles structure in Pockwock water.

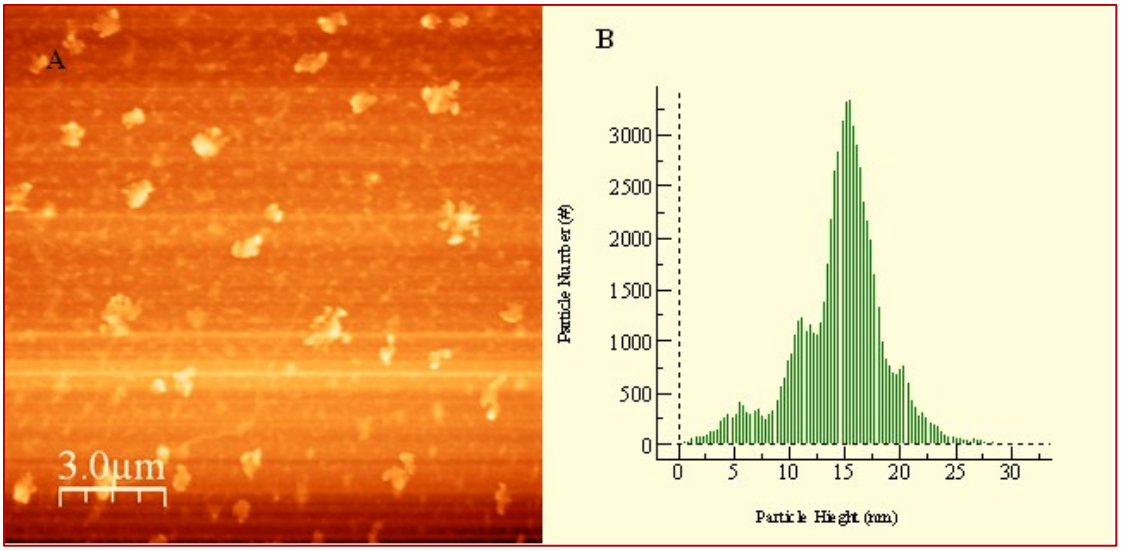

Figure 5.3A: AFM Image of Nanoparticles in Pockwock Water and B) AFM Nanoscale Colloids Height Distribution Histogram.

Figure 5.4 presents the structure of nanoparticles observed in the Pockwock water samples. The profile of the rectangular region in Figure 5.4A is depicted in Figure 5.4B. The same structure seems to be dominant in Pockwock water, as it appears throughout

the entire image (Figures 5.3A and 5.4A). These morphological structures can be considered clay nanoparticles in Pockwock water, as has been reported by others. Figure 5.4C presents the 3D plot of these structures; they appear to have a hill-like structure with a sharp apex and a mean height of around 3.5 nm. Similar topographical structures of nanoparticle formations have been reported for clay particles coated with humic acids in Gorleben groundwater that are spherical, fibrous, platelet, and irregular in shape (Plaschke et al., 2002).

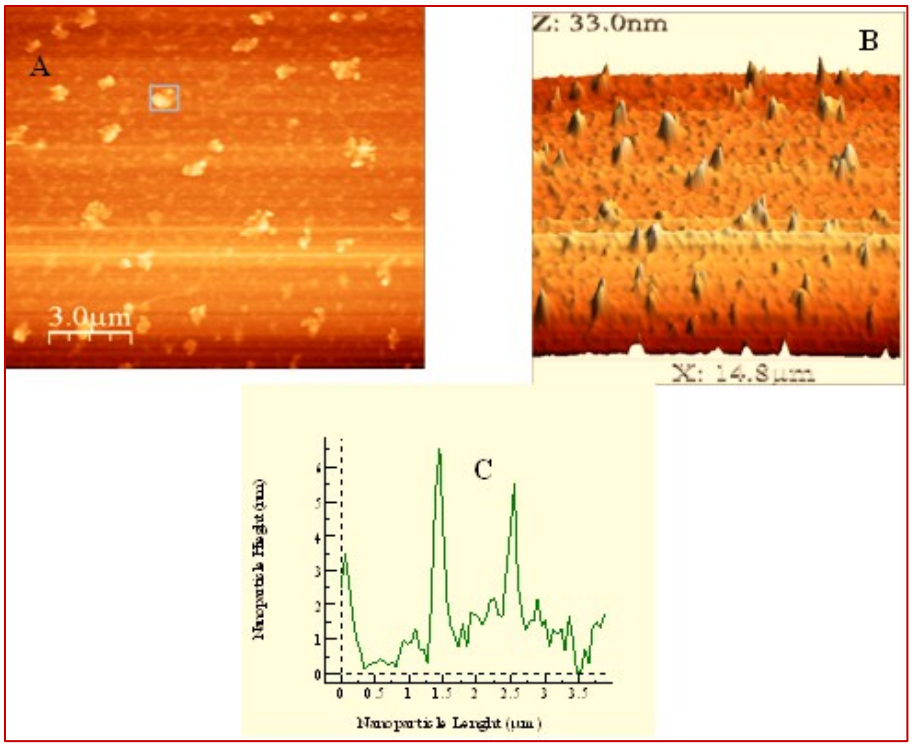

Figure 5.4A: AFM Images of Raw Pockwock Water: B) 3D View of the Nanoparticles in Pockwock Water C) Line Profile of the selected gray area.

Figure 5.5 displays the height distribution histograms of the 0.45 µm (Figure 5.5 A), 0.1 µm (Figure 5.5 B), and 0.05 µm (Figure 5.5 C) filtered water samples generated by AFM. The height histograms show that the height of the right fractions has been detected for

each corresponding filter pore size, and the nanoparticles in the sample were distributed in a wide size range of 0.5 – 44 nm. Figures 5.5A, 5.5B, and 5.5C also show that nanoparticles with mean heights of 35 nm, 21 nm, and 3 nm for the 0.45, 0.1, and 0.05 μm were observed in the filtered samples, respectively. These sizes agree with the sizes reported by Plaschke et al. (2002) for spherical humic acids in Gorleben groundwater, and it is assumed that these structures to be humic acids or clay nanoparticles that remained in the filtrate after larger particles were removed.

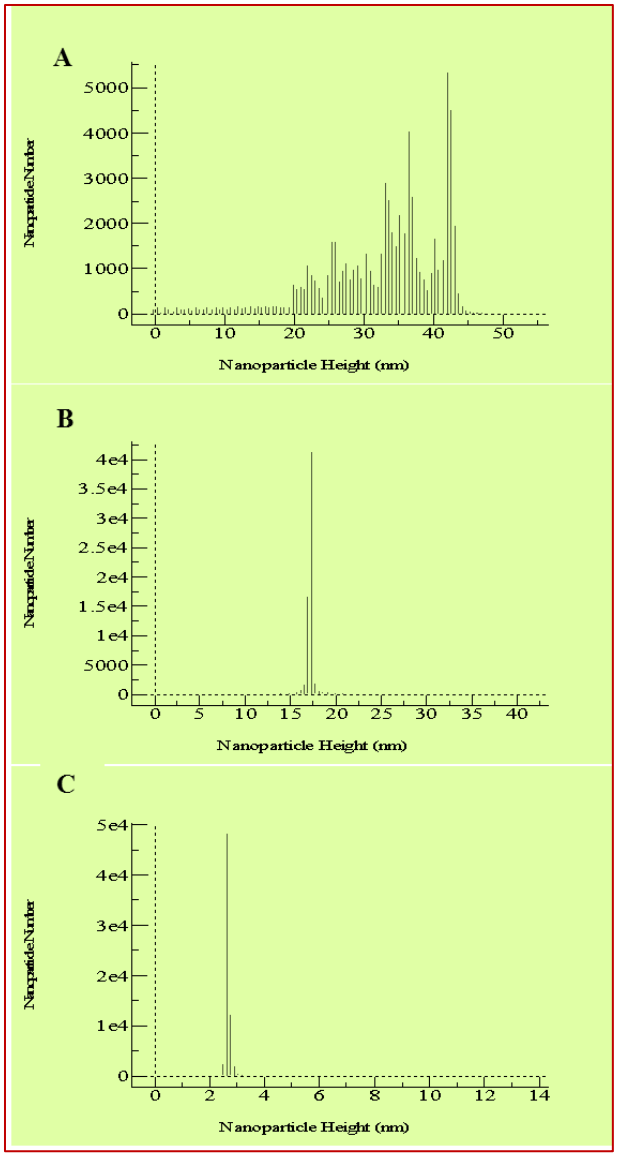

Figure 5.5A, B and C: Histograms of the 0.45, 0.1, and 0.05 µm Stepwise Filtered Fractions of Nanoparticles in Pockwock Water Generated by AFM.

5.5. Conclusions

Water samples from Pockwock Lake were characterized for natural nanoparticle size using three analytical techniques: transmission electron microscopy (TEM), dynamic light scattering (DLS), and atomic force microscopy (AFM). The combination of application of these techniques allowed validation the results by comparison. With the

three used techniques; TEM and AFM images, three distinctive naturally occurring nanoparticle populations with spherical, elongated and irregular shapes were detected in Pockwock water.

It is expected that these spherical structures to be of humic acid aggregates or inorganic matter coated with humic substances, and that the elongated structures to be fibrous polysaccharides or some other nano-scale structure. Despite the limitations associated with each of these analytical techniques, the results obtained through the DLS, TEM, and AFM show strong agreement. The study results represent a key step in characterizing low turbidity water for natural nanoparticles, and it is anticipated that its findings to assist in the optimization of filtration treatment for the removal of these kinds of particles.

CHAPTER 6: EVALUATING FILTER PERFORMANCE FOR THE DEPOSITION OF TiO_2 NANOPARTICLES UNDER DIFFERENT WATER CHEMISTRY AND SIMULATED CONDITIONS

6.1. Abstract

The objective of this study was to evaluate filter performance for the deposition of TiO_2 nanoparticles onto the porous medium (glass beads) under different water chemistry and simulated conditions. It is found that changing water chemistry (e.g., pH, ionic strength, etc.) can drastically affect particle stability leading to particle aggregation and deposition onto porous media. In this study, the deposition of TiO_2 nanoparticles onto glass bead media was evaluated. Sodium chloride and calcium nitrate of two ionic strengths of 10 and 20 mmol/L, were used. These ionic strengths were applied with and without alum addition. Results from the experiment showed that collision attachment efficiencies (α) of 0.001, 0.002, and 0.01 and filter coefficients (λ) of -0.003, -0.01 and -0.02 were calculated. These attachment efficiencies were then used to evaluate filter efficiency under simulated conditions for the removal of different particle sizes of naturally occurring nanoparticles (1 – 100 nm). The study found that the TiO_2 nanoparticle deposition was affected by solution ionic strength and that aggregation increased with increasing ionic strength, specifically in cases where no alum was added. The study also determined that the nanoparticles remained dispersed in water and became more stable with alum additions, due to excessive positive charges. Therefore, changing the ionic strength of water assists in the destabilization of nanoparticles during filtration. The study findings are significant, as data consistent with practice have not been shown for small particles such as TiO_2 nanoparticles.

6.2. Introduction

Deposition of colloidal particles onto porous media involves destabilization, transport and attachment processes (Crittenden et al., 2005; Tobiason & O'Melia, 1988; Yao et al., 1971). Deposition occurs at two sequential stages: transport and attachment. The transport stage brings a particle close to the surface of a "collector" or medium grain, and the attachment binds the two surfaces together in a way that allows their aggregation and subsequent deposition (Espinasse et al., 2007; Hahn & O'Melia, 2004; Lecoanet et al., 2004). However, nanoparticle transport in water is expected to be mainly governed by Brownian diffusion, which is the random movement of particles due to the thermal energy of fluid (Yiacoumi and Letterman, 2011). For particles of extremely small size (5-25 nm), such as TiO_2 nanoparticles, transport through a porous medium is expected to follow Brownian diffusion (Jegatheesan & Vigneswaran, 2005), while particle attachment is dictated by their surface charge and interaction with other particles in water (Hahn & O'Melia, 2004; Wiesner et al., 2007; Sellers et al., 2009).

The effect of water chemistry on the filtration process has drawn significant attention due to the inability of physical theories to predict filter performance (Guzman et al., 2006). The behavior, interaction and stability of colloid particulates in water can be explained by the Derjaguin Landu Verwey and Overbeek (DLVO) theory which explains what happens when two surfaces of dispersed particles in a suspension are brought into close contact with one another (Yiacoumi and Letterman, 2011). According to DLVO theory, the total interaction energy or forces acting at a certain distance between dispersed particles consist of electrostatic coulombic interaction, which can be repulsive or attractive, as well as Van der Waals attractive interaction (Hahn & O'Melia, 2004,

McDowell-Boyer et al., 1986). Most particles in water possess a surface charge due to ionization, ion binding or ion exchange. It is found that changing water chemistry (e.g., pH, ionic strength) can drastically affect particle stability in a way that could lead to their aggregation and subsequent deposition onto porous media.

Investigations of water chemistry on filtration process have been carried out to explain the inability of physical microscopic models to predict filter performance. O'Melia and Stumm (1967) found that chemical effects, other than those of coulombic origin, play a major role in particle deposition during the filtration process. For instance, Ionic strength, which is the measurement of ion concentration in a solution, is crucial for particle stability in water. As the ionic strength of a solution is increased, the extent of the electrical double layer decreases, which in turn reduces particle surface (zeta) potential (Bratby, 2006). While it is possible to reduce the thickness of the electrical double layer by increasing solution ionic strength, however, such an approach is not standard practice for particle destabilization in drinking water treatment.

In general, particles are deemed to be stable in freshwater due to low ionic strength and high electrical repulsive forces, but they are considered unstable and rapidly flocculated in salt water due to high ionic strength and low electrical repulsive forces (Limbach et al., 2008). It is believed that changing the ionic strength in water characterized by low particle content can help stimulate particle deposition during the filtration process. The objective of this study was to evaluate filter performance for the deposition of TiO_2 nanoparticles onto the well-defined porous medium (glass beads) under various water

chemistries, and to use the experimentally generated data for the simulation of natural nanoparticle removal.

6.3. Materials and Methods

Filter Media: Glass beads purchased from (Sigma Aldrich, Mississauga, Ontario) with a particle size of 425 – 600 μm (30-40 US sieve) were used in this study. The beads were soaked for 24 hours in 10% nitric acid and rinsed with Milli-Q water until a pH of 6.5 – 7 was reached. The beads were then oven-dried at 105 ºC for 24 hours and brought to room temperature (20 ºC) before being packed to the filter columns.

Water Source: Milli-Q water produced by – Millipore SAS 67120, Molsheim, France was used in all filter experiments. The water's ionic strength was altered through the addition of monovalent ions of sodium chloride (NaCl) in two different concentrations of 3.33mmol and 6.66mmol or divalent ions of calcium nitrate $Ca(NO_3)_2$, at the same concentrations used for sodium chloride (two concentrations for $Ca(NO_3)_2$). The pH was adjusted to 7 using 0.1 N NaOH, after which a concentration of 5μg/L of TiO_2 nanoparticles was added to the water samples. To establish a baseline (control), a set of experiments was conducted using Milli-Q water without chemical addition and with the pH adjusted to 7 and dosed with 5 μg/L TiO_2 nanoparticles before the column run. During the experiments, all glassware used for sample collections were thoroughly cleaned before use, as described previously in this thesis.

Ionic Strength Adjustment: NaCl and Ca $(NO_3)_2$ were used to evaluate the effect of water chemistry on TiO_2 nanoparticle deposition. To prepare water samples for the two

ionic strengths of Ca $(NO_3)_2$ used, 0.5 L of Milli-Q water was mixed once with 0.273g and once with 0.546 g of Ca $(NO_3)_2$ to obtain 10 and 20 mmol/L of Ca $(NO_3)_2$. The pH was adjusted to 7.0 by the addition of a pH 6.5 – 7 Borate buffer with an appropriate amount of 0.1N NaOH. The same procedure was repeated to obtain ionic strengths of 3.3 and 10 mmol/L of NaCl using 0.0975g and 0.195g of NaCl mixed in 0.5L of Mill-Q water, with the pH adjusted to 7 as well. Following ionic strength adjustment, samples were taken and analyzed for zeta potential, using the Zetasizer Nano Series (Malvern Instruments Inc.).

Experimental Setup: The experimental setup consisted of a feed reservoir (glass container filled with 10 L of ionic-strength-adjusted Milli-Q water), a peristaltic pump, and filter columns; Plexiglas columns – 2.5 cm I.D. x 22 cm length (see Figure 6.1). The 10L container was placed on a magnetic stirrer and continuously slow-mixed using a stir bar throughout the duration of the experiment. The peristaltic pump drew the water from the glass container and passed it through the columns at a flow rate of 50mL/min. Experiments were run for three hours each. The columns' effluent was collected every 15 minutes and analyzed for residual TiO_2 concentration using micro flow imaging (MFI). Two sets of experiments were performed with a 8mg/L alum dose and without alum addition. All experiments were conducted in duplicate and the data were averaged and plotted after a pair t-test was conducted at a 95% confidence interval.

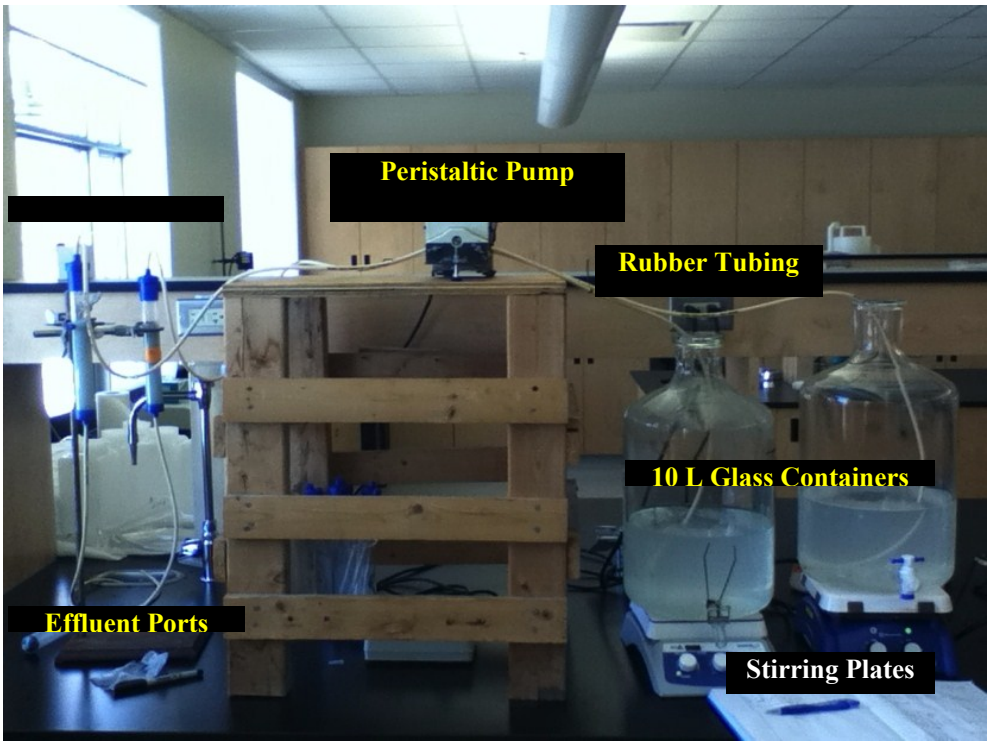

Figure 6.1: Filter Columns Experimental Setup

Sample Analysis: Samples were analyzed for zeta potential, initial TiO_2 concentration, and then collected at the start of each experiment after 2.5 minutes, and then every 15 minutes for the three-hour duration of the experiment. One millilitre of the collected effluent was analyzed using the MFI machine for TiO_2 residual concentrations. Afterward, paired t-test analysis was conducted to obtain the data average.

Filter efficiency under simulated conditions: Collision attachment efficiencies calculated for TiO_2 nanoparticles in this study were used to predict filter performance for the removal of natural nanoparticles (1-100 nm) under the following simulated conditions: collision attachment efficiencies, (α) of 0.001, 0.002 and 0.01 (calculated using equation 6.1); filtration rate (V) of 0.167 cm/s (50 mL/min); media depth (L) of 15

cm; and media grain size (d_c) of 500 µm. Equations 2.10 (Chapter 2) and 6.2 were used to calculate the filter removal efficiency (η_o) and filter coefficient (λ). A log removal was then plotted as a function of particle diameter for the aforementioned attachment efficiencies using equations 2.4 through 2.9 (see chapter 2) and equations 6.1 and 6.2.

$$\frac{C}{C_o} = \mathrm{e}^{\frac{-3(1-\varepsilon)\alpha\eta_o L}{2d_c}} \tag{6.1}$$

$$\lambda = \frac{-3(1-\varepsilon)\alpha\eta_o}{2d_c} \tag{6.2}$$

Where C and C_o are the effluent and influent TiO_2 concentrations, ε is the porosity.

6.4. Results and Discussion

Table 6.1 shows the ionic strengths calculated for the two concentrations of sodium chloride and calcium nitrate added to Milli-Q water. Table 6.1 also shows the zeta potentials measured after 2.5 minutes from the columns' startup, along with their standard deviation, with and without an 8 mg/L alum dose. From basic chemistry, it is established that both sodium and calcium, when added to water, dissociate and impart positive charge to the water. Additionally, the zeta potential measurements (both with and without alum) showed that there was significant variation between the two conditions.

Table 6.1: Solution Ionic Strength and Zeta Potential of TiO_2 Nanoparticles without and with Alum Addition.

Chemical con., mmol/L	*Ionic strength, mmol/L*	*Zeta potential (std), mV without alum addition*	*Zeta potential (std), mV with alum addition*
3.33 $Ca(NO_3)_2$	*10*	*-5.68(3.55)*	*26.8(3.99)*
3.33 NaCl	*3.3*	*-25.70(4.01)*	*24.2(3.61)*
6.66 $Ca(NO_3)_2$	*20*	*-2.64(4.16)*	*28.4(3.85)*
6.66 NaCl	*10*	*-15.60(4.39)*	*25.0(3.72)*

In cases where no alum was added, increasing the ionic strength of both calcium nitrate and sodium chloride increased the overall zeta potential of the water from -5.68 to -2.64 mV and from -25.7 to -15.6 mV, respectively. When alum was added, the overall charge of the water slightly increased due to enhanced ionic strength in both calcium and sodium concentrations (e.g., the zeta potential increased from 24.2 to 25 and from 26.8 to 28.4 mV for both Na and Ca, respectively). From the charge destabilization theory (Crittenden et al., 2005), it is known that when a suspension has a zeta potential beyond ± 30 mV, it becomes more stable. TiO_2 nanoparticles should become more dispersed and stable in water due to the increased positive charge of the suspension and therefore the potential removal by filtration should be reduced.

6.4.1 Column Experiments

The averaged results of the column experiments for TiO_2 nanoparticle deposition on glass beads are plotted as breakthrough curves in Figures 6.2 and 6.3. The fraction of TiO_2 nanoparticle concentrations (C/C_o) measured in the filter effluent samples was used to calculate the collision attachment efficiency (α) and the filter coefficient (λ) for each of the experiments performed (i.e. with and without the addition of alum). The value of C/C_o is plotted as a function of dimensionless time, t/t_{calc}. Dimensionless time is the ratio of the elapsed time, t, to the mean hydraulic residence time (t_{calc}) for the columns. The t_{calc} value used in the experiments was 1.5 minutes.

Figure 6.2 illustrates results for no alum added to the samples. At the beginning of the column run, the 10 mmol/L ionic strength of $Ca(NO_3)_2$ and the control showed relatively higher TiO_2 concentrations compared to the other samples tested. Whereas, the 3.3 and

10 mmol/L of NaCl, and the 20 mmol/L of both $Ca(NO_3)_2$ showed low TiO_2 concentrations in the filter effluent. During the filter's steady-state period, it was noted that all samples tested and the control, with exception to the 10 mmol/L of $Ca(NO_3)_2$, showed a similar reduction of TiO_2 concentrations in the filter effluent. This can be attributed to the fact that, as time goes by, TiO_2 nanoparticles (where chemicals were added) were aggregated in larger particle sizes (i.e. TiO_2 are negatively charged) and deposited onto the glass bead media.

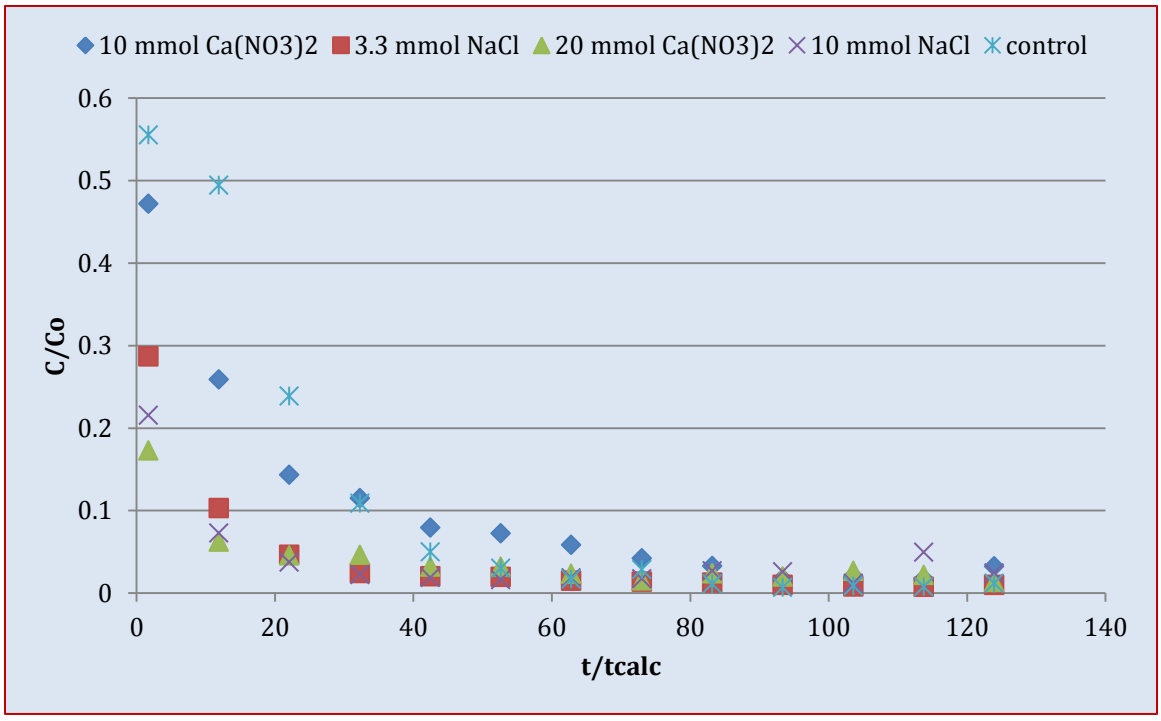

Figure 6.2: Fraction of TiO_2 Nanoparticle Concentration Remaining in the Filter Effluent as a Function of Dimensionless Time – without Alum Addition.

Figure 6.3 presents results when alum was added to the samples. Here, the plot of C/C_o versus the dimensionless time looks completely different than the plot in Figure 6.2. It shows plateau values for the remaining TiO_2 nanoparticles in the effluent when alum was added. At the beginning of the column run (Figure 6.3), the TiO_2 concentrations in the

effluent monotonically increased for all tested samples. As filtration continued, plateau values were observed for all tested samples and the control alike. However, the 10 mmol/L ionic strength of $Ca(NO_3)_2$ and NaCl showed more TiO_2 concentration in the filter effluent compared to the other three ionic strengths tested (20 mmol/L of $Ca(NO_3)_2$, 10 mmol/L of NaCl, and the control). The plateau values in Figure 6.3 could be explained by the increased positive charge in the water due to the addition of alum (in addition to the Ca^{2+} and Na^{+} cations already in the water). Repulsive forces become more dominant in the sample and created a more stable suspension, thus preventing TiO_2 nanoparticles from adhering together, thereby resisting flocculation. The excessive positive charge in the water resulted in TiO_2 nanoparticles dispersion.

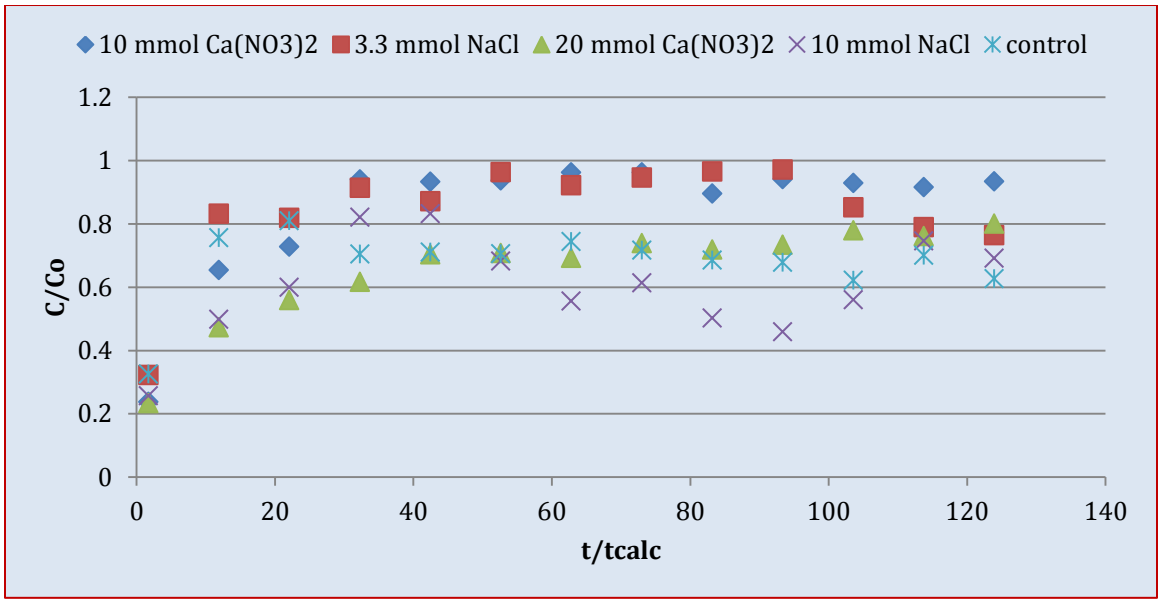

Figure 6.3: Fraction of TiO_2 Nanoparticles Influent Concentration Remaining in the Filter Effluent as a Function of Dimensionless Time – with alum Addition (averaged data).

Nonetheless, it is observed that the lower ionic strength of 10 and 3.3 mmol/L of both Ca $(NO_3)_2$ and NaCl, had a similar effect on the dispersion of TiO_2 in the samples, whereas

the higher ionic strength of 10 and 20 mmol/L of NaCl and Ca $(NO_3)_2$, respectively also had a similar impact on TiO_2 concentration dispersion in the samples (Figure 6.3). However, from the plots in Figure 6.2, it is clear that the higher ionic strength of 20 mmol/L of the divalent Ca^{2+} performed similar to the two ionic strengths of 3.3 and 10 mmol/L of the monovalent Na^+ in terms of TiO_2 nanoparticle destabilization and removal throughout the experiment. This indicates that sodium is more electrostatically attracted to the negatively charged TiO_2 nanoparticles than calcium (Bourgeois et al., 2004). Although both Ca^{2+} and Na^+ attached to TiO_2 nanoparticles, higher ionic strengths of 20 and 10 mmol/L of Ca^{2+} and Na^+, similarly reduced the electrical double layer around the TiO_2 nanoparticles at the column starts. However, during the steady state of the filter, there was no significant difference between the two elements (Na^+, Ca^{2+}). Therefore, the two ionic strengths created by the addition of sodium chloride and calcium nitrate affected TiO_2 nanoparticle removal only at the beginning of the filtration process.

With the addition of alum, Figure 6.3 shows that the 3.3 mmol/L and 20 mmol/L ionic strength of NaCl and Ca $(NO_3)_2$ had similar performances throughout the column run. The deviation observed for the higher ionic strength (10 mmol/L) of sodium chloride can be attributed to a column upset. Of particular interest is the observed performance of the control in both cases, as it followed the same trend: Figure 6.2 shows the identical performance of the 10 and 20 mmol/L concentrations of the two chemicals (sodium chloride and calcium nitrate). This trend can be explained by the fact that TiO_2 nanoparticles consistently tend to form aggregates with larger particles in the water, and thus were prone to deposition onto the media's surface.

From a water treatment perspective, this experiment emphasizes that, if TiO_2 nanoparticles were present in the water, the use of lime/carbon dioxide addition followed by coagulation with alum, as the case with JD Kline Water Supply Plant, would enhance their removal. Moreover, the addition of carbon dioxide does not decrease alkalinity but adds more carbonic acid to the water, which lowers the pH due to the shifting of the carbonate species balance. And lime ($Ca(OH)_2$), which contains calcium, helps remove particles from water by maintaining the proper pH for the most effective coagulation conditions while at the same time not increasing the carbonate content of the water.

From the column experiments, it is evident that for both Ca $(NO_3)_2$ and NaCl, the particle removal (without alum addition) was greater than 99.2% at the high ionic strength of 20 and 10 mmol/L. Therefore, altering water chemistry by changing its ionic strength can affect the removal of TiO_2 nanoparticles. The findings of this study indicate that the deposition of TiO_2 nanoparticles in the porous medium of glass beads increased with increasing ionic strength. This is consistent with the DLVO theory, which predicted a reduction of electrostatic repulsive forces between particles due to increased ionic strength. Similar findings were reached by other researchers for TiO_2 nanoparticles (Espinasse et al., 2007; Hahn & O'Melia, 2004; Lecoanet et al., 2004). In cases where alum was added, the increased positive charge led to the formation of a more stable system of TiO_2 nanoparticles, which again agrees with classical chemistry fundamentals regarding particle interaction (i.e. similar charges repel each other).

6.4.2 Collision Attachment Efficiency (α)

Figures 6.4 and 6.5 present the collision attachment efficiency plotted as a function of the remnant TiO_2 nanoparticle concentrations in the filter effluent for the experiments without and with alum addition, respectively. An exponential decay can be observed from the averaged data in the case of no alum addition (Figure 6.4). From the graph, it is observed that α was high when the TiO_2 concentration in the effluent was low. The attachment efficiency, α decreased for higher turbidity in the filter effluent, which was observed at the beginning of the filter run. Stable α values were observed when the filter was under steady state conditions. In the case when alum was added (Figure 6.5), semi-linear decay was observed which indicated stability of particles in the water.

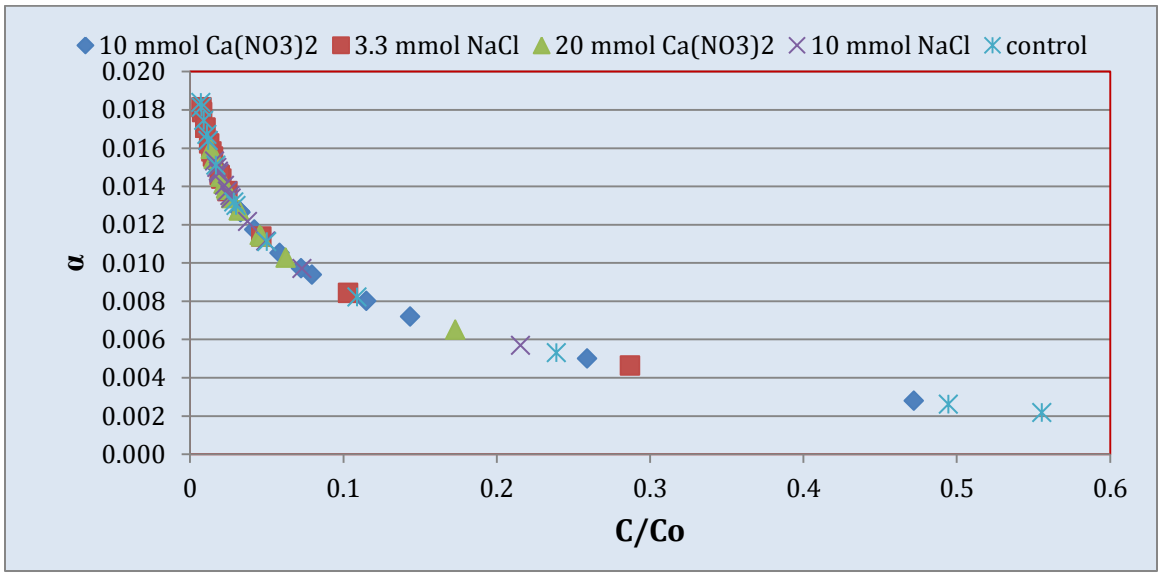

Figure 6.4: Collision Attachment Efficiency as a Function of TiO_2 Nanoparticle Influent Concentration Remaining in the Filter Effluent – without Alum Added.

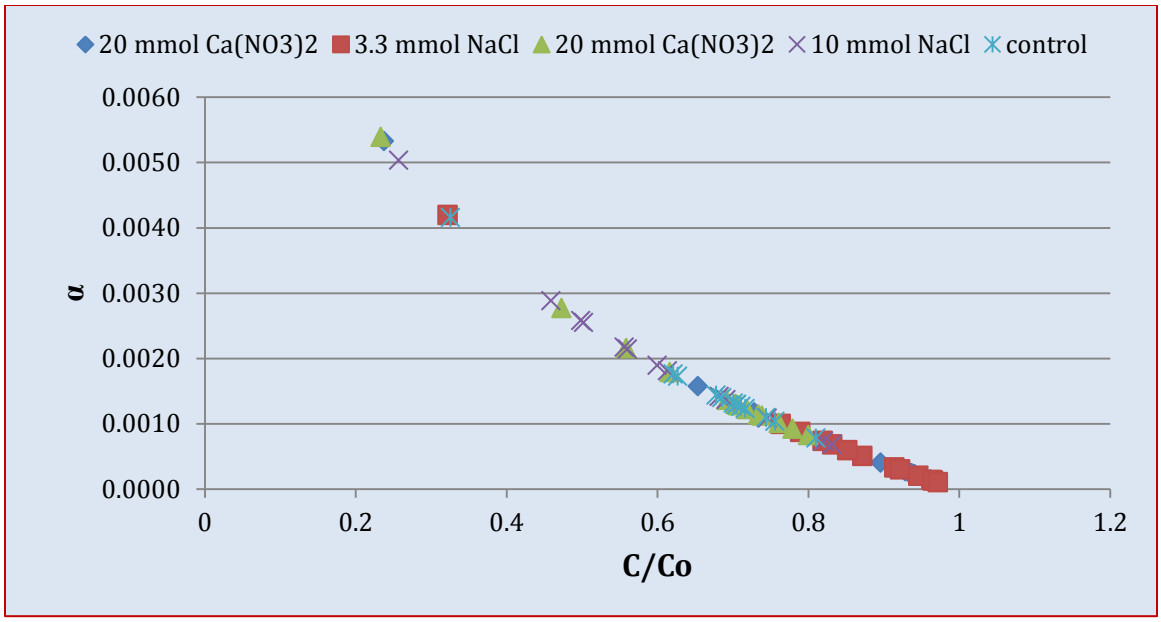

Figure 6.5: Collision Attachment Efficiency as a Function of TiO_2 Nanoparticle Influent Concentration Remaining in the Filter Effluent – with Alum Addition.

Studies conducted by Tobiason and O'Melia (1988) found α values ranging from 1 to 0.02 under both favorable and unfavorable chemical conditions. An attachment efficiency, α of 0.03 was calculated for C60 or fullerene nanoparticle deposition onto spherical silicate glass beads using sodium chloride with an ionic strength of 10 mmol/L by Espinasse et al., (2007). However, in this study, α values in the range of 0.01 to 0.02 were calculated (the focus was to investigate the unfavorable chemical conditions only, and to test how they can affect TiO_2 nanoparticle deposition). The difference between Tobiason et al., (1988) and this study is that latex particles were used in the former, whereas TiO_2 nanoparticles were used in the current study. The results above indicate that TiO_2 nanoparticles form aggregates in both solutions of Ca $(NO_3)_2$ and NaCl in the absence of alum, and that a removal efficiency greater than 99 % was achieved for both

Ca $(NO_3)_2$ and NaCl. The experiments with alum showed that no significant removal of TiO_2 nanoparticles was achieved.

Figures 6.6 and 6.7 displays filter coefficient as a function of the fraction of the TiO_2 nanoparticle concentrations remaining in the effluent. Filter coefficient is usually used to determine filter performance. However, it is site specific and depends on several factors; media properties (grain shape and size distribution, porosity, and depth), water turbidity, particle size and concentration, water density and viscosity, water temperature, level of pretreatment, and operating conditions (Crittenden et al., 2005). Figures 6.6 and 6.7 show that exponential and non-linear functions of the filter coefficient were observed in the treatment condition with and without alum. From these figures, it is apparent that the filter coefficient was slightly changed, with ionic strength increasing when no alum was added. However, it kept its value constant when alum was added, although there was a poor attachment.

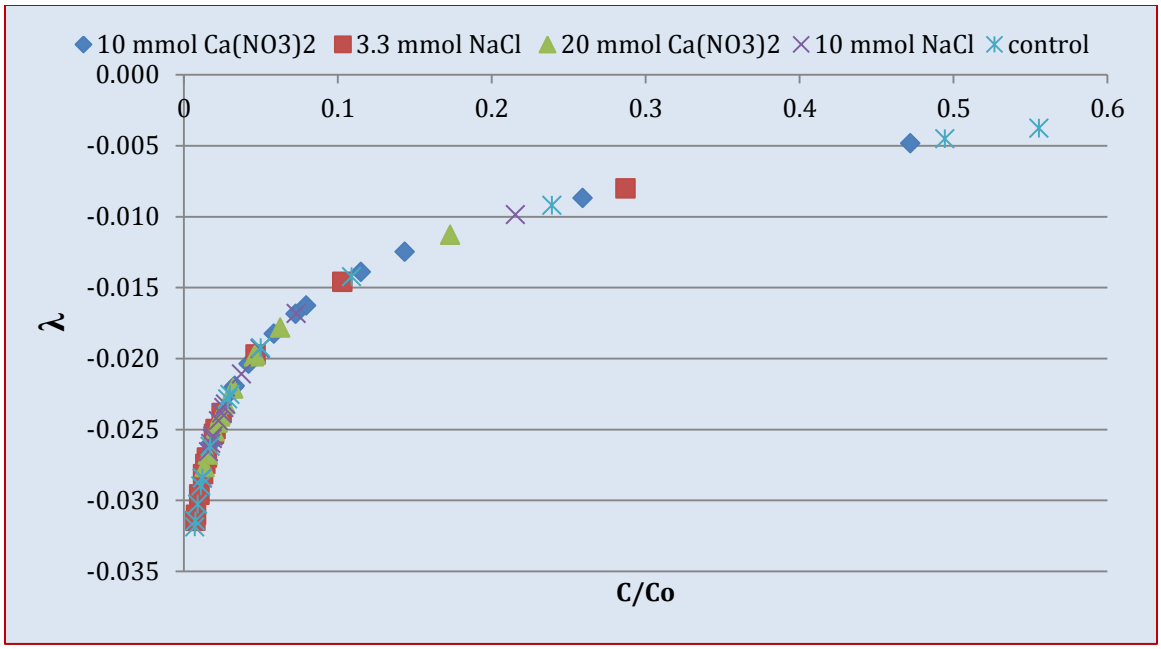

Figure 6.6: Filter Coefficient Fraction as a Function of TiO2 Nanoparticle Influent Concentration Remaining in the Filter Effluent – without Alum Addition.

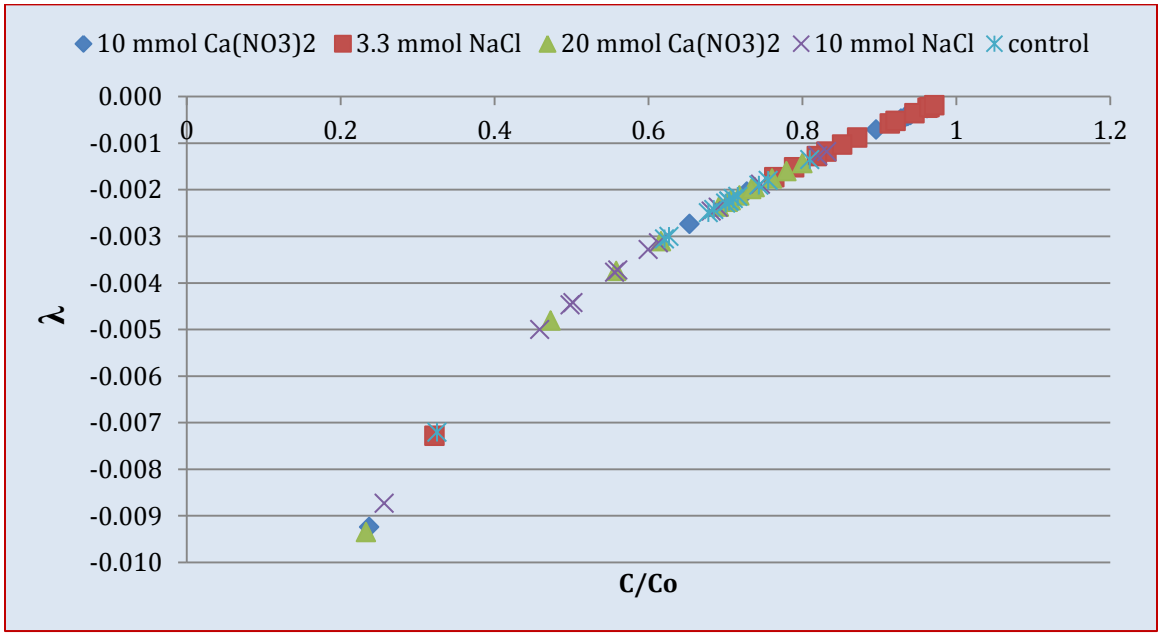

Figure 6.7: Filter Coefficient Fraction as a Function of TiO2 Nanoparticle Influent Concentration Remaining in the Filter Effluent – with Alum Addition.

6.4.3 Application of the Collision Attachment Efficiency for Nanoparticle Removal

This section aims to apply the calculated collision attachment efficiencies to simulate the removal or deposition of natural nanoparticles (1 – 100 nm). Figure 6.8 presents simulated log removal versus particle diameter for nanoparticles, calculated for the three attachment efficiencies of 0.001, 0.002, and 0.01 (obtained from the filtration experiments – see appendix C). Parameters used in the calculations were: superficial velocity (V) of 0.167 cm/s (50 ml/min); filter bed depth (L) of 15 cm; porosity of 0.4; medium grain size of 500 μm; the absolute temperature (T) of 293 K; Hamaker constant (A) of 10E-20 J, and particle density (ε) of 1.05g/cm^3.

Figure 6.8 shows that very low log removals can be achieved for the nanoparticles and that the minimal removal efficiency can be seen for nanoparticles of 100 nm size. The figure also shows that, under the simulated conditions, these nanoparticles cannot be removed but rather remain dispersed in the effluent. This can be explained by the fact that the attachment efficiency (α) bears a value ranging from zero to one. When α has a value of one, it means that every collision between a particle and media grain results in attachment. On the other hand, when α has a value of zero, it means that no particle adherence occurs, and the only way to achieve high attachment efficiency would be through proper destabilization of particles by coagulation.

Thus, it is evident from the figure that the higher α value of 0.01 provided better removal compared to the lower α values of 0.001 and 0.002. Nevertheless, these results are consistent with those reported by others (Yao et al., 1971), who noticed low removal of particles of approximately 1 μm size and increased removal of larger particles (> 1μm).

In the future, similar experiments can be conducted to simulate nanoparticle removal for different filtration rates, different filter bed depths, and higher attachment efficiencies (e.g., greater than 0.1).

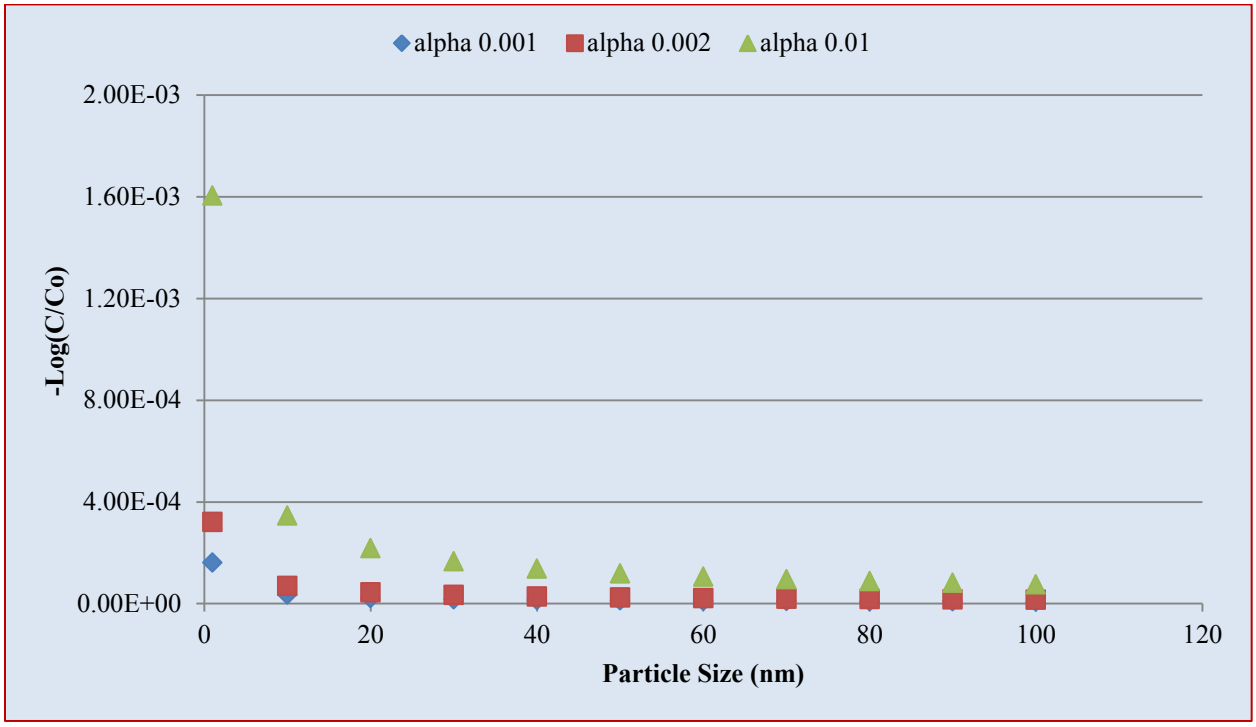

Figure 6.8: Simulated Log Removal versus Particle Size for nanoparticle sizes ranging from 1 to 100 nm calculated for filtration at three different attachment efficiencies. Parameters used in the calculations: V = 0.167 cm/s, L = 15 cm, ε = 0.4, d_c = 500 µm, T = 293 K, A= 10e-20 J, ρ_p = 1.05 g/cm.

6.5. Conclusions

In this study, the deposition of TiO_2 nanoparticles onto the well-defined porous medium (glass beads) using sodium chloride and calcium nitrate for the ionic strength alteration was evaluated. The results indicate that TiO_2 nanoparticles form aggregates with both calcium nitrate and sodium chloride in the absence of alum, and that TiO_2 removal greater than 99% was achieved for the used chemicals. Experiments with alum showed

poor deposition of TiO_2 nanoparticles due to the creation of particle stability resulting from the addition of alum, which imparts an excessive positive charge in the water.

The study showed that changing water's ionic strength assists in nanoparticle destabilization during filtration. Based on the calculated attachment efficiencies and under the simulated conditions, natural nanoparticles remain dispersed in water. The study findings are very noteworthy, as data consistent with practice has not been shown for TiO_2 nanoparticles. In the future, similar experiments can be conducted to simulate nanoparticle removal for different filtration rates, different filter bed depths, and higher attachment efficiencies (e.g., greater than 0.1).

CHAPTER 7: EXAMINING REMOVAL OF TiO_2 BY DIRECT FILTRATION UNDER BENCH-SCALE CONDITIONS

7.1. Abstract

The objective of this study was to examine the removal of TiO_2 nanoparticles from drinking water at a bench - scale level, and under operating conditions similar to those practiced at the James Douglas Kline Water Supply Plant. The physicochemical characteristics dictating fate and mobility of TiO_2 nanoparticles in water were determined. Jar tests using both raw and oxidized water from Pockwock Lake and the JD Kline Water Supply Plant, dosed with 5µg/L TiO_2 were conducted. Filter column experiments at three different coagulant dosages of 8, 15 mg/L alum, and a combined dose of 8 mg/L alum + 0.05 mg/L polymer were conducted. Visual observations from the jar testing showed that oxidized water coagulated with 8 mg/L alum gave clear supernatant, well-formed pinpoint floc and significant turbidity reduction (from 4.2 to 0.25 NTU), whereas the raw water jar testing showed a cloudy supernatant and poor floc formation, though there was a reduction in turbidity (from 1.9 to 0.4 NTU). Results from filter experiments showed that the alum dose of 15 mg/L and the combined dose of 8 + 0.05 mg/L of alum plus polymer outperformed the 8 mg/L dose of alum in terms of turbidity reduction. However, during the filter steady state period, the three doses showed a similar performance and achieved almost the same turbidity removal (less than 0.2 NTU). After a two-hour filter run time, a column experiment with an 8 mg/L alum dose started to break through, while the other two doses did not break through until the end of the experiments (i.e., after three hours). Samples were collected from column effluent, filter paper soakage, and media for TiO_2 analysis using ICP-MS. All samples analyzed for TiO_2 showed that no titanium was detected in the effluent and that the removal of titanium dioxide greater than 99.5 % was achieved. Therefore, this study demonstrated that TiO_2 nanoparticles were successfully coagulated by alum and removed by the direct filtration treatment under operating conditions similar to those practiced at the JD Kline Water Supply Plant.

7.2. Introduction

Water utilities in Nova Scotia face numerous challenges treating low turbidity water and complying with stringent guidelines and treatment standards (Eisnor et al, 2001, O'Leary et al, 2003, and Knowles 2011). Problems associated with the treatment of low-turbidity water are not confined to Nova Scotia; several other provinces such as British Columbia, Manitoba and Ontario (Braul et al., 2001) share similar water characteristics of drinking water sources. The treatment of low turbidity water is a challenge for these utilities as it requires maintaining the appropriate coagulant dosage that will ensure adequate particle and natural organic matter removal, while at the same time not enhancing the formation of disinfection by-products (Bratby 2006, Crittenden et al., 2005).

Another concern associated with the treatment of such water is that when the particle content of the water is very low, charge neutralization will not be effective due to the weak contact between destabilized particles (Petrusevski 1996). Currently, nanoparticles are not regulated as water contaminants, and thus it is unclear whether the existing filtration treatment practices are capable of removing them from drinking water. Additionally, obtaining in-depth information on their characteristics in drinking water sources would provide a valuable resource that could assist in the development of future treatment strategies.

Different particles have been used as a source in filtration studies to evaluate particle removal; styrene beads, inactivated *Giardia* and *Cryptosporidium parvum* (Assavasilavasukul et al., 2008). However, these particles are too large in size (e.g. 3 – 8 μm) for many of the naturally occurring particles in water. Thus, particles with size less

than 1 μm can be used to examine the filter's ability for the removal of nanoparticles. Problems associated with the treatment of low-turbidity water are not confined to Nova Scotia, several other provinces; British Columbia, Manitoba and Ontario (Braul et al., 2001) share similar water characteristics of drinking water sources. The objective of this study was to examine the removal of TiO_2 nanoparticles from drinking water characterized by low turbidity, alkalinity and pH, at a bench - scale level and under operating conditions similar to those practiced at the JD. Kline Water Supply Plant, Halifax, Nova, Scotia, Canada.

7.3. Materials and Methods

TiO_2 nanoparticles: Commercial TiO_2 nanoparticles (anatase, particle size 10 – 25 nm and refractive index 2.5) were purchased from Sigma Aldrich (Mississauga, Ontario, Canada). The TiO_2 physicochemical characteristics are presented in Table 7.1. These characteristics were determined using the following characterization techniques: dynamic light scattering (DLS), ultrasonic acoustic attenuation spectrometry (U/AAS), Transmission Electron Microscopy (TEM) and Brunauer-Emmet-Teller (BET) surface area techniques (Note: TEM image is not shown here). Details on these characterization techniques are described in Zhang and Kumar (2009).

Table 7.1: Physicochemical Characteristics of TiO_2 in Milli-Q Water Along with the Analytical Techniques Used for Their Determination.

Parameter	Value	Analytical Technique
Molecular Weight, g/mol	79.9	Mendeleev Periodic Table
Average particle size, nm (10 % w/v TiO_2)	120, 350	U/AAS
Average particle size, nm (0.01 w/v % TiO_2)	120 - 250	DLS and TEM
Zeta potential, mV	-20.8	Zeta Meter and DLS
pH_{zpc}	5.4	DLS
pH_{zpc}	6.2	U/AAS
BET surface area, m^2/g	120	N_2- absorption Method

Water sources: Water sources used in this study were: Milli-Q water, raw water from Pockwock Lake, and oxidized/ flocculated water from the J.D. Kline Water Supply Plant. The J.D. Kline Water Supply Plant treats water from Pockwock Lake by coagulation with alum, hydraulic flocculation, direct filtration, and chlorine disinfection. In order to work at concentrations closer to those detected for titanium dioxide in natural waters; 5 to 16 µg/L (Wigginton et al., 2007) without substantially changing water turbidity, a minimum concentration of 5 µg/L TiO_2 was used during the filter experiments, which created a turbidity of 4.2 NTU.

Jar test and Filtration Experiments: Oxidized water from the J.D. Kline Water Supply Plant was used to perform the jar test experiments. To create ideal coagulation conditions, the pH of the oxidized water was adjusted to 5.5 – 6 using 0.1 N HCl. Next, 5µg/l TiO_2 was added, creating a turbidity of 4.2 NTU. The oxidized water was then jar-tested with alum following the protocol adopted by the J.D. Kline Water Supply Plant: rapid mixing for a minute at 142 rpm (i.e. G = 100 s^{-1}) was followed by mixing at slower rates of 12.5 min at 37rpm (G = 30 s^{-1}), 26 rpm (G = 20 s^{-1}), and 17 rpm (G = 10 s^{-1}),

respectively. Following jar testing, the coagulated and flocculated water was immediately run through laboratory columns, in an attempt to mimic direct filtration treatment.

Duplicate or triplicate filtration experiments were carried out using Plexiglas columns (2.5 cm I.D. x 22 cm length). The columns were filled with two layers of media (a 10 cm layer of anthracite, with a uniformity coefficient of 1.7, over a 50 cm layer of Ottawa sand, with a uniformity coefficient of 1.5). The columns were run at a filtration rate of 50 ml/min for three hours. A set of filtration experiments was performed to determine the optimum turbidity point at which samples can be collected for TiO_2 analysis during the experiment. Three different coagulant doses; 8 and 15 mg/L of alum, and 8 mg/L of alum plus 0.05 mg/L polymer (polyacrylamide, CARUSTM 3250 – zinc and phosphate dry blend from Carus Phosphate Incorporation, LaSalle, Illinois, USA) were used. These dosages represent the same dosages used at the JD. Kline Water Supply Plant. The oxidized water was collected from the plant, jar-tested as described above, and directly fed into the filter columns with slow continuous mixing.

Effluent samples from the filter columns were collected every 15 minutes and analyzed for TiO_2. TiO_2 was analyzed for in the filter effluent, the 0.45 μm filter paper, and the upper layer of the media. Effluent samples were filtered through 0.45 μm filters, and the filtrate was preserved with 3 to 4 drops of concentrated phosphoric acid before being analyzed for TiO_2. The 0.45 μm filter paper was soaked in Milli-Q water with a pH of 4 for 20 minutes, after which it was removed and the soakage was filtered and analyzed for TiO_2. After the completion of the filtration test, the upper 1.5 cm of the media was

collected and soaked in Milli-Q water with a pH of 4 as well, mixed thoroughly, after which the soakage was again 0.45 μm filtered and analyzed for TiO_2.

Analytical Equipment: HACH 2100 Spectrophotometer (HACH Thunder Bay, Ontario, Canada) and Inductively Coupled Plasma Mass Spectrometry, ICP-MS (Thermo Fisher Scientific – Mississauga, Ontario, Canada) were used to analyze samples for turbidity and titanium residual concentration (the detection limit of the ICP-MS used for TiO_2 analysis was 2 μg/L).

7.4. Results and Discussion

7.4.1. TiO_2 Characteristics

Previous studies indicated that the physicochemical properties of TiO_2 nanoparticles determined their fate and mobility in Milli-Q water (Zhang et al., 2008). Table 7.1 represents some of the measured physicochemical characteristics for TiO_2 nanoparticles in water. Figure 7.1 shows the particle size distribution measured by U/AAS for TiO_2 in Milli-Q water, it is clear that TiO_2 nanoparticles had bimodal particle size distribution (two peaks of average sizes of 120 and 350 nm). Additionally, average particle sizes in the range of 120 to 250 were obtained for TiO_2 nanoparticles through DLS at lower concentrations (0.01 w/v % TiO_2 concentrations) and TEM (see Table 7.1). These particle sizes seem to correlate well with each other regardless of analytical equipment used. This result shows that TiO_2 in water agglomerate and form aggregates with large size in comparison to the initial size reported by the vendors. This also can be explained by the large surface area (120 m^2/g) that TiO_2 possesses.

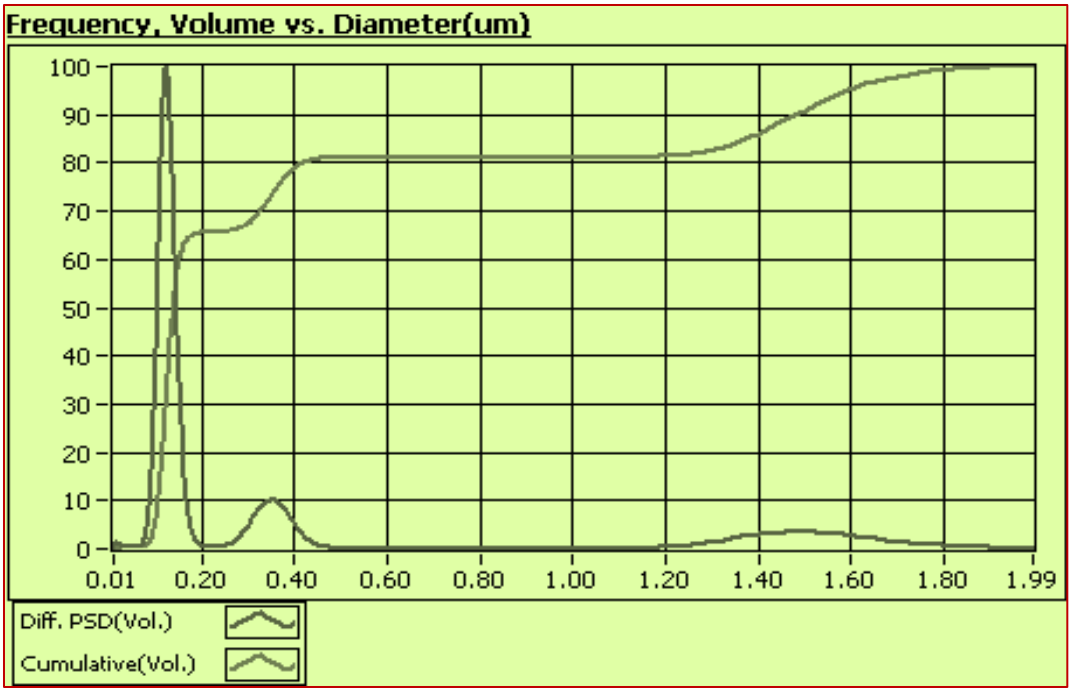

Figure 7.1: Average TiO_2 Particle Size Distribution in Milli-Q Water Determined by Ultrasound or Acoustic Attenuation Spectroscopy (U/AAS).

Figure 7.2 shows the plot of zeta potential versus pH determined for TiO_2 nanoparticles in Milli-Q water (10 w/v % TiO_2 concentration) using ultrasonic acoustic attenuation spectrometry (U/AAS). This figure shows that TiO_2 had a zero point of charge of 6.2 (pH_{zpc}), which means that TiO_2 had a positive zeta potential at acidic pH and negative zeta potentials beyond its zero point of charge. At a concentration of 0.01 w/v %, TiO_2 nanoparticles had a zero point of charge of 5.4 (Table 7.1) measured by dynamic light scattering. This result indicates that the concentration of TiO_2 nanoparticles in water influenced its size distribution and pHzpc. Other investigators found that TiO_2 pHzpc is dependent to some extent on its crystalline structure. For example, Guzman et al. (2007) reported pH_{zpc} of 5.9 and 6.3 for rutile and anatase titanium dioxide nanoparticles, respectively, Kosmulski (2002) reported pH_{zpc} of 5.4 and 5.9 for the two forms of TiO_2, and Zhang et al. (2008) reported pH_{zpc} of 5.2 for titanium dioxide nanoparticle. However,

in this study, anatase titanium dioxide was used but different analytical techniques were employed to perform the measurement. Therefore, the discrepancy in the results can be attributed not only to TiO_2 concentration but also to the type of analytical equipment used. Thus, the findings of the current study indicate that both the concentration of TiO_2 and the analytical techniques used to determine its particle size distribution and surface charge, which is why different pHzpc have been reported in literature regarding TiO_2 nanoparticles.

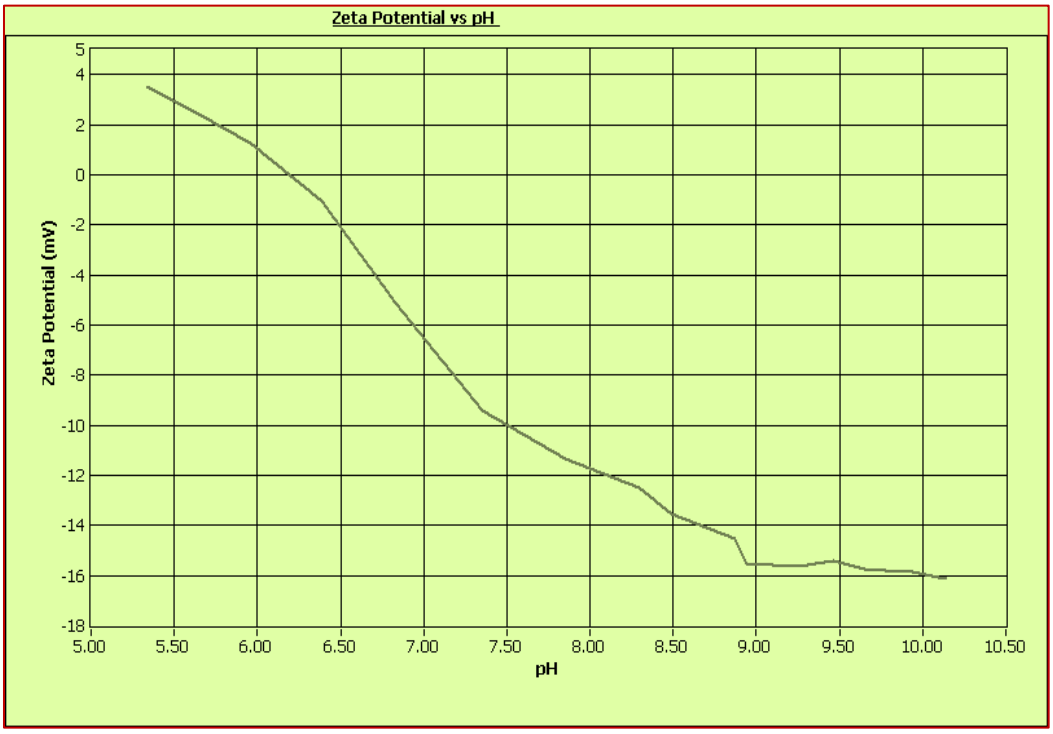

Figure 7.2: A Plot of TiO_2 Zeta Potential versus pH Determined by Titration Method Using Ultrasound or Acoustic Attenuation (U/AAS).

As stated in the objective, the core of this study was to assess the ability of direct filtration to remove TiO_2 nanoparticles under operating conditions similar to those practiced at the JD Kline Water Supply Plant. However, most researchs conducted so far

to study TiO_2 in water have been conducted at higher concentrations than those encountered in the environment (Zhang et al., 2008; Joo et al., 2009). Some researchers believed that higher concentrations might promote TiO_2 nanoparticle aggregation, and that at more realistic concentrations, TiO_2 nanoparticles might remain dispersed in water. Therefore, this study attempted to examine the removal of TiO_2 nanoparticles from water at very low concentrations (i.e. 5 μg/L).

7.4.2. Jar Test Results

Jar testing was conducted using raw water from Pockwock Lake and oxidized water from the JD Kline Water Supply Plant, both before and after the addition of TiO_2 nanoparticles. The purpose of the jar testing was to provide some indication of which water sample would provide the lowest turbidity for filtration testing (described below). Results are provided in Figure 7.3. The raw and oxidized water samples were dosed with 5μg/L TiO_2, which resulted in an initial water turbidity of 1.9 and 4.2 NTU, respectively. Visual observations of the jar test results show that oxidized water produced a clear supernatant with a well-formed fine flocs and reduction of turbidity from 4.2 to 0.3 NTU, whereas the raw water jar test showed a cloudy supernatant with poor flocs formation, though there was also a reduction in turbidity, from 1.9 to 0.4 NTU (Figure 7.3). Based on the jar test results, oxidized water was used to conduct all filter experiments.

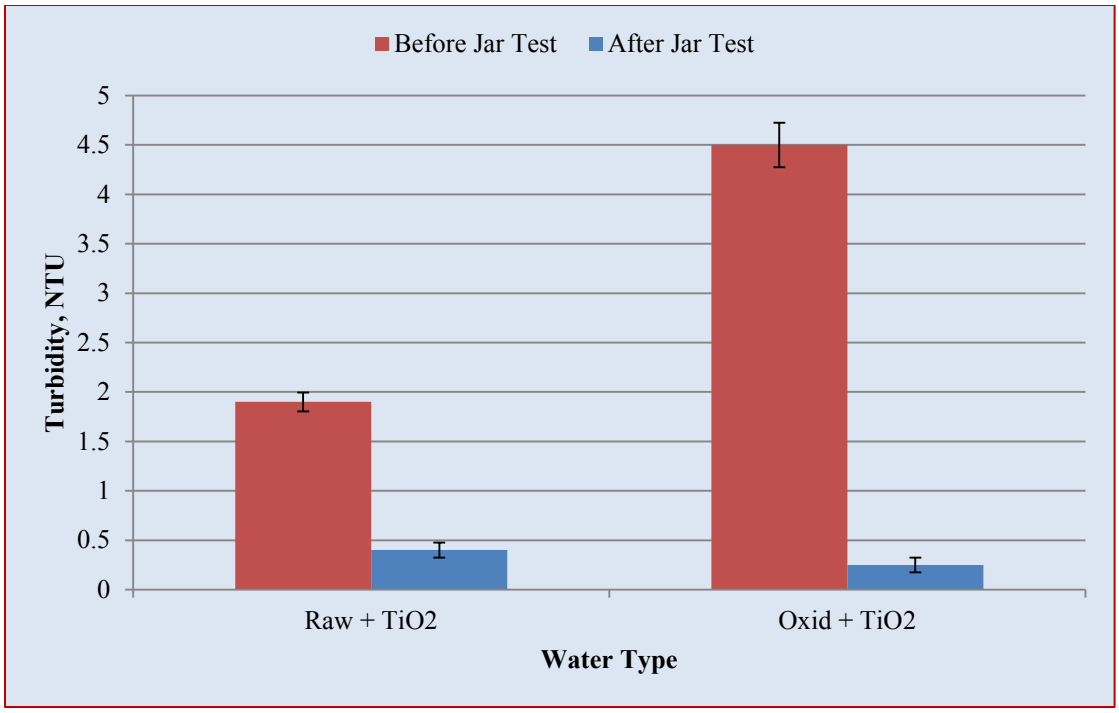

Figure 7.3: Turbidity Reduction Before and After the Jar Test of the Raw and Oxidized Water from Pockwock Lake and JD Kline Water Supply Plant, respectively.

7.4.3. Filter Experiment Results

Figure 7.4 presents breakthrough curves of the bed volumes of oxidized water spiked with the TiO_2, passed through the column media versus turbidity. This plot represents the average of three trials of the filtration experiment; with the error bars represent the standard error. The results show that a turbidity of less than 0.08 NTU was achieved after 100 bed volumes of water were passed through the filter. All samples analyzed for TiO_2 using ICP-MS showed no titanium was detected in the effluent (less than the method detection limit < 2 µg/L). This suggests that TiO_2 nanoparticles were successfully coagulated and removed by direct filtration under operating conditions similar to those practiced by the JD Kline Water Supply Plant.

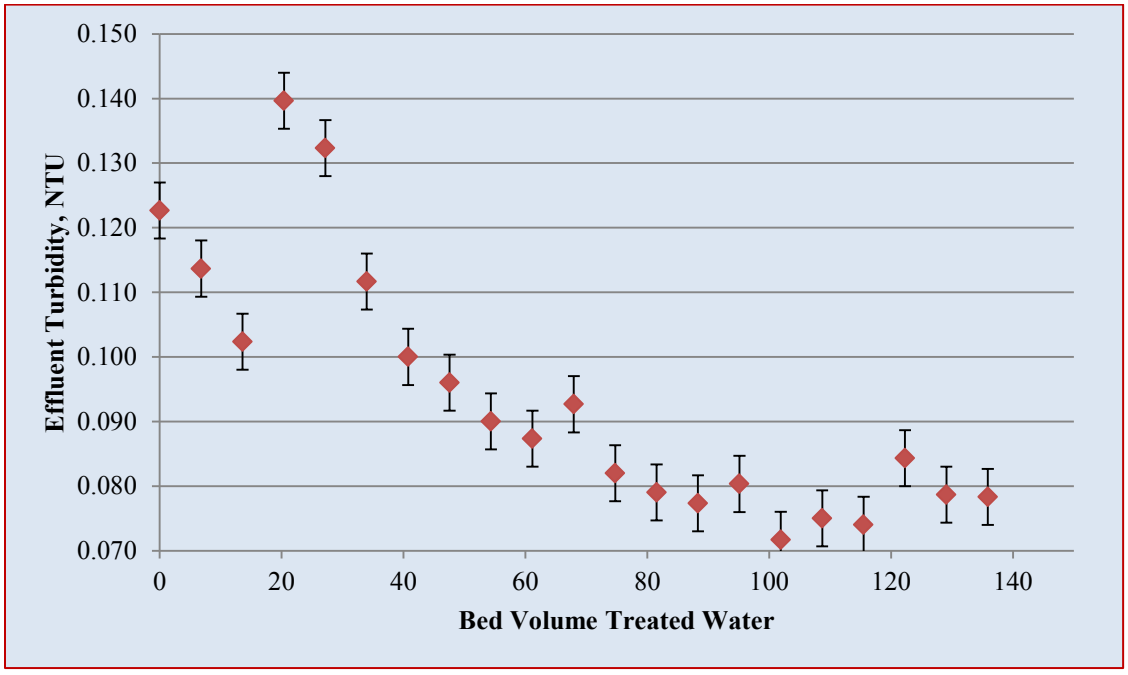

Figure 7.4: Filtration Trials for the Validation of Optimal Turbidity Point for Samples Collection of TiO_2 Residual Analysis.

Figure 7.5 shows the results of the filtration experiments for the TiO_2 nanoparticles removal at different alum dosages. From the breakthrough curves, it is clear that the higher alum dose of 15 mg/L and the combined dose of 8 plus 0.05 mg/L of alum plus polymer outperformed the lower dose of 8 mg/L of alum in terms of turbidity removal. At the filter steady state period, however, the three doses had almost similar performance and achieved similar degrees of turbidity reduction. Additionally, 133 bed volumes after the filter start time, the experiment with the low alum dose of 8 mg/L started to break through, while for the two other doses, breakthrough did not occur until the end of the experiments three hours later.

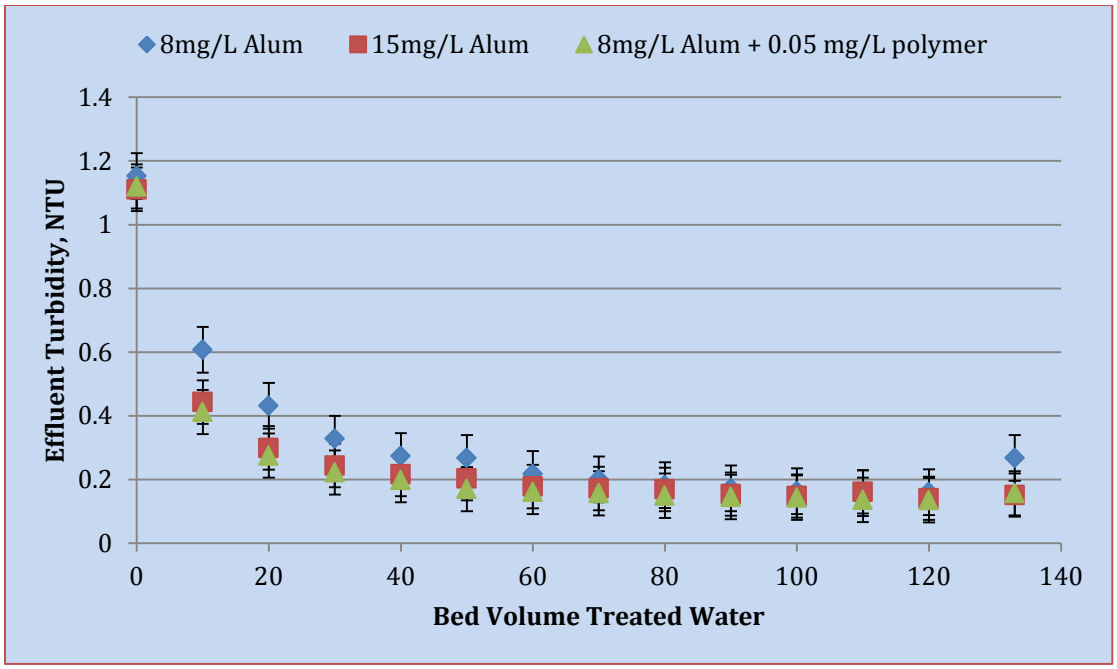

Figure 7.5: Plot of Bed Volume of Treated Water as a Function of Turbidity Reduction throughout the Filtration Experiments at Different Alum and Polymer Dosages.

The removal of TiO_2 nanoparticles in this study can be explained by the fact that TiO_2 had a negative zeta potential in water (- 20.8 mV), which promoted TiO_2 nanoparticles to be destabilized by alum. This destabilization, when combined with the filtration by the anthracite sand filter achieved low turbidity with the treatment train performed. Previous research indicated that nanoparticle removal in bed filters was found to be dominated by phenomena such as attractive Van der Waals and electrostatic repulsive forces within the electrical double layer between particles and water molecules (Bratby 2006; Wiesner and Bottero 2007). In these experiments, however, it is believed that most of the filtration work was done by the anthracite the top layer of the filter), based on an adsorption mechanism (Crittenden et al., 2005).

These findings are consistent with Gregory and Carlson (2003), who examined the effect of coagulation pH, zeta potential, and floc formation kinetics on particle removal during filtration. Specific to the water source examined in this paper, Knowles (2011) conducted a pilot-scale coagulation study at the JD Kline Water Supply Plant and clearly showed that at a higher alum dose of 15 mg/L (without polymer), filters required to be backwashed more frequently. This was attributed to the 15 mg/L alum dose tending to generate more floc formation and consequently more rapid filter clog. Nonetheless, this study showed that the higher alum dose of 15 mg/L can be used to replace the combined alum polymer dose when rapid changes in water quality are expected. However, a cost analysis and environmental viability study should first be performed to evaluate implications related to aluminum release in water before a decision is made.

To evaluate filter performance for TiO_2 removal, filter coefficient, λ needs to be calculated. Filter coefficient, λ is found to be site specific as it depends on water quality, characteristics of particulate matter, media characteristics and operating parameters. To calculate the filter coefficient, it demands to calculating the transport efficiency factor, η and attachment efficiency, α; α has values varying from 1 to 0, zero value means that no particles adhere to filter media, while a value of 1 means that every collision between a particle and medium grain leads to attachment, and proper destabilization of particles by coagulation results in achieving high attachment efficiency.

Based on this study, α and λ of 0.21 and -82.85, respectively were obtained using equations 2.3, 2.4, and 2.10 (see chapter 2). These values of α and λ when compared with

those values of 0.001, 0.002, and 0.01calculated for α, and -0.003, -0.02, and -0.01 values obtained for λ during filter performance evaluation for the deposition of TiO_2 nanoparticle under different water chemistry (chapter 6), it is clear that higher TiO_2 removal was achieved due to the proper coagulation and flocculation conditions under which the experiment was conducted.

7.5. Conclusions

Direct filtration treatment was examined for the removal of TiO_2 nanoparticles from low turbidity water, at low concentrations, and under operating conditions similar to those practiced at the JD Kline Water Supply Plant. The physicochemical characteristics of TiO_2 in water were measured using different analytical techniques. The results show that titanium dioxide had different particle size distributions and pHzpc depending on the concentration and analytical techniques used. Titanium dioxide in the water formed aggregates with particle sizes larger than its initial size reported by suppliers and had negative surface charge. Therefore, it is easily coagulated by alum, which has a positive surface charge, and subsequently removed by direct filtration.

Visual observations of the jar testing performed showed that oxidized water coagulated with 8 mg/L of alum gave a clear supernatant, well-formed flocs and noticeable turbidity reduction, whereas the raw water jar test showed a cloudy supernatant and poor flocs formation, though there was also a reduction in turbidity. Results from filtration experiments showed that the alum dose of 15 mg/L and the combined dose of 8 plus 0.05 mg/L of alum plus polymer outperformed the 8 mg/L dose of alum in terms of turbidity reduction. All samples analyzed for TiO_2 showed no titanium was detected in the

effluent, and removal in excess of 99.5% was achieved under the study conditions. This study demonstrates that TiO_2 nanoparticles can successfully be coagulated by alum and removed by direct filtration treatment under operating conditions similar to those practiced at the JD Kline Water Supply Plant, at least from the bench scale perspective.

CHAPTER 8: SUMMARY

The fundamental hypothesis of this dissertation was that synthetic nanoparticles can aggregate in a similar manner to natural particles and therefore can be removed by direct filtration from surface water characterized by low levels of pH, turbidity and alkalinity. The main objective of the dissertation was to examine direct filtration treatment for the removal of synthetic nanoparticles as a surrogate for natural nanoparticles in low turbidity water, and under operating conditions similar to those practiced at the JD Kline Water Supply Plant. Several characterizations and bench scale filter experiments were conducted to test the thesis hypothesis and satisfy its objective.

Characterization of synthetic nanoparticles in water: To choose a suitable synthetic nanoparticle as a surrogate for particle removal in filtration studies, four commercially available nanoparticles were selected and used in this research: cerium dioxide (CeO_2), ferric oxide (Fe_2O_3), silicon dioxide (SiO_2), and titanium dioxide (TiO_2). These metal oxide nanoparticles were characterized in Milli-Q water for shape, particle size, surface area and surface charge. The effect of solution pH and ionic strength on these nanoparticles at 10 and 20 mmol NaCl concentrations and pH of 4 and 10 was also studied.

Characterization experiments showed that these nanoparticles aggregate in water in a manner similar to natural particles and form aggregates with particle sizes far larger than the initial sizes declared by the suppliers. For instance, average particle sizes of 163, 370, 1554 and 2169 nm were measured for CeO_2, Fe_2O_3, SiO_2 and TiO_2, respectively. Surface

areas of 35.7, 455.9 and 120.1 m^2/g were measured for Fe_2O_3, SiO_2 and TiO_2, respectively. (A surface area for CeO_2 was not measured but instead taken from Limbach et al. [2008]). The zeta potentials and zero points of charge (pH_{zpc}) of 22.5, 16.02, -20.8 and -23.8 mV, and 8.2, 7.5, 1.8 and 5.4 were measured for CeO_2, Fe_2O_3, SiO_2 and TiO_2, respectively (measured at a pH of 6±0.02 and ionic strengths of 0.1 M $NaNO_3$ in 10 mg/L nanoparticle concentrations).

From the pH and ionic strength experiments, it was found that increasing water's ionic strength at pH 4 decreased the zeta potential for TiO_2 and Fe_2O_3 and increased it for CeO_2, whereas the zeta potential for SiO_2 was only slightly changed. Meanwhile, increasing the ionic strength from 10 to 20 mmol NaCl increased the zeta potential of the four investigated metal oxide nanoparticles, with the average particle size of the studied nanoparticles appeared to be pH- and ionic strength-dependent. Based on these results and on interpretations of zeta potential values, titanium dioxide (TiO_2) was selected as the surrogate to examine particle removal with in all filtration experiments.

Characterization of Pockwock water for naturally occurring nanoparticles: Water samples from Pockwock Lake were characterized for naturally occurring nanoparticles by applying a stepwise filtration procedure, through which larger particles (> 0.45 μm) were separated from the samples. Three techniques – atomic force microscopy (AFM), transmission electronic microscopy (TEM), and dynamic light scattering (DLS) – were used for characterization. The results obtained through these techniques correlate perfectly with each other with regards to particle size, shape, and structure. Three distinct

populations of naturally occurring nanoparticles were identified in Pockwock water through DLS, with average particle sizes of 2.3, 15.7 and 58.8 nm. The TEM images showed nanoparticles of spherical, elongated and irregular shapes, with diameters ranging from 1 to 200 nm.

AFM images revealed the same structures as those imaged by TEM and emphasized the spherical and irregular shape aggregates for the natural nanoparticles in Pockwock water. A 3D AFM plot revealed that the structural morphology of those natural nanoparticles appeared to have hill-like structures, with a sharp apex, a diameter of 0.5 – 40 nm, and a height of 0.5 – 33 nm. Similar topographical structures, whether spherical, fibrous or irregular, have been reported for clay and humic acid nanoparticles in ground- and freshwater. However, AFM images of Pockwock water filtered through 0.45, 0.1 and 0.05 μm showed only spherical structures, with diameters and heights of 44 and 20 nm, 33 and 4 nm, and 15.5 and 1.4 nm, respectively. These dimensions were in agreement with those reported in the literature for humic acids in groundwater. It is believed that natural nanoparticles in Pockwock water could be regarded as a complex mixture of humic acids, clay, and other inorganic nanoparticles, and that these nanoparticles could impair or enhance deposition or transport of other particles in water.

Evaluating filter performance for the deposition of TiO_2 nanoparticles: To evaluate the filter performance of the TiO_2 nanoparticle deposition onto well-defined porous media (glass beads), bench scale filter experiments were conducted at various water ionic strengths, and the generated data were used to calculate collision attachment efficiency

(α) and filter coefficients (λ). The calculated filter parameters (i.e., α and λ) were then used to simulate the removal of naturally occurring nanoparticles. Sodium chloride and calcium nitrate of two ionic strengths each (3.3 and 10 mmol/L, and 10 and 20 mmol/L, respectively) with and without alum, were used to study TiO_2 nanoparticle deposition and attachment. A very low attachment coefficient (α) of 0.01 and 0.002, and a filter coefficient (λ) of -0.003 and -0.02 were calculated, without and with alum addition, respectively. Filter experiments showed that TiO_2 nanoparticle deposition was affected by the water's ionic strength, and that aggregation increased as the ionic strength increased, when no alum was added. However, with the addition of alum, the particles remained dispersed in water and became more stable, due to excessive positive charges. The study showed that changing the ionic strength of the water helps to simulate particle deposition during filtration treatment. Based on the calculated attachment efficiencies and under the simulated conditions, natural nanoparticles are unlikely to be removed from water by direct filtration treatment.

Examining direct filtration for the removal of TiO_2 nanoparticles: Jar test and bench scale filtration experiments were conducted to test the ability of direct filtration treatments to remove titanium dioxide nanoparticles from water under operating conditions similar to those practiced at the JD Kline Water Supply Plant. Observations from the jar test showed that oxidized water coagulated with 8 mg/L alum gave a clear supernatant, well-formed fine flocs, and significant turbidity reduction (from 4.2 to 0.25 NTU), whereas the raw water jar test showed a cloudy supernatant and poor flocs formation, although there was a reduction in turbidity (from 1.9 to 0.4 NTU). Results of

filtration experiments showed that the alum dose of 15 mg/L and the combined dose of 8 + 0.05 mg/L of alum plus polymer worked better than the 8 mg/L dose of alum in terms of turbidity removal after the filter start and ripening period. However, during the filter steady state period, the three doses showed a similar performance and achieved almost the same turbidity values less than 0.2 NTU.

Moreover, two hours following the filter start time, the experiment with the 8 mg/L alum dose started to breakthrough, while the two other doses did not break through until the end of the experiments (after three hours). Titanium was not detected in the effluent (less than the method detection limit < 2 μg/L) for all samples analyzed for TiO_2 using ICP-MS. These findings demonstrate that TiO_2 nanoparticles were successfully coagulated with alum and easily removed by direct filtration under operating conditions similar to those practiced at the JD Kline Water Supply Plant. This work represents a key step in the characterization of source waters with low turbidity and particle content such as Pockwock Lake, and is the first of its kind in Atlantic Canada.

CHAPTER 9: CONCLUSIONS AND RECOMMENDATIONS

9.1. Conclusions

This research project was successful with regards to the characterization and removal of synthetic nanoparticles through direct filtration treatment in water exhibiting low particle content and turbidity. Additionally, this research is considered to be a road map for other utilities with similar water characteristics to optimize their filtration treatment for particle removal. The dissertation hypothesis and objectives were successfully tested and satisfied. Moreover, based on the experimental results described throughout the dissertation, the following conclusions can be made.

1 Characterization experiments show that synthetic nanoparticles did aggregate in a similar fashion to natural particles, and form aggregate with sizes larger than their initial sizes reported to them by the vendors. Among the four studied synthetic nanoparticles, only TiO_2 nanoparticles can easily be coagulated with alum due to their negative surface potential and zero point of charge, and could easily be coagulated by 8 mg/L alum dose and therefore removed by direct filtration. Based on the interpretation of characterization results, TiO_2 nanoparticles were selected to carry out all bench scale filter experiments with.

2 A stepwise filtration procedure for water sample preparation and detection was developed. Through this procedure, water samples from Pockwock Lake were characterized for the naturally occurring and synthetic nanoparticles. Three analytical techniques – transmission electron microscopy (TEM), dynamic light

scattering (DLS), and atomic force microscopy (AFM) – were used to analyze for nanopartilces. The use of these three techniques allowed for the comparison and validation of the results. Three distinctive populations of naturally occurring nanoparticles were identified in Lake Pockwock water, with average sizes of 2.3, 15.7, and 58.8 nm, and with spherical, elongated and irregular shapes. The identified natural nanoparticles are believed to be humic acids, clay, or inorganic nano-colloid structures. These findings are consistent with what has been reported in the literature.

3 TiO_2 deposition on a well-defined porous medium showed that TiO_2 nanoparticles form aggregates with both calcium nitrate and sodium chloride in the absence of alum. A removal efficiency of greater than 99 % was achieved for both Ca $(NO_3)_2$ and NaCl chemicals, respectively. However, experiments with alum showed a poor deposition of TiO_2 nanoparticles due to the creation of nanoparticle stability resulting from the addition of alum, which imparts an excessive positive charge in the water.

4 Direct filtration treatment was examined for the removal of TiO_2 nanoparticles from water characterized by low turbidity and particle content, under operating conditions similar to those practiced at the JD Kline Water Supply Plant. This research results demonstrate that TiO_2 nanoparticles can successfully be coagulated by 8 mg/L alum dose. Removal greater than 95 % was, and all samples analyzed for TiO_2 residual showed that no titanium was detected in the filter effluent.

5 The overall research findings represent a major step forward in nanoparticle characterization and removal in drinking water source such as Pockwock Lake, as data consistent with practice had not previously been shown for smaller particles such as TiO_2 nanoparticles. And as such, the research findings contribute to the optimization of water treatment processes for nanoparticle removal in water characterized by low turbidity.

9.2. Recommendations

Based on the findings of this research project, several recommendations for further investigation related to nanoparticle characterization and removal in drinking water can be made.

1 Further research on additional nanoparticle characteristics in other drinking water sources, at environmentally sound concentrations, should be carried out on both raw and treated water samples. This would be of great value to JD Kline Water Supply Plant and other utilities dealing with water of similar quality characteristics. Moreover, a timely source of data and information that can assist in developing informative treatment solutions could be created; bearing in mind the stringent water quality guidelines and standards that may require water utilities to meet certain limits for nanoparticles as water contaminants.

2 Pilot scale studies should be performed to investigate nanoparticle removal throughout a complete treatment train to determine the actual particle removal rate of the filters. This might help optimize filtration treatment for nanoparticle removal along with disinfection by-products created from the natural organic matter removal and chlorine disinfection processes.

3 Site-specific analytical procedures for nanoparticle detection, along with reliable monitoring protocols that can aid a better understanding of nanoparticle behavior in water in terms of dispersion, transport, deposition and removal, should be developed.

References

Abdallah, E., & Gagnon, G. (2009). Arsenic removal from groundwater through iron oxyhydroxide coated waste products. *Canadian Journal of Civil Engineering, 36*(5), 881-888.

Amirtharajah, A. (1988). Some theoretical and conceptual views of filtration. *Journal American Water Works Association, 80*(12), 36-46.

Assavasilavasukul, P., Lau, B. L. T., Harrington, G. W., Hoffman, R. M., & Borchardt, M. A. (2008). Effect of pathogen concentrations on removal of< i> Cryptosporidium</i> and< i> Giardia</i> by conventional drinking water treatment. *Water Research, 42*(10), 2678-2690.

Bourgeois, J., Walsh, M., & Gagnon, G. (2004). Treatment of drinking water residuals: Comparing sedimentation and dissolved air flotation performance with optimal cation ratios. *Water Research, 38*(5), 1173-1182.

Bratby, J. (2006). *Coagulation and flocculation in water and wastewater treatment* Intl Water Assn.

Braul, L., Viraraghavan, T., & Corkal, D. (2001). Cold water effects on enhanced coagulation of high DOC, low turbidity water. *Water Quality Research Journal of Canada, 36*(4), 701-717.

Cleasby, J., & Logsdon, G. (1999). Granular bed and precoat filtration. *Water Quality and Treatment.New York, McGraw Hill, Inc,* , 8.1-8.99.

Crittenden, J., & Harza, M. W. (2005). *Water treatment: Principles and design* John Wiley & Sons.

De Momi, A., & Lead, J. R. (2008). Behaviour of environmental aquatic nanocolloids when separated by split-flow thin-cell fractionation (SPLITT). *Science of the Total Environment, 405*(1-3), 317-323. Retrieved from http://dx.doi.org/10.1016/j.scitotenv.2008.05.032

Domingos, R. F., Baalousha, M. A., Ju-Nam, Y., Reid, M. M., Tufenkji, N., Lead, J. R., Wilkinson, K. J. (2009). Characterizing manufactured nanoparticles in the environment: Multimethod determination of particle sizes. *Environmental Science & Technology, 43*(19), 7277-7284.

Eisnor, J. D., O'Leary, K. C., & Gagnon, G. A. (2001). Evaluation of particle removal at water treatment plants in nova scotia. *Water Quality Research Journal of Canada, 36*(1), 105-119.

U.S. EPA (2010). Nanomaterial Case Studies: Nanoscale Titanium Dioxide in Water Treatment and in Topical Sunscreen (Final). U.S. Environmental Protection Agency, Washington, DC, EPA/600/R-09/057F, 2010.

Espinasse, B., Hotze, E. M., & Wiesner, M. R. (2007). Transport and retention of colloidal aggregates of C60 in porous media: Effects of organic macromolecules, ionic composition, and preparation method. *Environmental Science & Technology, 41*(21), 7396-7402.

Filella, M., Zhang, J., Newman, M. E., & Buffle, J. (1997). Analytical applications of photon correlation spectroscopy for size distribution measurements of natural colloidal suspensions: Capabilities and limitations. *Colloids and Surfaces A: Physicochemical and Engineering Aspects, 120*(1-3), 27-46.

Franson, M. A. H. (1995). *Standard methods for the examination of water and wastewater* CRC Press.

French, R. A., Jacobson, A. R., Kim, B., Isley, S. L., Penn, R. L., & Baveye, P. C. (2009). Influence of ionic strength, pH, and cation valence on aggregation kinetics of titanium dioxide nanoparticles. *Environmental Science & Technology, 43*(5), 1354-1359.

Gregory, D., & Carlson, K. (2003). Relationship of pH and floc formation kinetics to granular media filtration performance. *Environmental Science & Technology, 37*(7), 1398-1403.

Gregory, J. (2005). *Particles in water: Properties and processes*. Boca Raton, FL: CRC Press.

Guo, J., & Ma, J. (2006). AFM study on the sorbed NOM and its fractions isolated from river songhua. *Water Research, 40*(10), 1975-1984.

Guzman, K. A. D., Finnegan, M. P., & Banfield, J. F. (2006). Influence of surface potential on aggregation and transport of titania nanoparticles. *Environmental Science & Technology, 40*(24), 7688-7693.

Hahn, M. W., & O'Melia, C. R. (2004). Deposition and reentrainment of brownian particles in porous media under unfavorable chemical conditions: Some concepts and applications. *Environmental Science & Technology, 38*(1), 210-220.

Hassellöv, M., & Kaegi, R. (2009). Analysis and characterization of manufactured nanoparticles in aquatic environments. *Environmental and Human Health Impacts of Nanotechnology,* , 211-266.

Hassellöv, M., Readman, J. W., Ranville, J. F., & Tiede, K. (2008). Nanoparticle analysis and characterization methodologies in environmental risk assessment of engineered nanoparticles. *Ecotoxicology, 17*(5), 344-361.

Health Canada, (2004). Guidelines for Canadian drinking Water Quality: Guideline Technical Document – Giardia and Cryptosporidium. Water Quality and Health Bureau, Healthy Environments and Consumer Safety Branch, Ottawa, Canada.

Horcas, I., Fernández, R., Gómez-Rodríguez, J., Colchero, J., Gómez-Herrero, J., & Baro, A. (2007). Top 20 most downloaded articles. *Rev. Sci. Instrum., 78*, 013705.

Hunter, R. J. (1981). *Zeta potential in colloid science: Principles and applications* Academic press London.

Instruments, M. (2007). Zetasizer nano user manual. *Malvern Instruments Ltd., Worcestershire WR14 1XZ, UK,*

Jegatheesan, V., & Vigneswaran, S. (2005). Deep bed filtration: Mathematical models and observations. *Critical Reviews in Environmental Science and Technology, 35*(6), 515-569.

Jing, C., Meng, X., Liu, S., Baidas, S., Patraju, R., Christodoulatos, C., & Korfiatis, G. P. (2005). Surface complexation of organic arsenic on nanocrystalline titanium oxide. *Journal of Colloid and Interface Science, 290*(1), 14-21.

Joo, S. H., Al-Abed, S. R., & Luxton, T. (2009). Influence of carboxymethyl cellulose for the transport of titanium dioxide nanoparticles in clean silica and mineral-coated sands. *Environmental Science & Technology, 43*(13), 4954-4959.

Kaegi, R., Wagner, T., Hetzer, B., Sinnet, B., Tzvetkov, G., & Boller, M. (2008). Size, number and chemical composition of nanosized particles in drinking water

determined by analytical microscopy and LIBD. *Water Research, 42*(10-11), 2778-2786.

Kawamura, S. (1975). Design and operation of high-rate filters-part 1. *Journal American Water Works Association, 67*(10), 535-544.

Kim, J., & Tobiason, J. E. (2004). Particles in filter effluent: The roles of deposition and detachment. *Environmental Science & Technology, 38*(22), 6132-6138.

Knowles, A. (2011). Optimizing the removal of natural organic matter in drinking water while avoiding unintended consequences following coagulation.

Korich, D., Mead, J., Madore, M., Sinclair, N., & Sterling, C. R. (1990). Effects of ozone, chlorine dioxide, chlorine, and monochloramine on cryptosporidium parvum oocyst viability. *Applied and Environmental Microbiology, 56*(5), 1423-1428.

Kosmulski, M. (2002). The significance of the difference in the point of zero charge between rutile and anatase. *Advances in Colloid and Interface Science, 99*(3), 255-264.

Lead, J., Davison, W., Hamilton-Taylor, J., & Buffle, J. (1997). Characterizing colloidal material in natural waters. *Aquatic Geochemistry, 3*(3), 213-232.

Lead, J., Muirhead, D., & Gibson, C. (2005). Characterization of freshwater natural aquatic colloids by atomic force microscopy (AFM). *Environmental Science & Technology, 39*(18), 6930-6936.

Lecoanet, H. F., Bottero, J. Y., & Wiesner, M. R. (2004). Laboratory assessment of the mobility of nanomaterials in porous media. *Environmental Science & Technology, 38*(19), 5164-5169.

Lien, H. L., & Zhang, W. (2001). Nanoscale iron particles for complete reduction of chlorinated ethenes. *Colloids and Surfaces A: Physicochemical and Engineering Aspects, 191*(1-2), 97-105.

Limbach, L. K., Bereiter, R., Müller, E., Krebs, R., Gälli, R., & Stark, W. J. (2008). Removal of oxide nanoparticles in a model wastewater treatment plant: Influence of agglomeration and surfactants on clearing efficiency. *Environmental Science & Technology, 42*(15), 5828-5833.

Mahmood, T., Amirtharajah, A., Sturm, T. W., & Dennett, K. E. (2000). A micromechanics approach for attachment and detachment of asymmetric colloidal particles. *Colloids and Surfaces A: Physicochemical and Engineering Aspects, 177*(2-3), 99-110.

McDowell-Boyer, L. M., Hunt, J. R., & Sitar, N. (1986). Particle transport through porous media. *Water Resour.Res, 22*(13), 1901-1921.

Muirhead, D., & Lead, J. (2003). Measurement of the size and structure of natural aquatic colloids in an urbanised watershed by atomic force microscopy. *Hydrobiologia, 494*(1), 65-69.

Nowack, B., & Bucheli, T. D. (2007). Occurrence, behavior and effects of nanoparticles in the environment. *Environmental Pollution, 150*(1), 5-22.

Nurmi, J. T., Tratnyek, P. G., Sarathy, V., Baer, D. R., Amonette, J. E., Pecher, K., . . . Penn, R. L. (2005). Characterization and properties of metallic iron nanoparticles: Spectroscopy, electrochemistry, and kinetics. *Environmental Science & Technology, 39*(5), 1221-1230.

O'Leary, K., Eisnor, J., & Gagnon, G. (2003). Examination of plant performance and filter ripening with particle counters at full-scale water treatment plants. *Environmental Technology, 24*(1), 1-9.

O'Melia, C. R., & Stumm, W. (1967). Theory of water filtration.

Perret, D., Newman, M. E., Negre, J. C., Chen, Y., & Buffle, J. (1994). Submicron particles in the rhine river--I. physico-chemical characterization. *Water Research, 28*(1), 91-106.

Petrusevski, B. (1996). Algae and particle removal in direct filtration of biesbosch water : Influence of algal characteristics, oxidation and other pre-treatment conditions. Rotterdam ;Brookfield, VT: A.A. Balkema.

Pettibone, J. M., Cwiertny, D. M., Scherer, M., & Grassian, V. H. (2008). Adsorption of organic acids on TiO2 nanoparticles: Effects of pH, nanoparticle size, and nanoparticle aggregation. *Langmuir, 24*(13), 6659-6667.

Plaschke, M., Römer, J., & Kim, J. (2002). Characterization of gorleben groundwater colloids by atomic force microscopy. *Environmental Science & Technology, 36*(21), 4483-4488.

Rajagopalan, R., & Tien, C. (1976). Trajectory analysis of deep-bed filtration with the sphere-in-cell porous media model. *AICHE Journal, 22*(3), 523-533.

Rose, J., Thill, A., & Brant, J. (2007). Methods for structural and chemical characterization of nanomaterials. *Environmental Nanotechnology.Applications and Impacts of Nanomaterials,* 105-154.

Santschi, P. H., Balnois, E., Wilkinson, K. J., Zhang, J., Buffle, J., & Guo, L. (1998). Fibrillar polysaccharides in marine macromolecular organic matter as imaged by

atomic force microscopy and transmission electron microscopy. *Limnology and Oceanography,* 896-908.

Sellers, K. (2009). *Nanotechnology and the environment*. Boca Raton: CRC Press.

Sharma, D. K., King, D., Oma, P., & Merchant, C. (2010). Micro-flow imaging: Flow microscopy applied to sub-visible particulate analysis in protein formulations. *The AAPS Journal, 12*(3), 455-464.

Tien, C., & Payatakes, A. C. (1979). Advances in deep bed filtration. *AICHE Journal, 25*(5), 737-759.

Tobiason, J. E., & O'melia, C. R. (1988). Physicochemical aspects of particle removal in depth filtration. *Journal American Water Works Association, 80*(12), 54-64.

Tufenkji, N., & Elimelech, M. (2004). Correlation equation for predicting single-collector efficiency in physicochemical filtration in saturated porous media. *Environmental Science & Technology, 38*(2), 529-536.

Vadasarukkai, Y. S., Gagnon, G. A., Campbell, D. R., & Clark, S. C. (2011). Assessment of hydraulic flocculation processes using CFD. *Journal AWWA, 103*(11)

Wang, C. B., & Zhang, W. X. (1997). Synthesizing nanoscale iron particles for rapid and complete dechlorination of TCE and PCBs. *Environmental Science & Technology, 31*(7), 2154-2156.

Wiesner, M. R., & Jean-Yves. Bottero. (2007). *Environmental nanotechnology* McGraw-Hill Professional.

Wigginton, N. S., Haus, K. L., & Hochella Jr, M. F. (2007). Aquatic environmental nanoparticles. *J.Environ.Monit., 9*(12), 1306-1316.

Wolf, R. E. (2005). What is ICP-MS? … and more importantly, what can it do? Retrieved from http://minerals.cr.usgs.gov/icpms/What_is_ICPMS.pdf.

Yao, K. M., Habibian, M. T., & O'Melia, C. R. (1971). Water and waste water filtration. concepts and applications. *Environmental Science & Technology, 5*(11), 1105-1112.

Yiacoumi, S. (2010). Coagulation and flocculation. *Water Quality & Treatment: A Handbook on Drinking Water,*

Zeta-APS Operation Manual, version 1.0, (2004). Particle size and zeta potential analysis… at high solids. Matec Applied Sciences, 56 Hudson St. Northborough, MA 01532.

Zhang, S., Li, L., & Kumar, A. (2009). *Materials characterization techniques* CRC Press.

Zhang, Y., Chen, Y., Westerhoff, P., & Crittenden, J. (2009). Impact of natural organic matter and divalent cations on the stability of aqueous nanoparticles. *Water Research, 43*(17), 4249-4257.

Zhang, Y., Chen, Y., Westerhoff, P., Hristovski, K., & Crittenden, J. C. (2008). Stability of commercial metal oxide nanoparticles in water. *Water Research, 42*(8-9), 2204-2212.

APPENDIX A NANOPARTICLES CHARACTERIZATION RAW DATA

BET Surface Area of Nanoparticles

Sample mass		1st, (m^2/g)	2nd (m^2/g)	Mean (m^2/g)	S.A (m^2/g)	BET aver
CeO_2	Adsorbed		NA	NA	32	32
	Desorbed		NA	NA	32	
SiO_2	Adsorbed	22.8	22.7	22.75	455	455.9
	Desorbed	22.89	22.79	22.84	456.8	
TiO_2	Adsorbed	21.53	21.57	21.55	120.39	120.11
	Desorbed	21.49	21.41	21.45	119.83	
Fe_2O_3	Adsorbed		NA	NA	35.8	35.65
	Desorbed		NA	NA	35.5	

NA* not available

	Nanoparticles Zeta Potentials in mV			
	Fe_2O_3	TiO_2	SiO_2	CeO_2
	15.3	-27.8	-20.77	22.63
	16.35	-23.33	-20.81	22.02
	16.15	-22.42	-19.89	21.61
	16.03	-22.37	-21.8	23.49
	16.23	-22.9	-21.36	22.84
average	16.01	-23.76	-20.93	22.52
Std	0.37	2.05	0.64	0.65
95%	0.010	0.057	0.018	0.018

APPENDIX B FILTRATION EXPERIMENTS RAW DATA

Filter Columns Experiments for TiO2 Removal

Time, min	Column 1	Column2	d	average	STD	SEM	PVT
0	0.25	0.23	0.0200	0.240	0.014	0.010	0
5	0.26	0.24	0.0200	0.250	0.014	0.010	3
10	0.23	0.23	0.0000	0.230	0.000	0.000	7
15	0.21	0.21	0.0000	0.210	0.000	0.000	10
20	0.20	0.19	0.0100	0.195	0.007	0.005	13
25	0.18	0.17	0.0100	0.175	0.007	0.005	17
30	0.16	0.15	0.0100	0.155	0.007	0.005	20
35	0.15	0.14	0.0775	0.145	0.007	0.005	23
40	0.14	0.12	0.0750	0.130	0.014	0.010	27
45	0.15	0.12	0.0825	0.135	0.021	0.015	30
50	0.14	0.13	0.0725	0.135	0.007	0.005	33
55	0.13	0.13	0.0650	0.130	0.000	0.000	37
60	0.13	0.12	0.0675	0.125	0.007	0.005	40
65	0.11	0.12	0.0575	0.115	0.007	0.005	43
70	0.11	0.13	0.0600	0.120	0.014	0.010	47
75	0.11	0.10	0.0100	0.105	0.007	0.005	50
80	0.11	0.10	0.0100	0.105	0.007	0.005	53
85	0.11	0.10	0.0100	0.105	0.007	0.005	57
90	0.11	0.10	0.0100	0.105	0.007	0.005	60
95	0.10	0.10	0.0000	0.100	0.000	0.000	63
100	0.10	0.09	0.0100	0.095	0.007	0.005	67
105	0.09	0.09	0.0000	0.090	0.000	0.000	70
110	0.09	0.09	0.0000	0.090	0.000	0.000	73
115	0.09	0.09	0.0000	0.090	0.000	0.000	77
120	0.09	0.09	0.0000	0.090	0.000	0.000	80
Average	0.14	0.14	0.03				
Std. Deviation	0.0516398	0.048487	0.030701				
Std. error	0.010328	0.009697	0.00614				
95% Confidence Interval		0.014427	**< δ <**	0.039773			

FILTRATION TRIALS FOR OPTIMUM TURBIDITY DETERMINATION

	First Trial	Second Trial	Third Trial	Mean	STD	SEM	Column area	Q	column length	velocity	PVT
Time, min	Turbidity, NTU	Turbidity, NTU	Turbidity, NTU	Turbidity, NTU	NTU		m^2	m^3/h	m	m/h	unit less
0	0.123	0.12	0.125	0.123	0.003	0.070822	0.0005	0.003	0.15	6.11	0
10	0.111	0.116	0.114	0.114	0.003	0.065625	0.0005	0.003	0.15	6.11	7
20	0.103	0.103	0.101	0.102	0.001	0.059082	0.0005	0.003	0.15	6.11	14
30	0.139	0.138	0.142	0.140	0.002	0.080637	0.0005	0.003	0.15	6.11	20
40	0.191	0.104	0.102	0.132	0.051	0.076403	0.0005	0.003	0.15	6.11	27
50	0.123	0.107	0.105	0.112	0.010	0.064471	0.0005	0.003	0.15	6.11	34
60	0.103	0.094	0.103	0.100	0.005	0.057735	0.0005	0.003	0.15	6.11	41
70	0.107	0.088	0.093	0.096	0.010	0.055426	0.0005	0.003	0.15	6.11	48
80	0.094	0.087	0.089	0.090	0.004	0.051962	0.0005	0.003	0.15	6.11	54
90	0.093	0.084	0.085	0.087	0.005	0.050422	0.0005	0.003	0.15	6.11	61
100	0.104	0.088	0.086	0.093	0.010	0.053501	0.0005	0.003	0.15	6.11	68
110	0.081	0.083	0.082	0.082	0.001	0.047343	0.0005	0.003	0.15	6.11	75
120	0.074	0.084	0.079	0.079	0.005	0.045611	0.0005	0.003	0.15	6.11	82
130	0.079	0.077	0.076	0.077	0.002	0.044648	0.0005	0.003	0.15	6.11	88
140	0.091	0.071	0.079	0.080	0.010	0.04638	0.0005	0.003	0.15	6.11	95
150	0.072	0.07	0.073	0.072	0.002	0.041377	0.0005	0.003	0.15	6.11	102
160	0.073	0.076	0.076	0.075	0.002	0.043301	0.0005	0.003	0.15	6.11	109
170	0.077	0.072	0.073	0.074	0.003	0.042724	0.0005	0.003	0.15	6.11	115
180	0.090	0.086	0.077	0.084	0.007	0.04869	0.0005	0.003	0.15	6.11	122
190	0.077	0.079	0.08	0.079	0.002	0.045418	0.0005	0.003	0.15	6.11	129
200	0.074	0.078	0.083	0.078	0.005	0.045226	0.0005	0.003	0.15	6.11	136

FILTRATION EXPERIMENTS FOR TiO_2 REMOVAL AT DIFFERENT ALUM DOSES

8mg/L Alum

		Barrel 1	Barrel 2				
	pH	9.3	9.4				
	Time (mins)	May 12th Column 1 Turbidity (NTU)	May 12th Column 2 Turbidity (NTU)	May 13th Column 3 Turbidity (NTU)	Mean Turbidity (NTU)	STD	Standard mean error
Sample Collected	0	0.950	1.740	0.769	1.153	0.5163	0.298
	15	0.669	0.729	0.422	0.607	0.1627	0.094
	30	0.501	0.521	0.272	0.431	0.1383	0.080
	45	0.342	0.422	0.220	0.328	0.1017	0.059
	60	0.304	0.320	0.198	0.274	0.0663	0.038
	75	0.259	0.355	0.189	0.268	0.0833	0.048
	90	0.244	0.238	0.170	0.217	0.0411	0.024
	105	0.224	0.215	0.162	0.200	0.0335	0.019
	120	0.196	0.194	0.155	0.182	0.0231	0.013
	135	0.179	0.189	0.148	0.172	0.0214	0.012
Sample Collected	150	0.171	0.177	0.142	0.163	0.0187	0.011
	165	0.158	0.168	0.145	0.157	0.0115	0.007
Sample Collected	180	0.151	0.182	0.146	0.160	0.0195	0.011
190	200	0.198	0.330	0.275	0.268	0.0663	0.038

Samples sent for TiO2 analysis

		Column 1	Column 2	Column 3
		TiO2, µg/L	TiO2, µg/L	TiO2, µg/L
	Filtrate	< 2	< 2	< 2
pH 4 water washed	Filter Paper	< 2	< 2	< 2
pH 4 water washed	Media	< 2	< 2	< 2

		15mg/L Alum						
		Barrel 1	Barrel 2	Barrel 3				
	pH	8.76	6.86	9.58				
	Time (mins)	May 17th Column 1 Turbidity (NTU)	May 18th Column 2 Turbidity (NTU)	May 19th Column 3 Turbidity (NTU)	Mean Turbidity (NTU)	STD	Standard mean error	Confidence
	0	1.250	0.662	1.420	1.111	0.398	0.230	0.450
	15	0.429	0.267	0.633	0.443	0.183	0.106	0.208
	30	0.303	0.213	0.381	0.299	0.084	0.049	0.095
	45	0.243	0.204	0.285	0.244	0.041	0.023	0.046
	60	0.207	0.187	0.253	0.216	0.034	0.020	0.038
	75	0.205	0.180	0.225	0.203	0.023	0.013	0.026
	90	0.174	0.161	0.198	0.178	0.019	0.011	0.021
	105	0.160	0.161	0.195	0.172	0.020	0.012	0.023
	120	0.154	0.160	0.193	0.169	0.021	0.012	0.024
	135	0.147	0.134	0.182	0.154	0.025	0.014	0.028
Sample Collected	150	0.144	0.127	0.174	0.148	0.024	0.014	0.027
	165	0.194	0.125	0.163	0.161	0.035	0.020	0.039
	180	0.135	0.125	0.164	0.141	0.020	0.012	0.023
190	200	0.143	0.142	0.169	0.151	0.015	0.009	0.017

Samples sent for TiO2 analysis

		Column 1 TiO2, µg/L	Column 2 TiO2, µg/L	Column 3 TiO2, µg/L
	Filtrate	< 2	< 2	2
pH 4 water washed	Filter Paper	< 2	< 2	< 2
pH 4 water washed	Media	< 2	< 2	<2

8mg/L+ Polymer

Barrel 1 Polymer added = 0.1ml (0.05 mg/L)

pH 9.3

	Time (mins)	May 20th Column 1 Turbidity (NTU)	May 21th Column 2 Turbidity (NTU)	May 21th Column 3 Turbidity (NTU)	Mean Turbidity (NTU)	STD	Standard Error mean
	0	0.970	1.440	0.950	1.120	0.277	0.1601
	15	0.411	0.413	0.412	0.412	0.001	0.0006
	30	0.285	0.287	0.252	0.275	0.020	0.0113
	45	0.232	0.222	0.212	0.222	0.010	0.0058
	60	0.213	0.197	0.185	0.198	0.014	0.0081
	75	0.177	0.169	0.163	0.170	0.007	0.0041
	90	0.163	0.160	0.161	0.161	0.002	0.0009
	105	0.155	0.155	0.160	0.157	0.003	0.0017
	120	0.146	0.147	0.155	0.149	0.005	0.0028
	135	0.143	0.142	0.149	0.145	0.004	0.0022
Sample Collected	150	0.140	0.142	0.148	0.143	0.004	0.0024
	165	0.132	0.136	0.139	0.136	0.004	0.0020
	180	0.132	0.136	0.138	0.135	0.003	0.0018
190	200	0.148	0.185	0.138	0.157	0.025	0.0143

Samples sent for TiO2 analysis

		Column 1 TiO2, µg/L	Column 2 TiO2, µg/L	Column 3 TiO2, µg/L
	Filtrate	< 2	< 2	< 2
pH 4 water washed	Filter Paper	< 2	< 2	< 2
pH 4 water washed	Media	< 2	< 2	<2

	8mg/L Alum	15mg/L Alum	8mg/L Alum + polymer					
Time	Mean	Mean	Mean	Q	column length	Velocity	column area	PVT
(min)	Turbidity (NTU)	Turbidity (NTU)	Turbidity (NTU)	m^3/h	m	m^2/h	m^2	unit less
0	1.153	1.111	1.120	0.003	0.15	6	0.0005	0
15	0.607	0.443	0.412	0.003	0.15	6	0.0005	10
30	0.431	0.299	0.275	0.003	0.15	6	0.0005	20
45	0.328	0.244	0.222	0.003	0.15	6	0.0005	30
60	0.274	0.216	0.198	0.003	0.15	6	0.0005	40
75	0.268	0.203	0.170	0.003	0.15	6	0.0005	50
90	0.217	0.178	0.161	0.003	0.15	6	0.0005	60
105	0.2	0.172	0.157	0.003	0.15	6	0.0005	70
120	0.182	0.169	0.149	0.003	0.15	6	0.0005	80
135	0.172	0.154	0.145	0.003	0.15	6	0.0005	90
150	0.163	0.148	0.143	0.003	0.15	6	0.0005	100
165	0.157	0.161	0.136	0.003	0.15	6	0.0005	110
180	0.16	0.141	0.135	0.003	0.15	6	0.0005	120
200	0.268	0.151	0.157	0.003	0.15	6	0.0005	133

APPENDIX C FILTER EFFICIENCY CALCULATION FORMULAS

Particle Dia.	dp=	0.000002	m
Collector Dia.	dc=	0.0005	m
Porosity	E=	0.4	dimensionless
porosity function	γ=	0.843432665	dimensionless
Boltzmann const.	kB=	1.381E-23	J/K
Temperature	T=	25	Celcius
absolute Temp.	T=	298	K
Flow	Q=	50	ml/min
Flow	Q=	0.003	m3/h
Column Dia.	D=	2.5	cm
Column Area	A=	0.000490874	m2
Superficial vel.	v=	6.111549815	m/h
Viscosity	μ=	0.001	kg/m.s
Filtration rate	VF=v	6.111549815	m/h
Hamaker const.	Ha=	1E-20	J(kg.m^2/S^2)
particle density	ρs=	4230	kg/m^3
water density	ρw=	998	kg/m^3
depth of filter	L	0.15	m
	t cal	1.472621556	

$$A_s = \frac{2(1-\gamma^5)}{2-3\gamma+3\gamma^5-2\gamma^6} \qquad N_R = \frac{d_p}{d_c}$$

As
37.979096

NR
0.004

$$N_{LO} = \frac{4Ha}{9\pi\mu {d_p}^2 \nu} \qquad N_G = \frac{V_s}{V_F} = \frac{(\rho_s-\rho_w)g{d_p}^2}{18\mu V_F}$$

NLO	NG
2.083E-04	1.153E-06

$$Pe = \frac{3\pi\mu d_p d_c \nu}{k_B T}$$

Pe
3.888E+06

$$\eta_\circ = 4{A_s}^{1/3} Pe^{-2/3} + A_s {N_{LO}}^{1/8} {N_R}^{15/8} + 3.88\times10^{-3} A_s {N_G}^{1.2} {N_R}^{-0.4}$$

η
9.639E-04

$$ln\left(\frac{C}{C_o}\right) = -\frac{3}{2}\frac{(1-\varepsilon)\alpha\eta_o L}{d_c}$$

$$\lambda = \frac{-3(1-f)\alpha\eta}{2d_c}$$

FILTER EFFICIENCY CALCULATION RAW DATA WITHOUT ALUM (FIRST TRIAL DUPLICATED)

3.33E-3 $Ca(NO_3)_2$, pH 7

Time, mins	Total PC (#)		PC # (2-2.25 µm)	C/Co	α	α(2-2.25 µm)	t/t_{cal}
	Co	8038	45040				
2.5	C1	6248	4382	0.777308	0.001	0.009	1.70
17.5	C2	3537	2276	0.440035	0.003	0.011	11.88
32.5	C3	2047	1337	0.254665	0.005	0.013	22.07
47.5	C4	1691	1126	0.210376	0.006	0.014	32.26
62.5	C5	1138	718	0.141578	0.007	0.015	42.44
77.5	C6	1045	637	0.130007	0.008	0.016	52.63
92.5	C7	820	494	0.102015	0.008	0.017	62.81
107.5	C8	610	353	0.07589	0.010	0.018	73.00
122.5	C9	473	286	0.058845	0.010	0.019	83.18
137.5	C10	214	152	0.026624	0.013	0.021	93.37
152.5	C11	264	192	0.032844	0.013	0.020	103.56
167.5	C12	227	136	0.028241	0.013	0.021	113.74
182.5	C13	465	260	0.05785	0.011	0.019	123.93

6.66E-3 $Ca(NO_3)_2$, pH 7

Time, mins	Total PC (#)		PC # (2-2.25 µm)	C/Co	α	α(2-2.25 µm)	t/t_{cal}
	Co	77943	52923				
2.5	C1	8323	6049	0.107	0.008	0.008	1.70
17.5	C2	3940	2664	0.051	0.011	0.011	11.88
32.5	C3	3675	2246	0.047	0.011	0.012	22.07
47.5	C4	4801	2393	0.062	0.010	0.011	32.26
62.5	C5	2973	1509	0.038	0.012	0.013	42.44
77.5	C6	3213	1661	0.041	0.012	0.013	52.63
92.5	C7	2925	1247	0.038	0.012	0.014	62.81
107.5	C8	1949	996	0.025	0.014	0.015	73.00
122.5	C9	3128	1595	0.040	0.012	0.013	83.18
137.5	C10	2430	1113	0.031	0.013	0.014	93.37
152.5	C11	3229	1673	0.041	0.012	0.013	103.56
167.5	C12	2724	1122	0.035	0.012	0.014	113.74
182.5	C13	1694	1026	0.022	0.014	0.015	123.93

3.33E-3 $Ca(NO_3)_2$, pH 7

Time, mins	Total PC (#)		PC # (2-2.25 µm)	C/Co	α	α(2-2.25 µm)	t/t_{cal}	λ	λ(2-2.25 µm)
	Co	8038	45040						
2.5	C1	6248	4382	0.777308	0.001	0.009	1.7	-0.002	-0.015
17.5	C2	3537	2276	0.440035	0.003	0.011	11.88	-0.005	-0.019
32.5	C3	2047	1337	0.254665	0.005	0.013	22.07	-0.009	-0.023
47.5	C4	1691	1126	0.210376	0.006	0.014	32.26	-0.010	-0.024
62.5	C5	1138	718	0.141578	0.007	0.015	42.44	-0.013	-0.027
77.5	C6	1045	637	0.130007	0.008	0.016	52.63	-0.013	-0.027
92.5	C7	820	494	0.102015	0.008	0.017	62.81	-0.015	-0.029
107.5	C8	610	353	0.07589	0.010	0.018	73	-0.017	-0.031
122.5	C9	473	286	0.058845	0.010	0.019	83.18	-0.018	-0.033
137.5	C10	214	152	0.026624	0.013	0.021	93.37	-0.023	-0.037
152.5	C11	264	192	0.032844	0.013	0.020	103.56	-0.022	-0.035
167.5	C12	227	136	0.028241	0.013	0.021	113.74	-0.023	-0.037
182.5	C13	465	260	0.05785	0.011	0.019	123.93	-0.018	-0.033

6.66E-3 $Ca(NO_3)_2$, pH 7

Time, mins	Total PC (#)		PC # (2-2.25 µm)	C/Co	α	α(2-2.25 µm)	t/t_{cal}	λ	λ(2-2.25 µm)
	Co	77943	52923						
2.5	C1	8323	6049	0.107	0.008	0.008	1.7	-0.014	-0.014
17.5	C2	3940	2664	0.051	0.011	0.011	11.88	-0.019	-0.019
32.5	C3	3675	2246	0.047	0.011	0.012	22.07	-0.020	-0.020
47.5	C4	4801	2393	0.062	0.010	0.011	32.26	-0.018	-0.020
62.5	C5	2973	1509	0.038	0.012	0.013	42.44	-0.021	-0.023
77.5	C6	3213	1661	0.041	0.012	0.013	52.63	-0.020	-0.022
92.5	C7	2925	1247	0.038	0.012	0.014	62.81	-0.021	-0.024
107.5	C8	1949	996	0.025	0.014	0.015	73	-0.024	-0.026
122.5	C9	3128	1595	0.040	0.012	0.013	83.18	-0.021	-0.023
137.5	C10	2430	1113	0.031	0.013	0.014	93.37	-0.022	-0.025
152.5	C11	3229	1673	0.041	0.012	0.013	103.56	-0.020	-0.022
167.5	C12	2724	1122	0.035	0.012	0.014	113.74	-0.022	-0.025
182.5	C13	1694	1026	0.022	0.014	0.015	123.93	-0.025	-0.025

3.33E-3 NaCl, pH 7

Time, mins	Total PC (#)		PC # (2-2.25 µm)	C/Co	α	α(2-2.25 µm)	t/t_{cal}
	Co	66188	48684				
2.5	C1	26652	19590	0.403	0.00337	0.00337	1.70
17.5	C2	8873	6419	0.134	0.00744	0.00750	11.88
32.5	C3	4310	3099	0.065	0.01012	0.01020	22.07
47.5	C4	2293	1606	0.035	0.01245	0.01264	32.26
62.5	C5	1912	1308	0.029	0.01313	0.01340	42.44
77.5	C6	1948	1265	0.029	0.01306	0.01352	52.63
92.5	C7	1221	824	0.018	0.01479	0.01511	62.81
107.5	C8	1202	718	0.018	0.01485	0.01562	73.00
122.5	C9	1068	790	0.016	0.01528	0.01526	83.18
137.5	C10	764	529	0.012	0.01652	0.01675	93.37
152.5	C11	813	551	0.012	0.01629	0.01660	103.56
167.5	C12	508	332	0.008	0.01804	0.01847	113.74
182.5	C13	907	591	0.014	0.01589	0.01634	123.93

6.66E-3 NaCl, pH 7

Time, mins	Total PC (#)		PC # (2-2.25 µm)	C/Co	α	α(2-2.25 µm)	t/t_{cal}
	Co	69043	48742				
2.5	C1	23603	17645	0.341859	0.00398	0.00376	1.70
17.5	C2	6197	4488	0.089756	0.00893	0.00883	11.88
32.5	C3	3292	3188	0.04768	0.01127	0.01010	22.07
47.5	C4	1671	1239	0.024202	0.01378	0.01360	32.26
62.5	C5	2000	1255	0.028967	0.01312	0.01355	42.44
77.5	C6	1555	1103	0.022522	0.01405	0.01403	52.63
92.5	C7	2013	820	0.029156	0.01309	0.01513	62.81
107.5	C8	1059	570	0.015338	0.01547	0.01648	73.00
122.5	C9	2723	1153	0.039439	0.01197	0.01387	83.18
137.5	C10	1924	811	0.027867	0.01326	0.01517	93.37
152.5	C11	611	392	0.00885	0.01751	0.01786	103.56
167.5	C12	6516	2055	0.094376	0.00874	0.01173	113.74
182.5	C13	1131	658	0.016381	0.01523	0.01594	123.93

3.33E-3 NaCl, pH 7

Time, mins	Total PC (#)		PC # (2-2.25 µm)	C/Co	α	α(2-2.25 µm)	t/t_{cal}	λ	λ(2-2.25 µm)
	Co	66188	48684						
2.5	C1	26652	19590	0.403	0.00337	0.00337	1.70	-0.006	-0.006
17.5	C2	8873	6419	0.134	0.00744	0.00750	11.88	-0.013	-0.013
32.5	C3	4310	3099	0.065	0.01012	0.01020	22.07	-0.018	-0.018
47.5	C4	2293	1606	0.035	0.01245	0.01264	32.26	-0.022	-0.022
62.5	C5	1912	1308	0.029	0.01313	0.01340	42.44	-0.023	-0.023
77.5	C6	1948	1265	0.029	0.01306	0.01352	52.63	-0.023	-0.023
92.5	C7	1221	824	0.018	0.01479	0.01511	62.81	-0.026	-0.026
107.5	C8	1202	718	0.018	0.01485	0.01562	73.00	-0.026	-0.027
122.5	C9	1068	790	0.016	0.01528	0.01526	83.18	-0.027	-0.026
137.5	C10	764	529	0.012	0.01652	0.01675	93.37	-0.029	-0.029
152.5	C11	813	551	0.012	0.01629	0.01660	103.56	-0.028	-0.029
167.5	C12	508	332	0.008	0.01804	0.01847	113.74	-0.031	-0.032
182.5	C13	907	591	0.014	0.01589	0.01634	123.93	-0.028	-0.028

6.66E-3 NaCl, pH 7

Time, mins	Total PC (#)		PC # (2-2.25 µm)	C/Co	α	α(2-2.25 µm)	t/t_{cal}	λ	λ(2-2.25 µm)
	Co	69043	48742						
2.5	C1	23603	17645	0.341859	0.00398	0.00376	1.70	-0.007	-0.007
17.5	C2	6197	4488	0.089756	0.00893	0.00883	11.88	-0.015	-0.015
32.5	C3	3292	3188	0.04768	0.01127	0.01010	22.07	-0.020	-0.018
47.5	C4	1671	1239	0.024202	0.01378	0.01360	32.26	-0.024	-0.024
62.5	C5	2000	1255	0.028967	0.01312	0.01355	42.44	-0.023	-0.024
77.5	C6	1555	1103	0.022522	0.01405	0.01403	52.63	-0.024	-0.024
92.5	C7	2013	820	0.029156	0.01309	0.01513	62.81	-0.023	-0.026
107.5	C8	1059	570	0.015338	0.01547	0.01648	73.00	-0.027	-0.029
122.5	C9	2723	1153	0.039439	0.01197	0.01387	83.18	-0.021	-0.024
137.5	C10	1924	811	0.027867	0.01326	0.01517	93.37	-0.023	-0.026
152.5	C11	611	392	0.00885	0.01751	0.01786	103.56	-0.030	-0.031
167.5	C12	6516	2055	0.094376	0.00874	0.01173	113.74	-0.015	-0.020
182.5	C13	1131	658	0.016381	0.01523	0.01594	123.93	-0.026	-0.028

Base Solution, pH 7

Time, mins	Total PC (#)		PC # (2-2.25 µm)	C/Co	α	α(2-2.25 µm)	t/t_{cal}
	Co	62983	58575				
2.5	C1	34042	20730	0.540495	0.00228	0.00385	1.70
17.5	C2	54245	25543	0.861264	0.00055	0.00307	11.88
32.5	C3	13836	8845	0.219678	0.00561	0.00700	22.07
47.5	C4	12052	6021	0.191353	0.00612	0.00843	32.26
62.5	C5	5460	2925	0.08669	0.00906	0.01110	42.44
77.5	C6	5240	24260	0.083197	0.00921	0.00326	52.63
92.5	C7	1605	1018	0.025483	0.01359	0.01501	62.81
107.5	C8	3152	1521	0.050045	0.01109	0.01352	73.00
122.5	C9	730	472	0.01159	0.01651	0.01786	83.18
137.5	C10	448	300	0.007113	0.01832	0.01953	93.37
152.5	C11	470	317	0.007462	0.01814	0.01933	103.56
167.5	C12	402	290	0.006383	0.01872	0.01966	113.74
182.5	C13	970	486	0.015401	0.01546	0.01775	123.93

Base Solution trial 2, pH 7

Time, mins	Total PC (#)		PC # (2-2.25 µm)	C/Co	α	α(2-2.25 µm)	t/t_{cal}
	Co	76475	55478				
2.5	C1	43687	29056	0.571259	0.00207	0.00240	1.70
17.5	C2	9809	6778	0.128264	0.00761	0.00779	11.88
32.5	C3	19747	16366	0.258215	0.00501	0.00452	22.07
47.5	C4	2077	1435	0.027159	0.01336	0.01354	32.26
62.5	C5	1001	730	0.013089	0.01606	0.01604	42.44
77.5	C6	2344	1583	0.030651	0.01291	0.01317	52.63
92.5	C7	665	477	0.008696	0.01757	0.01762	62.81
107.5	C8	525	392	0.006865	0.01845	0.01834	73.00
122.5	C9	766	581	0.010016	0.01705	0.01689	83.18
137.5	C10	556	494	0.00727	0.01824	0.01749	93.37
152.5	C11	814	527	0.010644	0.01683	0.01725	103.56
167.5	C12	652	456	0.008526	0.01765	0.01778	113.74
182.5	C13	707	471	0.009245	0.01735	0.01766	123.93

FILTER EFFICIENCY CALCULATION RAW DATA WITHOUT ALUM (SECOND TRIAL DUPLICATED)

3.33E-3 $Ca(NO_3)_2$, pH 7

Time, mins	Total PC (#)		PC # (2-2.25 μm)	C/Co	α	α(2-2.25 μm)	t/t_{cal}
	Co	68888	66535				
2.5	C1	11504	8253	0.166996	0.007	0.008	1.70
17.5	C2	5341	3564	0.077532	0.009	0.011	11.88
32.5	C3	2179	1507	0.031631	0.013	0.014	22.07
47.5	C4	1398	935	0.020294	0.014	0.016	32.26
62.5	C5	1180	1066	0.017129	0.015	0.015	42.44
77.5	C6	1000	662	0.014516	0.016	0.017	52.63
92.5	C7	1015	556	0.014734	0.016	0.018	62.81
107.5	C8	522	338	0.007578	0.018	0.020	73.00
122.5	C9	473	286	0.006866	0.018	0.020	83.18
137.5	C10	544	346	0.007897	0.018	0.019	93.37
152.5	C11	531	341	0.007708	0.018	0.020	103.56
167.5	C12	507	325	0.00736	0.018	0.020	113.74
182.5	C13	465	260	0.00675	0.019	0.021	123.93

6.66E-3 $Ca(NO_3)_2$, pH 7

Time, mins	Total PC (#)		PC # (2-2.25 μm)	C/Co	α	α(2-2.25 μm)	t/t_{cal}
	Co	49494	46975				
2.5	C1	11848	9011	0.239	0.005	0.006	1.70
17.5	C2	3687	2816	0.074	0.010	0.010	11.88
32.5	C3	2192	1666	0.044	0.012	0.012	22.07
47.5	C4	1521	1143	0.031	0.013	0.014	32.26
62.5	C5	1269	868	0.026	0.014	0.015	42.44
77.5	C6	1117	941	0.023	0.014	0.014	52.63
92.5	C7	459	309	0.009	0.017	0.019	62.81
107.5	C8	285	215	0.006	0.019	0.020	73.00
122.5	C9	393	263	0.008	0.018	0.019	83.18
137.5	C10	423	405	0.009	0.018	0.018	93.37
152.5	C11	623	326	0.013	0.016	0.018	103.56
167.5	C12	461	278	0.009	0.017	0.019	113.74
182.5	C13	248	163	0.005	0.020	0.021	123.93

3.33E-3 $Ca(NO_3)_2$, pH 7

Time, mins	Total PC (#)		PC # (2-2.25 µm)	C/Co	α	α(2-2.25 µm)	t/t_{cal}	λ	λ(2-2.25 µm)
	Co	68888	66535						
2.5	C1	11504	8253	0.166996	0.007	0.008	1.70	-0.012	-0.013
17.5	C2	5341	3564	0.077532	0.009	0.011	11.88	-0.016	-0.019
32.5	C3	2179	1507	0.031631	0.013	0.014	22.07	-0.022	-0.024
47.5	C4	1398	935	0.020294	0.014	0.016	32.26	-0.025	-0.027
62.5	C5	1180	1066	0.017129	0.015	0.015	42.44	-0.026	-0.027
77.5	C6	1000	662	0.014516	0.016	0.017	52.63	-0.027	-0.030
92.5	C7	1015	556	0.014734	0.016	0.018	62.81	-0.027	-0.031
107.5	C8	522	338	0.007578	0.018	0.020	73.00	-0.031	-0.034
122.5	C9	473	286	0.006866	0.018	0.020	83.18	-0.032	-0.035
137.5	C10	544	346	0.007897	0.018	0.019	93.37	-0.031	-0.034
152.5	C11	531	341	0.007708	0.018	0.020	103.56	-0.031	-0.034
167.5	C12	507	325	0.00736	0.018	0.020	113.74	-0.032	-0.034
182.5	C13	465	260	0.00675	0.019	0.021	123.93	-0.032	-0.036

6.66E-3 $Ca(NO_3)_2$, pH 7

Time, mins	Total PC (#)		PC # (2-2.25 µm)	C/Co	α	α(2-2.25 µm)	t/t_{cal}	λ	λ(2-2.25 µm)
	Co	49494	46975						
2.5	C1	11848	9011	0.239	0.005	0.006	1.70	-0.009	-0.011
17.5	C2	3687	2816	0.074	0.010	0.010	11.88	-0.017	-0.018
32.5	C3	2192	1666	0.044	0.012	0.012	22.07	-0.020	-0.021
47.5	C4	1521	1143	0.031	0.013	0.014	32.26	-0.022	-0.024
62.5	C5	1269	868	0.026	0.014	0.015	42.44	-0.024	-0.026
77.5	C6	1117	941	0.023	0.014	0.014	52.63	-0.024	-0.025
92.5	C7	459	309	0.009	0.017	0.019	62.81	-0.030	-0.032
107.5	C8	285	215	0.006	0.019	0.020	73.00	-0.033	-0.035
122.5	C9	393	263	0.008	0.018	0.019	83.18	-0.031	-0.033
137.5	C10	423	405	0.009	0.018	0.018	93.37	-0.031	-0.031
152.5	C11	623	326	0.013	0.016	0.018	103.56	-0.028	-0.032
167.5	C12	461	278	0.009	0.017	0.019	113.74	-0.030	-0.033
182.5	C13	248	163	0.005	0.020	0.021	123.93	-0.034	-0.036

3.33E-3 NaCl, pH 7

Time, mins	Total PC (#)		PC # (2-2.25 µm)	C/Co	α	α(2-2.25 µm)	t/t_{cal}
	Co	67285	48548				
2.5	C1	11494	8670	0.171	0.00654	0.00638	1.70
17.5	C2	4817	3243	0.072	0.00977	0.01002	11.88
32.5	C3	1866	1380	0.028	0.01328	0.01319	22.07
47.5	C4	940	645	0.014	0.01582	0.01600	32.26
62.5	C5	804	494	0.012	0.01640	0.01699	42.44
77.5	C6	661	428	0.010	0.01712	0.01752	52.63
92.5	C7	790	470	0.012	0.01646	0.01718	62.81
107.5	C8	653	348	0.010	0.01717	0.01829	73.00
122.5	C9	637	490	0.009	0.01726	0.01702	83.18
137.5	C10	534	669	0.008	0.01791	0.01587	93.37
152.5	C11	273	175	0.004	0.02040	0.02084	103.56
167.5	C12	439	194	0.007	0.01864	0.02045	113.74
182.5	C13	427	217	0.006	0.01874	0.02004	123.93

6.66E-3 NaCl, pH 7

Time, mins	Total PC (#)		PC # (2-2.25 µm)	C/Co	α	α(2-2.25 µm)	t/t_{cal}
	Co	73631	51814				
2.5	C1	6585	5119	0.089432	0.00894	0.00857	1.70
17.5	C2	4112	2934	0.055846	0.01069	0.01063	11.88
32.5	C3	1952	1267	0.026511	0.01345	0.01374	22.07
47.5	C4	1520	717	0.020643	0.01437	0.01585	32.26
62.5	C5	685	472	0.009303	0.01732	0.01740	42.44
77.5	C6	666	458	0.009045	0.01743	0.01751	52.63
92.5	C7	624	363	0.008475	0.01767	0.01837	62.81
107.5	C8	1507	1913	0.020467	0.01440	0.01222	73.00
122.5	C9	1141	611	0.015496	0.01543	0.01645	83.18
137.5	C10	1791	762	0.024324	0.01376	0.01563	93.37
152.5	C11	1102	539	0.014967	0.01556	0.01691	103.56
167.5	C12	374	228	0.005079	0.01957	0.02010	113.74
182.5	C13	2463	1138	0.033451	0.01258	0.01414	123.93

3.33E-3 NaCl, pH 7

Time, mins	Total PC (#)		PC # (2-2.25 µm)	C/Co	α	α(2-2.25 µm)	t/t_{cal}	λ	λ(2-2.25 µm)
	Co	67285	48548						
2.5	C1	11494	8670	0.179	0.00654	0.00638	1.70	-0.011	-0.011
17.5	C2	4817	3243	0.067	0.00977	0.01002	11.88	-0.017	-0.017
32.5	C3	1866	1380	0.028	0.01328	0.01319	22.07	-0.023	-0.023
47.5	C4	940	645	0.013	0.01582	0.01600	32.26	-0.027	-0.028
62.5	C5	804	494	0.010	0.01640	0.01699	42.44	-0.028	-0.029
77.5	C6	661	428	0.009	0.01712	0.01752	52.63	-0.030	-0.030
92.5	C7	790	470	0.010	0.01646	0.01718	62.81	-0.029	-0.030
107.5	C8	653	348	0.007	0.01717	0.01829	73.00	-0.030	-0.032
122.5	C9	637	490	0.010	0.01726	0.01702	83.18	-0.030	-0.030
137.5	C10	534	669	0.014	0.01791	0.01587	93.37	-0.031	-0.028
152.5	C11	273	175	0.004	0.02040	0.02084	103.56	-0.035	-0.036
167.5	C12	439	194	0.004	0.01864	0.02045	113.74	-0.032	-0.035
182.5	C13	427	217	0.004	0.01874	0.02004	123.93	-0.033	-0.035

6.66E-3 NaCl, pH 7

Time, mins	Total PC (#)		PC # (2-2.25 µm)	C/Co	α	α(2-2.25 µm)	t/t_{cal}	λ	λ(2-2.25 µm)
	Co	73631	51814						
2.5	C1	6585	5119	0.089432	0.00894	0.00857	1.70	-0.016	-0.015
17.5	C2	4112	2934	0.055846	0.01069	0.01063	11.88	-0.019	-0.018
32.5	C3	1952	1267	0.026511	0.01345	0.01374	22.07	-0.023	-0.024
47.5	C4	1520	717	0.020643	0.01437	0.01585	32.26	-0.025	-0.028
62.5	C5	685	472	0.009303	0.01732	0.01740	42.44	-0.030	-0.030
77.5	C6	666	458	0.009045	0.01743	0.01751	52.63	-0.030	-0.030
92.5	C7	624	363	0.008475	0.01767	0.01837	62.81	-0.031	-0.032
107.5	C8	1507	1913	0.020467	0.01440	0.01222	73.00	-0.025	-0.021
122.5	C9	1141	611	0.015496	0.01543	0.01645	83.18	-0.027	-0.029
137.5	C10	1791	762	0.024324	0.01376	0.01563	93.37	-0.024	-0.027
152.5	C11	1102	539	0.014967	0.01556	0.01691	103.56	-0.027	-0.029
167.5	C12	374	228	0.005079	0.01957	0.02010	113.74	-0.034	-0.035
182.5	C13	2463	1138	0.033451	0.01258	0.01414	123.93	-0.022	-0.025

Base Solution, pH 7

Time, mins	Total PC (#)		PC # (2-2.25 µm)	C/Co	α	α(2-2.25 µm)	t/t_{cal}	λ	λ(2-2.25 µm)
	Co	62983	58575						
2.5	C1	34042	20730	0.540495	0.00228	0.00385	1.70	-0.004	-0.007
17.5	C2	54245	25543	0.861264	0.00055	0.00307	11.88	-0.001	-0.005
32.5	C3	13836	8845	0.219678	0.00561	0.00700	22.07	-0.010	-0.012
47.5	C4	12052	6021	0.191353	0.00612	0.00843	32.26	-0.011	-0.015
62.5	C5	5460	2925	0.08669	0.00906	0.01110	42.44	-0.016	-0.019
77.5	C6	5240	24260	0.083197	0.00921	0.00326	52.63	-0.016	-0.006
92.5	C7	1605	1018	0.025483	0.01359	0.01501	62.81	-0.024	-0.026
107.5	C8	3152	1521	0.050045	0.01109	0.01352	73.00	-0.019	-0.023
122.5	C9	730	472	0.01159	0.01651	0.01786	83.18	-0.029	-0.031
137.5	C10	448	300	0.007113	0.01832	0.01953	93.37	-0.032	-0.034
152.5	C11	470	317	0.007462	0.01814	0.01933	103.56	-0.031	-0.034
167.5	C12	402	290	0.006383	0.01872	0.01966	113.74	-0.032	-0.034
182.5	C13	970	486	0.015401	0.01546	0.01775	123.93	-0.027	-0.031

Base Solution, pH 7

Time, mins	Total PC (#)		PC # (2-2.25 µm)	C/Co	α	α(2-2.25 µm)	t/t_{cal}	λ	λ(2-2.25 µm)
	Co	76475	55478						
2.5	C1	43687	29056	0.571259	0.00207	0.00240	1.70	-0.004	-0.004
17.5	C2	9809	6778	0.128264	0.00761	0.00779	11.88	-0.013	-0.014
32.5	C3	19747	16366	0.258215	0.00501	0.00452	22.07	-0.009	-0.008
47.5	C4	2077	1435	0.027159	0.01336	0.01354	32.26	-0.023	-0.023
62.5	C5	1001	730	0.013089	0.01606	0.01604	42.44	-0.028	-0.028
77.5	C6	2344	1583	0.030651	0.01291	0.01317	52.63	-0.022	-0.023
92.5	C7	665	477	0.008696	0.01757	0.01762	62.81	-0.030	-0.031
107.5	C8	525	392	0.006865	0.01845	0.01834	73.00	-0.032	-0.032
122.5	C9	766	581	0.010016	0.01705	0.01689	83.18	-0.030	-0.029
137.5	C10	556	494	0.00727	0.01824	0.01749	93.37	-0.032	-0.030
152.5	C11	814	527	0.010644	0.01683	0.01725	103.56	-0.029	-0.030
167.5	C12	652	456	0.008526	0.01765	0.01778	113.74	-0.031	-0.031
182.5	C13	707	471	0.009245	0.01735	0.01766	123.93	-0.030	-0.031

FILTER EFFICIENCY CALCULATION AVERAGED DATA WITHOUT ALUM

3.33mmol Ca(NO3)2

	(C/Co)1	(C/Co)2	d	(C/Co)avg	α	λ	t/tcalc	-Log (C/Co)
	0.777	0.167	0.61	0.472	0.003	-0.005	1.7	0.33
	0.44	0.078	0.362	0.259	0.005	-0.009	11.88	0.59
	0.255	0.032	0.223	0.1435	0.007	-0.012	22.07	0.84
	0.21	0.02	0.19	0.115	0.008	-0.014	32.26	0.94
	0.142	0.017	0.125	0.0795	0.009	-0.016	42.44	1.10
	0.13	0.015	0.115	0.0725	0.010	-0.017	52.63	1.14
	0.102	0.015	0.087	0.0585	0.011	-0.018	62.81	1.23
	0.076	0.008	0.068	0.042	0.012	-0.020	73	1.38
	0.059	0.007	0.052	0.033	0.013	-0.022	83.18	1.48
	0.027	0.008	0.019	0.0175	0.015	-0.026	93.37	1.76
	0.033	0.008	0.025	0.0205	0.014	-0.025	103.56	1.69
	0.028	0.007	0.021	0.0175	0.015	-0.026	113.74	1.76
	0.058	0.007	0.051	0.0325	0.013	-0.022	123.93	1.49
Average	0.179769	0.029923	0.149846		0.01031	-0.01789		
Std. Deviation	0.213897	0.045493	0.169521					
Std. error	0.059324	0.012617	0.047017					
		0.047397	**< δ <**	0.25229536				

6.66mmolM Ca(NO3)2

	(C/Co)1	(C/Co)2	d	(C/Co)avg	α	λ	t/tcalc	-Log (C/Co)
	0.107	0.239	-0.132	0.173	0.006498	-0.011	1.7	0.76
	0.051	0.074	-0.023	0.063	0.010269	-0.018	11.88	1.20
	0.047	0.044	0.003	0.046	0.011445	-0.020	22.07	1.34
	0.062	0.031	0.031	0.047	0.011364	-0.020	32.26	1.33
	0.038	0.026	0.012	0.032	0.012748	-0.022	42.44	1.49
	0.041	0.023	0.018	0.032	0.012748	-0.022	52.63	1.49
	0.038	0.009	0.029	0.024	0.013892	-0.024	62.81	1.63
	0.025	0.006	0.019	0.016	0.015433	-0.027	73	1.81
	0.04	0.008	0.032	0.024	0.013814	-0.024	83.18	1.62
	0.031	0.009	0.022	0.020	0.014489	-0.025	93.37	1.70
	0.041	0.013	0.028	0.027	0.013377	-0.023	103.56	1.57
	0.035	0.009	0.026	0.022	0.014136	-0.025	113.74	1.66
	0.022	0.005	0.017	0.014	0.015945	-0.028	123.93	1.87
Average	0.044462	0.038154	0.006307692		0.012781	-0.02218		
Std. Deviation	0.021504	0.063451	0.044095322					
Std. error	0.005964	0.017598	0.012229842					
		-0.02034	**< δ <**	0.0329565				

3.33mmol NaCl

	(C/Co)1	(C/Co)2	d	(C/Co)avg	α	λ	t/tcalc	-Log (C/Co)
	0.403	0.171	0.232	0.287	0.004623	-0.008	1.7	0.54
	0.134	0.072	0.062	0.103	0.008419	-0.015	11.88	0.99
	0.065	0.028	0.037	0.047	0.011364	-0.020	22.07	1.33
	0.035	0.014	0.021	0.025	0.013737	-0.024	32.26	1.61
	0.029	0.012	0.017	0.021	0.014398	-0.025	42.44	1.69
	0.029	0.01	0.019	0.020	0.014583	-0.025	52.63	1.71
	0.018	0.012	0.006	0.015	0.015554	-0.027	62.81	1.82
	0.018	0.01	0.008	0.014	0.01581	-0.027	73	1.85
	0.016	0.009	0.007	0.013	0.01623	-0.028	83.18	1.90
	0.012	0.008	0.004	0.010	0.017056	-0.030	93.37	2.00
	0.012	0.004	0.008	0.008	0.017883	-0.031	103.56	2.10
	0.008	0.007	0.001	0.008	0.018122	-0.031	113.74	2.12
	0.014	0.006	0.008	0.010	0.017056	-0.030	123.93	2.00
Average	0.061	0.027923	0.033077		0.014218	-0.02467		
Std. Deviation	0.108234	0.04655	0.062048					
Std. error	0.030019	0.012911	0.017209					
		-0.00442	**< δ <**	0.07057516				

6.66mmol NaCl

	(C/Co)1	(C/Co)2	d	(C/Co)avg	α	λ	t/tcalc	-Log (C/Co)
	0.342	0.089	0.253	0.216	0.005684	-0.010	1.7	0.67
	0.09	0.056	0.034	0.073	0.009694	-0.017	11.88	1.14
	0.048	0.027	0.021	0.038	0.012161	-0.021	22.07	1.43
	0.024	0.021	0.003	0.023	0.014053	-0.024	32.26	1.65
	0.029	0.009	0.020	0.019	0.014679	-0.025	42.44	1.72
	0.023	0.009	0.014	0.016	0.015315	-0.027	52.63	1.80
	0.029	0.008	0.021	0.019	0.014778	-0.026	62.81	1.73
	0.015	0.02	-0.005	0.018	0.014984	-0.026	73	1.76
	0.039	0.015	0.024	0.027	0.013377	-0.023	83.18	1.57
	0.028	0.024	0.004	0.026	0.013517	-0.023	93.37	1.59
	0.009	0.015	-0.006	0.012	0.016381	-0.028	103.56	1.92
	0.094	0.005	0.089	0.050	0.011133	-0.019	113.74	1.31
	0.016	0.033	-0.017	0.025	0.013737	-0.024	123.93	1.61
Average	0.060462	0.025462	0.035		0.013038	-0.02262		
Std. Deviation	0.088664	0.02339	0.070468669					
Std. error	0.024591	0.006487	0.019544492					
		-0.00759	**< δ <**	0.0775874				

	Base Solution							
	(C/Co)1	(C/Co)2	d	(C/Co)avg	α	λ	t/tcalc	-Log (C/Co)
	0.54	0.571	-0.031	0.556	0.002177	-0.004	1.7	0.26
	0.861	0.128	0.733	0.495	0.002608	-0.005	11.88	0.31
	0.22	0.258	-0.038	0.239	0.005301	-0.009	22.07	0.62
	0.191	0.027	0.164	0.109	0.008209	-0.014	32.26	0.96
	0.087	0.013	0.074	0.050	0.011095	-0.019	42.44	1.30
	0.029	0.031	-0.002	0.030	0.012987	-0.023	52.63	1.52
	0.025	0.009	0.016	0.017	0.015091	-0.026	62.81	1.77
	0.05	0.007	0.043	0.029	0.013177	-0.023	73	1.55
	0.012	0.01	0.002	0.011	0.016703	-0.029	83.18	1.96
	0.007	0.007	0.000	0.007	0.018377	-0.032	93.37	2.15
	0.007	0.011	-0.004	0.009	0.017446	-0.030	103.56	2.05
	0.006	0.009	-0.003	0.008	0.018122	-0.031	113.74	2.12
	0.015	0.009	0.006	0.012	0.016381	-0.028	123.93	1.92
Average	0.157692	0.083846	0.073846		0.012129	-0.02104		
Std. Deviation	0.259257	0.163304	0.204806					
Std. error	0.071905	0.045292	0.056803					
		-0.04993	**< δ <**	0.19762002				

FILTER EFFICIENCY CALCULATION RAW DATA WITH ALUM (FIRST TRIAL DUPLICATED)

3.33E-3 $Ca(NO_3)_2$, pH 5.5

Time, min	Total PC (#)		C/Co	α	t/t_{cal}
	Co	114787			
2.5	C1	26064	0.227064	0.005	1.70
17.5	C2	90691	0.790081	0.001	11.88
32.5	C3	93507	0.814613	0.001	22.07
47.5	C4	101281	0.882339	0.000	32.26
62.5	C5	107153	0.933494	0.000	42.44
77.5	C6	103494	0.901618	0.000	52.63
92.5	C7	106840	0.930767	0.000	62.81
107.5	C8	106852	0.930872	0.000	73.00
122.5	C9	111765	0.973673	0.000	83.18
137.5	C10	114728	0.999486	0.000	93.37
152.5	C11	113273	0.98681	0.000	103.56
167.5	C12	114719	0.999408	0.000	113.74
182.5	C13	114538	0.997831	0.000	123.93

6.66E-3 $Ca(NO_3)_2$, pH 5.5

Time, min	Total PC (#)		C/Co	α	t/t_{cal}
	Co	52066			
2.5	C1	18592	0.357085	0.004	1.70
17.5	C2	31105	0.597415	0.002	11.88
32.5	C3	32456	0.623363	0.002	22.07
47.5	C4	34843	0.669208	0.001	32.26
62.5	C5	40925	0.786022	0.001	42.44
77.5	C6	39392	0.756578	0.001	52.63
92.5	C7	38555	0.740502	0.001	62.81
107.5	C8	42948	0.824876	0.001	73.00
122.5	C9	43374	0.833058	0.001	83.18
137.5	C10	44906	0.862482	0.001	93.37
152.5	C11	45288	0.869819	0.001	103.56
167.5	C12	43330	0.832213	0.001	113.74
182.5	C13	46963	0.90199	0.000	123.93

3.33E-3 NaCl, pH 5.5

Time, mins	Total PC (#)		C/Co	α	t/t cal
	Co	53428			
2.5	C1	18742	0.351	0.00388	1.70
17.5	C2	52729	0.987	0.00005	11.88
32.5	C3	49048	0.918	0.00032	22.07
47.5	C4	44835	0.839	0.00065	32.26
62.5	C5	51868	0.971	0.00011	42.44
77.5	C6	53789	1.007	0.0000	52.63
92.5	C7	52154	0.976	0.00009	62.81
107.5	C8	51460	0.963	0.00014	73.00
122.5	C9	51421	0.962	0.00014	83.18
137.5	C10	51826	0.970	0.00011	93.37
152.5	C11	49151	0.920	0.00031	103.56
167.5	C12	42724	0.800	0.00083	113.74
182.5	C13	41870	0.784	0.00090	123.93

6.66E-3 NaCl, pH 5.5

Time, mins	Total PC (#)		C/Co	α	t/t cal
	Co	150978			
2.5	C1	32385	0.214501	0.00570	1.70
17.5	C2	64675	0.428374	0.00314	11.88
32.5	C3	81673	0.54096	0.00228	22.07
47.5	C4	142888	0.946416	0.00020	32.26
62.5	C5	102699	0.680225	0.00143	42.44
77.5	C6	100086	0.662918	0.00152	52.63
92.5	C7	75438	0.499662	0.00257	62.81
107.5	C8	84735	0.561241	0.00214	73.00
122.5	C9	63447	0.42024	0.00321	83.18
137.5	C10	67358	0.446144	0.00299	93.37
152.5	C11	56280	0.37277	0.00365	103.56
167.5	C12	117859	0.780637	0.00092	113.74
182.5	C13	100819	0.667773	0.00150	123.93

Base Solution, pH 5.5

Time, mins	Total PC (#)		C/Co	α	t/t cal
	Co	110218			
2.5	C1	34091	0.309305	0.00435	1.70
17.5	C2	81568	0.740061	0.00111	11.88
32.5	C3	78201	0.709512	0.00127	22.07
47.5	C4	74726	0.677984	0.00144	32.26
62.5	C5	74911	0.679662	0.00143	42.44
77.5	C6	71333	0.647199	0.00161	52.63
92.5	C7	80112	0.72685	0.00118	62.81
107.5	C8	74161	0.672857	0.00147	73.00
122.5	C9	85603	0.77667	0.00094	83.18
137.5	C10	66317	0.601689	0.00188	93.37
152.5	C11	61899	0.561605	0.00214	103.56
167.5	C12	75994	0.689488	0.00138	113.74
182.5	C13	74904	0.679599	0.00143	123.93

FILTER EFFICIENCY CALCULATION RAW DATA WITH ALUM (SECOND TRIAL DUPLICATED)

3.33E-3 CaNO3, pH 5.5

Time, min	Total PC (#)		C/Co	α	t/t cal	λ
	Co	114787				
2.5	C1	26064	0.227064	0.005	1.70	-0.010
17.5	C2	90691	0.790081	0.001	11.88	-0.002
32.5	C3	93507	0.814613	0.001	22.07	-0.001
47.5	C4	101281	0.882339	0.000	32.26	-0.001
62.5	C5	117153	1.020612	0.000	42.44	0.000
77.5	C6	102494	0.892906	0.000	52.63	-0.001
92.5	C7	106840	0.930767	0.000	62.81	0.000
107.5	C8	106852	0.930872	0.000	73.00	0.000
122.5	C9	111765	0.973673	0.000	83.18	0.000
137.5	C10	114728	0.999486	0.000	93.37	0.000
152.5	C11	113273	0.98681	0.000	103.56	0.000
167.5	C12	114719	0.999408	0.000	113.74	0.000
182.5	C13	114538	0.997831	0.000	123.93	0.000

6.66E-3 CaNO3, pH 5.5

Time, mins	Total PC (#)		C/Co	α	t/t cal	λ
	Co	52066				
2.5	C1	18592	0.357	0.004	1.7	-0.007
17.5	C2	31105	0.597	0.002	11.88	-0.003
32.5	C3	32456	0.623	0.002	22.07	-0.003
47.5	C4	34843	0.669	0.001	32.26	-0.003
62.5	C5	40925	0.786	0.001	42.44	-0.002
77.5	C6	39392	0.757	0.001	52.63	-0.002
92.5	C7	38555	0.741	0.001	62.81	-0.002
107.5	C8	42948	0.825	0.001	73	-0.001
122.5	C9	43374	0.833	0.001	83.18	-0.001
137.5	C10	44906	0.862	0.001	93.37	-0.001
152.5	C11	45288	0.870	0.001	103.56	-0.001
167.5	C12	43330	0.832	0.001	113.74	-0.001
182.5	C13	46963	0.902	0.000	123.93	-0.001

3.33E-3 CaNO3, pH 5.5

Time, mins	Total PC (#)		C/Co	α	t/t cal	λ
	Co	140770				
2.5	C1	34865	0.247674	0.005	1.70	-0.009
17.5	C2	72755	0.516836	0.002	11.88	-0.004
32.5	C3	90313	0.641564	0.002	22.07	-0.003
47.5	C4	140467	0.997848	0.000	32.26	0.000
62.5	C5	131376	0.933267	0.000	42.44	0.000
77.5	C6	106876	0.759224	0.001	52.63	-0.002
92.5	C7	139856	0.993507	0.000	62.81	0.000
107.5	C8	139831	0.99333	0.000	73.00	0.000
122.5	C9	115164	0.8181	0.001	83.18	-0.001
137.5	C10	124327	0.883192	0.000	93.37	-0.001
152.5	C11	122504	0.870242	0.001	103.56	-0.001
167.5	C12	117077	0.83169	0.001	113.74	-0.001
182.5	C13	122394	0.869461	0.001	123.93	-0.001

6.66E-3 CaNO3, pH 5.5

Time, mins	Total PC (#)		C/Co	α	t/t cal	λ
	Co	146232				
2.5	C1	16005	0.109	0.008	1.70	-0.014
17.5	C2	50951	0.348	0.004	11.88	-0.007
32.5	C3	72153	0.493	0.003	22.07	-0.005
47.5	C4	82422	0.564	0.002	32.26	-0.004
62.5	C5	90796	0.621	0.002	42.44	-0.003
77.5	C6	96151	0.658	0.002	52.63	-0.003
92.5	C7	94061	0.643	0.002	62.81	-0.003
107.5	C8	95355	0.652	0.002	73.00	-0.003
122.5	C9	88260	0.604	0.002	83.18	-0.003
137.5	C10	141506	0.968	0.000	93.37	0.000
152.5	C11	100731	0.689	0.001	103.56	-0.002
167.5	C12	100812	0.689	0.001	113.74	-0.002
182.5	C13	102112	0.698	0.001	123.93	-0.002

3.33E-3 NaCl, pH 5.5

Time, mins	Total PC (#)		C/Co	α	t/t cal	λ
	Co	86410				
2.5	C1	25331	0.293	0.00454	1.70	-0.008
17.5	C2	58452	0.676	0.00145	11.88	-0.003
32.5	C3	62236	0.720	0.00122	22.07	-0.002
47.5	C4	85421	0.989	0.00004	32.26	0.000
62.5	C5	66735	0.772	0.00096	42.44	-0.002
77.5	C6	79446	0.919	0.00031	52.63	-0.001
92.5	C7	74909	0.867	0.00053	62.81	-0.001
107.5	C8	80234	0.929	0.00027	73.00	0.000
122.5	C9	83688	0.968	0.00012	83.18	0.000
137.5	C10	84085	0.973	0.00010	93.37	0.000
152.5	C11	67702	0.783	0.00090	103.56	-0.002
167.5	C12	67314	0.779	0.00092	113.74	-0.002
182.5	C13	64249	0.744	0.00110	123.93	-0.002

6.66E-3 NaCl, pH 5.5

Time, mins	Total PC (#)		C/Co	α	t/t cal	λ
	Co	128242				
2.5	C1	38403	0.299457	0.00447	1.70	-0.008
17.5	C2	72886	0.568347	0.00209	11.88	-0.004
32.5	C3	84460	0.658599	0.00155	22.07	-0.003
47.5	C4	89073	0.69457	0.00135	32.26	-0.002
62.5	C5	126105	0.983336	0.00006	42.44	0.000
77.5	C6	89912	0.701112	0.00132	52.63	-0.002
92.5	C7	78579	0.61274	0.00181	62.81	-0.003
107.5	C8	85274	0.664946	0.00151	73.00	-0.003
122.5	C9	74863	0.583764	0.00199	83.18	-0.003
137.5	C10	60502	0.47178	0.00278	93.37	-0.005
152.5	C11	95904	0.747836	0.00108	103.56	-0.002
167.5	C12	91168	0.710906	0.00126	113.74	-0.002
182.5	C13	91597	0.714251	0.00125	123.93	-0.002

Base Solution, pH 5.5

Time, mins	Total PC (#)		C/Co	α	t/t cal	λ
	Co	81801				
2.5	C1	27972	0.341952	0.00397	1.70	-0.007
17.5	C2	63142	0.771898	0.00096	11.88	-0.002
32.5	C3	74490	0.910625	0.00035	22.07	-0.001
47.5	C4	59854	0.731703	0.00116	32.26	-0.002
62.5	C5	60670	0.741678	0.00111	42.44	-0.002
77.5	C6	62409	0.762937	0.00100	52.63	-0.002
92.5	C7	62220	0.760626	0.00101	62.81	-0.002
107.5	C8	62186	0.760211	0.00102	73.00	-0.002
122.5	C9	48572	0.593782	0.00193	83.18	-0.003
137.5	C10	61690	0.754147	0.00105	93.37	-0.002
152.5	C11	55663	0.680468	0.00143	103.56	-0.002
167.5	C12	58214	0.711654	0.00126	113.74	-0.002
182.5	C13	46984	0.57437	0.00205	123.93	-0.004

FILTER EFFICIENCY CALCULATION AVERAGED DATA WITH ALUM

3.33mmol Ca(NO3)2

	(C/Co)1	(C/Co)2	d	(C/Co)avg	α	λ	t/tcalc	- log(C/Co)
	0.2271	0.2477	-0.02061	0.23736878	0.0053	-0.009	1.7	0.625
	0.7901	0.5168	0.273245	0.65345837	0.0016	-0.003	11.88	0.185
	0.8146	0.6416	0.173049	0.7280887	0.0012	-0.002	22.07	0.138
	0.8823	0.9978	-0.11551	0.94009307	0.0002	0.000	32.26	0.027
	0.9335	0.9333	0.000227	0.93338062	0.0003	0.000	42.44	0.030
	0.9016	0.9723	-0.07072	0.93697782	0.0002	0.000	52.63	0.028
	0.9308	0.9935	-0.06274	0.96213728	0.0001	0.000	62.81	0.017
	0.9309	0.9933	-0.06246	0.96210075	0.0001	0.000	73	0.017
	0.9737	0.8181	0.155573	0.89588671	0.0004	-0.001	83.18	0.048
	0.9995	0.8832	0.116294	0.94133922	0.0002	0.000	93.37	0.026
	0.9868	0.8702	0.116568	0.9285263	0.0003	0.000	103.56	0.032
	0.9994	0.8317	0.167718	0.91554879	0.0003	-0.001	113.74	0.038
	0.9978	0.8695	0.12837	0.93364579	0.0003	0.000	123.93	0.030
Average	0.874466	0.813004	0.061462		0.000814	-0.00141		
Std. Deviation	0.206032	0.221282	0.121802					
Std. error	0.057143	0.061373	0.033782					
		-0.01215	**< δ <**	0.13507263				

6.66mmol Ca(NO3)2

	(C/Co)1	(C/Co)2	d	(C/Co)avg	α	λ	t/tcalc	- log(C/Co)
	0.3571	0.1094	0.24763587	0.2332673	0.0054	-0.009	1.7	0.632
	0.5974	0.3484	0.24898903	0.4729203	0.0028	-0.005	11.88	0.325
	0.6234	0.4934	0.129948081	0.5583886	0.0022	-0.004	22.07	0.253
	0.6692	0.5636	0.105569711	0.6164235	0.0018	-0.003	32.26	0.210
	0.7860	0.6209	0.165117819	0.7034627	0.0013	-0.002	42.44	0.153
	0.7566	0.6575	0.099054528	0.7070509	0.0013	-0.002	52.63	0.151
	0.7405	0.6432	0.097271136	0.6918669	0.0014	-0.002	62.81	0.160
	0.8249	0.6521	0.172795863	0.7384782	0.0011	-0.002	73	0.132
	0.8331	0.6036	0.229496578	0.7183098	0.0012	-0.002	83.18	0.144
	0.8625	0.6052	0.257238512	0.733863	0.0011	-0.002	93.37	0.134
	0.8698	0.6888	0.180975321	0.7793314	0.0009	-0.002	103.56	0.108
	0.8322	0.6894	0.142815291	0.7608053	0.0010	-0.002	113.74	0.119
	0.9020	0.6983	0.20370213	0.8001387	0.0008	-0.001	123.93	0.097
Average	0.742662	0.567231	0.175431528		0.001717	-0.00298		
Std. Deviation	0.150093	0.167473	0.058550971					
Std. error	0.041628	0.046449	0.016239118					
		0.140046	**< δ <**	0.2108166				

3.33mmol NaCl

	(C/Co)1	(C/Co)2	d	(C/Co)avg	α	λ	t/tcalc	- log(C/Co)
	0.3508	0.2931	0.058	0.322	0.0042	-0.007	1.7	0.492
	0.9869	0.6764	0.310	0.832	0.0007	-0.001	11.88	0.080
	0.9180	0.7202	0.198	0.819	0.0007	-0.001	22.07	0.087
	0.8392	0.9886	-0.149	0.914	0.0003	-0.001	32.26	0.039
	0.9708	0.7723	0.198	0.872	0.0005	-0.001	42.44	0.060
	1.0068	0.9194	0.087	0.963	0.0001	0.000	52.63	0.016
	0.9762	0.8669	0.109	0.922	0.0003	-0.001	62.81	0.035
	0.9632	0.9285	0.035	0.946	0.0002	0.000	73	0.024
	0.9624	0.9685	-0.006	0.965	0.0001	0.000	83.18	0.015
	0.9700	0.9731	-0.003	0.972	0.0001	0.000	93.37	0.013
	0.9199	0.7835	0.136	0.852	0.0006	-0.001	103.56	0.070
	0.7997	0.7790	0.021	0.789	0.0009	-0.002	113.74	0.103
	0.7837	0.7435	0.040	0.764	0.0010	-0.002	123.93	
Average	0.880577	0.801013	0.079564		0.000755	-0.00131		
Std. Deviation	0.174954	0.185369	0.115369					
Std. error	0.048523	0.051412	0.031998					
		0.009841	**< δ <**	0.14928648				

6.66mmol NaCl

	(C/Co)1	(C/Co)2	d	(C/Co)avg	α	λ	t/tcalc	- log(C/Co)
	0.2145	0.2995	-0.085	0.2569794	0.0050	-0.009	1.7	0.590
	0.4284	0.5683	-0.140	0.4983605	0.0026	-0.004	11.88	0.302
	0.5410	0.6586	-0.118	0.5997791	0.0019	-0.003	22.07	0.222
	0.9464	0.6946	0.252	0.8204928	0.0007	-0.001	32.26	0.086
	0.6802	0.9833	-0.303	0.8317806	0.0007	-0.001	42.44	0.080
	0.6629	0.7011	-0.038	0.6820149	0.0014	-0.002	52.63	0.166
	0.4997	0.6127	-0.113	0.5562011	0.0022	-0.004	62.81	0.255
	0.5612	0.6649	-0.104	0.6130933	0.0018	-0.003	73	0.212
	0.4202	0.5838	-0.164	0.5020018	0.0026	-0.004	83.18	0.299
	0.4461	0.4718	-0.026	0.4589622	0.0029	-0.005	93.37	0.338
	0.3728	0.7478	-0.375	0.5603028	0.0021	-0.004	103.56	0.252
	0.7806	0.7109	0.070	0.7457714	0.0011	-0.002	113.74	0.127
	0.6678	0.7143	-0.046	0.691012	0.0014	-0.002	123.93	0.161
Average	0.555528	0.64705	-0.091521806		0.002028	-0.00352		
Std. Deviation	0.192061	0.158217	0.154692116					
Std. error	0.053268	0.043881	0.042903873					
		-0.18501	**< δ <**	0.0019657				

Base Solution

	(C/Co)1	(C/Co)2	d	(C/Co)avg	α	λ	t/tcalc	- log(C/Co)
	0.3093	0.3420	-0.033	0.326	0.0042	-0.007	1.7	0.487
	0.7401	0.7719	-0.032	0.756	0.0010	-0.002	11.88	0.121
	0.7095	0.9106	-0.201	0.810	0.0008	-0.001	22.07	0.091
	0.6780	0.7317	-0.054	0.705	0.0013	-0.002	32.26	0.152
	0.6797	0.7417	-0.062	0.711	0.0013	-0.002	42.44	0.148
	0.6472	0.7629	-0.116	0.705	0.0013	-0.002	52.63	0.152
	0.7269	0.7606	-0.034	0.744	0.0011	-0.002	62.81	0.129
	0.6729	0.7602	-0.087	0.717	0.0012	-0.002	73	0.145
	0.7767	0.5938	0.183	0.685	0.0014	-0.002	83.18	0.164
	0.6017	0.7541	-0.152	0.678	0.0014	-0.002	93.37	0.169
	0.5616	0.6805	-0.119	0.621	0.0018	-0.003	103.56	0.207
	0.6895	0.7117	-0.022	0.701	0.0013	-0.002	113.74	0.155
	0.6796	0.5744	0.105	0.627	0.0017	-0.003	123.93	0.203
Average	0.651729	0.699696	-0.04797		0.001524	-0.00264		
Std. Deviation	0.117052	0.136091	0.101611					
Std. error	0.032464	0.037745	0.028182					
		-0.10937	**< δ <**	0.01344139				

APPENDIX D CALCULATION FOR NANOPARTICLE SIZE VERSUS ATTACHMENT COLLISION EFFICIENCY

dp, m	As	NR	NLO	NG	Pe	α	ηo	λ	Ln(C/Co)	% C/Co	-Log(C/Co)	dp, nm	Log (dp)
1.00E-09	37.9791	2.00E-06	2.31E-01	4.61929E-15	7.12E+06	0.001	1.37E-03	-2.46E-03	-3.70E-04	0.99963	1.60E-04	1	0.00
1.00E-08	37.9791	2.00E-05	2.31E-03	4.61929E-13	7.12E+07	0.001	2.95E-04	-5.31E-04	-7.96E-05	0.99992	3.46E-05	10	1.00
2.00E-08	37.9791	4.00E-05	5.79E-04	1.84771E-12	1.42E+08	0.001	1.86E-04	-3.34E-04	-5.02E-05	0.99995	2.18E-05	20	1.30
3.00E-08	37.9791	6.00E-05	2.57E-04	4.15736E-12	2.14E+08	0.001	1.42E-04	-2.55E-04	-3.83E-05	0.99996	1.66E-05	30	1.48
4.00E-08	37.9791	8.00E-05	1.45E-04	7.39086E-12	2.85E+08	0.001	1.17E-04	-2.11E-04	-3.17E-05	0.99997	1.38E-05	40	1.60
5.00E-08	37.9791	1.00E-04	9.26E-05	1.15482E-11	3.56E+08	0.001	1.01E-04	-1.82E-04	-2.73E-05	0.99997	1.19E-05	50	1.70
6.00E-08	37.9791	1.20E-04	6.43E-05	1.66294E-11	4.27E+08	0.001	8.98E-05	-1.62E-04	-2.42E-05	0.99998	1.05E-05	60	1.78
7.00E-08	37.9791	1.40E-04	4.72E-05	2.26345E-11	4.98E+08	0.001	8.12E-05	-1.46E-04	-2.19E-05	0.99998	9.52E-06	70	1.85
8.00E-08	37.9791	1.60E-04	3.62E-05	2.95634E-11	5.69E+08	0.001	7.45E-05	-1.34E-04	-2.01E-05	0.99998	8.74E-06	80	1.90
9.00E-08	37.9791	1.80E-04	2.86E-05	3.74162E-11	6.41E+08	0.001	6.91E-05	-1.24E-04	-1.87E-05	0.99998	8.11E-06	90	1.95
1.00E-07	37.9791	2.00E-04	2.31E-05	4.61929E-11	7.12E+08	0.001	6.47E-05	-1.16E-04	-1.75E-05	0.99998	7.58E-06	100	2.00

dp, m	As	NR	NLO	NG	Pe	α	ηo	λ	Ln(C/Co)	% C/Co	Log(C/Co)	dp, nm	-Log (dp)
1.00E-09	37.9791	2.00E-06	2.31E-01	4.61929E-15	7.12E+06	0.002	1.37E-03	-4.93E-03	-7.39E-04	0.99926	3.21E-04	1	0.00
1.00E-08	37.9791	2.00E-05	2.31E-03	4.61929E-13	7.12E+07	0.002	2.95E-04	-1.06E-03	-1.59E-04	0.99984	6.92E-05	10	1.00
2.00E-08	37.9791	4.00E-05	5.79E-04	1.84771E-12	1.42E+08	0.002	1.86E-04	-6.69E-04	-1.00E-04	0.99990	4.36E-05	20	1.30
3.00E-08	37.9791	6.00E-05	2.57E-04	4.15736E-12	2.14E+08	0.002	1.42E-04	-5.11E-04	-7.66E-05	0.99992	3.33E-05	30	1.48
4.00E-08	37.9791	8.00E-05	1.45E-04	7.39086E-12	2.85E+08	0.002	1.17E-04	-4.22E-04	-6.33E-05	0.99994	2.75E-05	40	1.60
5.00E-08	37.9791	1.00E-04	9.26E-05	1.15482E-11	3.56E+08	0.002	1.01E-04	-3.64E-04	-5.47E-05	0.99995	2.37E-05	50	1.70
6.00E-08	37.9791	1.20E-04	6.43E-05	1.66294E-11	4.27E+08	0.002	8.98E-05	-3.23E-04	-4.85E-05	0.99995	2.11E-05	60	1.78
7.00E-08	37.9791	1.40E-04	4.72E-05	2.26345E-11	4.98E+08	0.002	8.12E-05	-2.92E-04	-4.39E-05	0.99996	1.90E-05	70	1.85
8.00E-08	37.9791	1.60E-04	3.62E-05	2.95634E-11	5.69E+08	0.002	7.45E-05	-2.68E-04	-4.02E-05	0.99996	1.75E-05	80	1.90
9.00E-08	37.9791	1.80E-04	2.86E-05	3.74162E-11	6.41E+08	0.002	6.91E-05	-2.49E-04	-3.73E-05	0.99996	1.62E-05	90	1.95
1.00E-07	37.9791	2.00E-04	2.31E-05	4.61929E-11	7.12E+08	0.002	6.47E-05	-2.33E-04	-3.49E-05	0.99997	1.52E-05	100	2.00

dp, m	As	NR	NLO	NG	Pe	α	ηo	λ	Ln(C/Co)	% C/Co	Log(C/Co)	dp, nm	Log(dp)
1.00E-09	37.9791	2.00E-06	2.31E-01	4.61929E-15	7.12E+06	0.01	1.37E-03	-2.46E-02	-3.70E-03	0.99631	1.60E-03	1	0.00
1.00E-08	37.9791	2.00E-05	2.31E-03	4.61929E-13	7.12E+07	0.01	2.95E-04	-5.31E-03	-7.96E-04	0.99920	3.46E-04	10	1.00
2.00E-08	37.9791	4.00E-05	5.79E-04	1.84771E-12	1.42E+08	0.01	1.86E-04	-3.34E-03	-5.02E-04	0.99950	2.18E-04	20	1.30
3.00E-08	37.9791	6.00E-05	2.57E-04	4.15736E-12	2.14E+08	0.01	1.42E-04	-2.55E-03	-3.83E-04	0.99962	1.66E-04	30	1.48
4.00E-08	37.9791	8.00E-05	1.45E-04	7.39086E-12	2.85E+08	0.01	1.17E-04	-2.11E-03	-3.17E-04	0.99968	1.38E-04	40	1.60
5.00E-08	37.9791	1.00E-04	9.26E-05	1.15482E-11	3.56E+08	0.01	1.01E-04	-1.82E-03	-2.73E-04	0.99973	1.19E-04	50	1.70
6.00E-08	37.9791	1.20E-04	6.43E-05	1.66294E-11	4.27E+08	0.01	8.98E-05	-1.62E-03	-2.42E-04	0.99976	1.05E-04	60	1.78
7.00E-08	37.9791	1.40E-04	4.72E-05	2.26345E-11	4.98E+08	0.01	8.12E-05	-1.46E-03	-2.19E-04	0.99978	9.52E-05	70	1.85
8.00E-08	37.9791	1.60E-04	3.62E-05	2.95634E-11	5.69E+08	0.01	7.45E-05	-1.34E-03	-2.01E-04	0.99980	8.74E-05	80	1.90
9.00E-08	37.9791	1.80E-04	2.86E-05	3.74162E-11	6.41E+08	0.01	6.91E-05	-1.24E-03	-1.87E-04	0.99981	8.11E-05	90	1.95
1.00E-07	37.9791	2.00E-04	2.31E-05	4.61929E-11	7.12E+08	0.01	6.47E-05	-1.16E-03	-1.75E-04	0.99983	7.58E-05	100	2.00